



**REPUBLIC OF IRAQ
MINISTRY OF HIGHER EDUCATION AND SCIENTIFIC
RESEARCH**

**AL-FURAT AL-AWSAT TECHNICAL UNIVERSITY
ENGINEERING TECHNICAL COLLEGE-NAJAF**

**STUDY THE EFFECT OF USING DIFFERENT TYPES
OF TWISTED TAPES ON THERMAL
PERFORMANCE IN SOLAR COLLECTOR**

A THESIS

**SUBMITTED TO THE DEPARTMENT OF MECHANICAL
ENGINEERING TECHNIQUES IN POWER AS PARTIAL
FULFILLMENT OF THE REQUIREMENTS FOR TECHNICAL
MASTER DEGREE IN MECHANICAL ENGINEERING
(THERMAL)**

BY

Ali Majeed Abdu AL Kareem

(B.SC MECH. ENG.)

Supervised by:

Asst. prof.

Dr. Ahmad Hashim Yousif

Prof.

Dr. Ali Shakir Baqir

July 2020

بِسْمِ اللَّهِ الرَّحْمَنِ الرَّحِيمِ

رَبِّ أَوْزَعْنِي أَنْ أَشْكُرَ نِعْمَتَكَ الَّتِي أَنْعَمْتَ عَلَيَّ
وَعَلَى وَالِدَيَّ وَأَنْ أَعْمَلَ صَالِحًا تَرْضَاهُ وَأَصْلِحْ لِي
فِي ذُرِّيَّتِي ۖ إِنَّي نُبْتُ إِلَيْكَ وَايَ مِنَ الْمُسْلِمِينَ

....

بِسْمِ اللَّهِ
الرَّحْمَنِ الرَّحِيمِ

سورة الأحقاف: آية ١٥

ACKNOWLEDGMENTS

*Full thanks to the Almighty God for the divine interference in a modest effort. Candid thanks are hereby extended to the following Never desisted in contributing to this thesis, **Asst. Prof. Dr. Ahmad Hashim Yousif** and **Prof. Dr. Ali Shakir baqir**, My supervisors, support me for their guidance and unlimited support during the research period. Present of mine gratitude with appreciation for everyone of the employers of the Power Techniques Department, College of Technical Engineering-Najaf Grateful and Special thanks for my parents, my late father, my mum, for mine brothers, my wife and my children for them unceasing assistance, inducement and Diligence in the hard time of my working life.*

*Special thanks to the Head of Department of Mechanical Engineering Techniques of Power **Asst. Prof. Dr. Dhafer Manea Hachim** in the Technical Engineering College /Al-Najaf, Al-Furat Al-Awsat Technical University, for their support and advice.*

Ali Majeed Abd ALkareem

July 2020

Devotion

To my late father..... The symbol of emotion

To my dear mother.....The flower of love

To my wife Inspirational....The symbol of Inspirational

To my children The spirit of life

To my wonderful brothers..... The source of strong

I dedicate this modest effort


Ali

July 2020

SUPERVISOR CERTIFICATION

We certify that this thesis titled” Study the effect of using different types of twisted tapes on thermal performance in solar collector” which is being submitted by **Ali Majeed Abd AL Kareem** was prepared under our supervision at the Power Techniques Engineering Department, Engineering Technical faculty-Najaf, AL- Furat Al-awsat Technical University, as partial fulfillment of the requirements for the degree of Master of technical in thermal Engineering.

Signature:



Name **Asst. Prof. Dr. Ahmad Hashim Yousif**
(Supervisor)

Date **9 / 12 / 2020**

Signature:



Name: **Prof. Dr. Ali Shakir Baqir**
(Co-supervisor)

Date **9 / 12 / 2020**

In view of the available recommendation, we forward this thesis for debate by the examining committee.

Signature:



Name: **Asst. Prof. Dr. Dhafer Manea Hachim**
Head of power mechanic Tech. Eng. Dept.

Date : / / 2020

THE EXAMING COMMITTEE CERTIFICATION

We certify that we have read this thesis titled” Study the effect of using different types of twisted tapes on performance of solar collector” which is being submitted by Ali Majeed Abd AL Kareem and as Examining Committee, examined the student in it is contents. In our opinion, the thesis is adequate for an award of degree of Master of Technical in Thermal Engineering.

Signature: 

Name Asst. Prof. Dr. Ahmad Hashim Yousif
(Supervisor)

Date 9/12 / 2020

Signature: 

Name: Prof. Dr. Ali Shakir Baqir
(Co-supervisor)

Date 9/12 / 2020

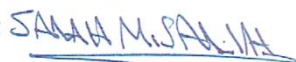
Signature: 

Name: Asst. Prof. Dr. Zaid M.

AL-Dulaimi

(Member)

Date 7/12 / 2020


Signature: 

Name :Lecturer Dr. Salah. M.

Salih

(Member)

Date 6/12 / 2020

Signature: 

Name: Prof. Dr. Qasim Saleh Mahdi

(Chairman)

Date 10/12 / 2020

Approval of the Engineering Technical College – Najaf.

Signature: 

Name: Asst. Prof. Dr. Hassanain Ghani Hameed

Dean of Technical Engineering College -Najaf

Date : / / 2020

IV

ABSTRACT

The goal of this research is to study experimentally the effect of the use of twisted aluminum strips as turbulence promoters on the heat transfer in terms of Nusselt number (Nu), the pressure drop in terms of the friction factor (f), the thermal performance factor TPF and the efficiency (η) of the flat plate solar collector. This research focuses with process of energy conversation under steady-state status in the laminar flow situation for uses drinkable water as the working fluid.

Experimental side includes design and construction of a simple solar collector (flat plate type) and four different kinds of twisted strips include curvatures and straight vortex generators (VGs) and twist ratio is $Y=2$ (twisted tape with curvature vortex generator in front flow TTFF, twisted tape with curvature vortex generator in opposite flow TTOF, twisted tape with straight vortex generator TTS and typical twisted tape TT), dimensions of the vortex generator 2mm high and 1mm thick. The measuring instruments used in this experiment were solar irradiance meter, volumetric flowmeter, manometer, temperature record meter, and temperature sensors. The experiments are carried out in Babal, Iraq with latitude $32^{\circ}, 13', 27$ N and longitude $44^{\circ}, 22', 36$ E, the volumetric flow rates used are (7, 5, 3 and 1.5) L / min .

The experimental result showed that the decrease in flow rate was found to increase the variation in temperature of the water between the exit and the inlet of tubes fitted with twisted tape, the higher difference in temperature was (18.3° C) in tubes fitted with TTFF at volumetric rate 1.5 liter / minute and the maximum outlet temperature of the fitted tube (TTFF) was 98° C for 1.5 L / min. Also, thermal transfer rate in term number of Nusselt (Nu) and pressure drop in term factor of friction (f) improved compared to other cases in the tube fitted with (TTFF), the Nusselt Number for riser tube equipped with (TTFF) enhanced to 31%, 38.2%, 40%, and 54.2% compared with the smooth tube at

laminar flow with Number of Reynolds range ($300 < Re < 2000$) respectively also the factor of friction increases with number of Reynolds Re decreases and for higher friction factor is achieved in the tube equipped with (TTFF, TTOF, and TTS) comparison with (TT) and plain tube, the parameter of friction (f) in the tube equipped with TTFF increases by about 18% to 30% above the plain tube. The empirical data also revealed the TPF thermal performance ratio for TTFF was higher than the other twisted tapes with the same pumping capacity, the maximum thermal performance factor was 1.4 and the maximum efficiency of the TTFF tube was 64.7%.

CONTENTS

| | |
|--|-----|
| Acknowledgements..... | I |
| Devotion..... | II |
| Supervisor Certification..... | III |
| The examining commttee certification..... | III |
| Contents..... | VII |
| List of Tables..... | X |
| List of Figures..... | XI |
| List of Nomenclature..... | XIV |
| Chapter One..... | 1 |
| Introduction..... | 1 |
| 1.1 preface..... | 1 |
| 1.2 Solar irradiance..... | 3 |
| 1.3 Solar radiation incidence on tilt surfaces..... | 3 |
| 1.4 Solar collectors:..... | 4 |
| 1.5 Flat plate collector..... | 7 |
| 1.6 Tilt angle for solar flat plate collector..... | 8 |
| 1.7 Thermal transfer improvement methods..... | 8 |
| 1.7.1 Effective Heat Transfer improvement methods..... | 9 |
| 1.7.2 Passive Heat Transfer improvement methods..... | 9 |
| 1.7.3 Compound Heat Transfer Augmentation Methods..... | 10 |
| 1.8 Inside Twisted strips Insert Devices..... | 10 |
| 1.8.1 Major groups of twisted tapes..... | 11 |
| 1.9 The goles of the experimental study..... | 13 |
| Chapter Two..... | 14 |
| literatuer survey..... | 14 |
| 2.1 Introduction..... | 14 |
| 2.2 The laminar flow..... | 14 |
| 2.3 Twist tapes as turbulence promoters..... | 15 |

| | |
|---|----|
| 2.4 Effect of twist ratio..... | 15 |
| 2.5 Effect of modulated twisted tape..... | 17 |
| 2.6 Effect of helical strips | 19 |
| 2.7 Effect of twisted tapes dimensions..... | 20 |
| 2.8 Effect of multiple twisted tapes..... | 23 |
| 2.9 Effect of the wire coil..... | 28 |
| 2.10 Effect the perforation | 31 |
| 2.11 Effect of winglet twisted tape | 35 |
| 2.12 Effect of twisted tape with ribs | 39 |
| 2.13 Scope of present work:..... | 41 |
| Chapter Three..... | 45 |
| Mathematical Background..... | 45 |
| 3.1 Introduction | 45 |
| 3.2 Twisted Tapes | 46 |
| 3.3 Twisted tape with vortex generators | 47 |
| 3.4 Transfer of heat and flowing of fluid into circular pipes..... | 47 |
| 3.5 Physical and thermal properties of working fluid (water) | 48 |
| 3.6 The performance of a solar collector | 49 |
| 3.7 The gross coefficient of heat loss for flat plate collector..... | 51 |
| 3.8 The internal convective coefficient of heat transfer for water flow (h_i) into riser pipe | 56 |
| 3.9 The efficiency of collector and useful energy..... | 56 |
| 3.10 Thermal performance factor (performance ratio) (TPF)..... | 58 |
| Chapter Four..... | 59 |
| Experimental Work..... | 59 |
| 4.1 Introduction | 59 |
| 4.2 Experimental Test Rig Description..... | 60 |
| 4.2.1 Specifications of Flat Plate type solar collector..... | 60 |
| 4.2.2 Experimental setup of the system | 62 |
| 4.2.3 Twisted tapes geometrical configuration and dimension..... | 65 |

| | |
|--|-----|
| 4.2.4 Water pump | 68 |
| 4.2.5 Pipes..... | 68 |
| 4.2.6 Valves..... | 69 |
| 4.2.7 The measuring devices | 69 |
| 4.3 Experimental procedure | 75 |
| Chapter Five | 77 |
| Results and Discussion..... | 77 |
| 5.1 Introduction | 77 |
| 5.2 The solar irradiance results | 78 |
| 5.3 The results of temperature difference | 80 |
| 5.4 The result of outlet temperature | 83 |
| 5.5 The thermal rate variation | 86 |
| 5.6 The Results of pressure drop..... | 90 |
| 5.7The factor of thermal performance (TPF)..... | 94 |
| 5.8 Collector efficiency | 97 |
| Chapter Six..... | 99 |
| Conclusion and Recommndations..... | 99 |
| 6.1 The conclusion | 99 |
| 6.2 The recommendations | 100 |
| References | 102 |
| Appendix(A)..... | A-1 |
| A. The calibration of Instruments used in the experiments..... | A-1 |
| A.1 Calibration of solar collector meter: | A-1 |
| A.2 Flow rate meter calibrate method..... | A-1 |
| A.3Calibration of temperature sensors of 8- channel data logger and 4K type thermocouples with digital thermometers..... | A-3 |
| A.4 Calibration differential pressure manometer:..... | A-6 |
| Appendix(B)..... | B-1 |
| B. Calculation of fin efficiency of straight configuration and the Average Transmittance-Absorptance ($\tau\alpha$) av | B-1 |

| | |
|--|-----|
| B.1 Calculating the efficiency (F) for rectangular shape and straight fins | B-1 |
| B.2 Calculate the Average Transmittance-Absorptance | B-2 |
| Appendix(C)..... | C-1 |
| C. Uncurtains analysis..... | C-1 |
| C.1 Friction factor derivation..... | C-2 |
| C.2 Nusselt number derivation..... | C-3 |
| C.3 collector efficiency derivation | C-4 |
| C.4 Uncertainty analysis for forced circulation condition:..... | C-5 |
| C.4.1 Friction factor evaluated..... | C-5 |
| C.4.2 The Nusselt number calculation | C-6 |
| C.4.3 Efficiency calculation | C-6 |
| Appendix(D)..... | D-1 |
| D. List of publications | D-1 |

LIST OF TABLES

| Table | page |
|---|-------------|
| No. | No. |
| Table – 1.1: The classification of solar collectors[web site] | 7 |
| Table- 2.1: The summary | 42 |
| Table- 4.1: The specification of flat plate solar collector | 64 |
| Table- 4.2: the specification of the centrifugal pump | 69 |
| Table A.1: calibration results of first 8- channels data logger with 8 sensors. A-3 | A-3 |
| Table A.2: calibration results of second 8- channels data logger for 8 sensors A-4 | A-4 |
| Table A.3: the calibration of 4 k- type | A-5 |
| Table C.1: The errors in the instruments used in experiments | C-5 |

LIST OF FIGURES

| Figure No. | Title of the Figure | Page No. |
|-----------------------|---|---------------------|
| Fig. 1.1 | The distribution of solar irradiance on the earth's surface[web site]..... | 3 |
| Fig.1.2 | The absorption bands with the wavelength[web site]. | 4 |
| Fig. 1.3: | Flat plate solar collector (FPC) [web site]..... | 5 |
| Fig. 1.4: | Evacuated tube solar collector[web site]..... | 6 |
| Fig. 1.1.5: | Parabolic trough collector[web site]..... | 6 |
| Fig.1.6: | Solar irradiance distribution over the flat plate collector[web site]. | 8 |
| Fig. 1.7: | The different categories of twisted tapes [4] | 12 |
| Fig. 1.8: | Typical twisted tape insertion into tube..... | 13 |
| Fig. 2.1 : | (a) SRTT and STT &(b) pictorial view of SRTT for different twist... .. | 16 |
| Fig. 2.2:(a) | Twisted tape with increase twist ratio&(b)-with decrease twist ratio[16]. | 17 |
| Fig. 2.3: | Three different twisted tapes[20]..... | 18 |
| Fig. 2.4: | Twisted tapes with an alternate axis [21]. | 19 |
| Fig. 2.5: | Spril device inserts with various twist orders [24]. | 20 |
| Fig. 2.6: | Twisted tapes in five different twisted ratios and width [32]. | 22 |
| Fig. 2.7: | Schematic layout of different thickness twisted tapes [33]. | 23 |
| Fig. 2.8: | Taper twisted tape with different taper angles (Θ) [34]. | 23 |
| Fig. 2.9: | The counter coupling, co-coupling and single twisted tapes [36]..... | 26 |
| Fig. 2.10: | Triple twisted tapes withe four different twist ratios [37]. | 27 |
| Fig. 2.11: | Typical, unilateral and cross hollow twisted tapes[38]. | 27 |
| Fig. 2.12: | The annular pipe fitted with co / counter swril convolute strips [40]. | 27 |
| Fig. 2.13: | Wire coil with three different pitch ratio Coiled Wire template Coil tabulator of pitch: (a) 5mm (b) 10mm (c) 15mm [46]. | 31 |
| Fig. 2.14: | Perforated torsion strip with punches in diverse size [54]. | 34 |
| Fig. 2.15: | Punched convolute strip with wings in parallel array (PTT)[55]. | 34 |
| Fig. 2.16: | Perforate-helical twisted tapes(P-HTT) [57]. | 35 |

| | |
|--|----|
| Fig. 2.17: Staggered-winglet typical tapes [58]. | 38 |
| Fig. 2.18: Traingle-wing convolute strip (a) normal convolute strips (b) upright tringle-wing torsion strips (c) incline triangle-wing convolute strips [59]. | 38 |
| Fig. 2.19: Normal convolute strips (TT), convolute strips with delta wings at center (WT), convolute strips at alternate pivots (T-A), convolute strips with wings at center for alternate-pivot (WT-A)[60]. | 39 |
| Fig. 2.20: Convolute strips with 30° v-ribs [64] | 40 |
| Fig. 2.21: Twisted tapewith ribs[65]. | 41 |
| Fig. 3.1: Schematic of twisted tape inside a tube. | 46 |
| Fig. 3.2: Twisted tapes with vortex generators. | 47 |
| Fig. 3.3: Distribution of solar irradiance over solar collectors [69]. | 51 |
| Fig. 3.4: Thermal resistance network for a solar collector with tow covers [69]. | 54 |
| Fig. 4.1: Flat plate solar collector. | 62 |
| Fig. 4.2: The main parts of the flat plate solar collector and measurement devices. | 63 |
| Fig. 4.3: Schematic of test rig construction and the measurement devices. | 65 |
| Fig. 4.4: Four different twisted tapes (TT, TTFF, TTOF, and TTS) | 66 |
| Fig. 4.5: Types of twisted tapes and dimensions of vortex generators. | 68 |
| Fig. 4.6: 8-Channel data logger. | 71 |
| Fig. 4.7: Eight temperature sensors. | 72 |
| Fig. 4.8: Digital thermometer. | 72 |
| Fig. 4.9: Positions and number of sensors. | 73 |
| Fig. 4.10: Number and positions of sensors. | 73 |
| Fig. 4.11: Volumetric flow meter. | 74 |
| Fig. 4.12: Manometer | 76 |
| Fig. 4.13: solar radiation meter. | 76 |
| Fig. 5.1: Solar radiation for(7,9,10)/1/2020. | 78 |
| Fig. 5.2: Solar radiation for(13,14,15)/2/2020. | 79 |
| Fig. 5.3:Solar radiation for(19,23,24)/3/2020. | 79 |

| | |
|--|----|
| Fig. 5.4: Temperature difference for typical twisted tapes(TT)..... | 81 |
| Fig. 5.5: Temperature difference for (TTFF)..... | 81 |
| Fig. 5.6: Temperature difference for (TTOF). | 82 |
| Fig. 5.7: Temperature Difference for (TTS). | 82 |
| Fig. 5.8: Temperature Difference for the plain tube. | 83 |
| Fig. 5.9: The outlet Temperature for 1.5 L/min. | 84 |
| Fig. 5.10: The outlet Temperature for 3L/min. | 84 |
| Fig. 5.11: The outlet Temperature for 5 L/min. | 85 |
| Fig. 5.12: The outlet Temperature for 7L/min. | 85 |
| Fig. 5.13: The variation of Nusselt number versus local Time at 7L/min. | 87 |
| Fig. 5.14: The variation of Nusselt number versus local Time at 5L/min. | 87 |
| Fig. 5.15: The change of Nusselt Number against Local Time at 3L/min. | 88 |
| Fig. 5.16: The change of Nusselt Number against local Time at 1.5 L/min. | 88 |
| Fig. 5.17: The change of Nusselt number against number of Reynolds Re with (smooth tube TT, TTFF, TTOF, and TTS). | 89 |
| Fig. 5.18: Nusselt number ratio versus The Re with (TT, TTFF, TTOF, and TTS)..... | 89 |
| Fig. 5.19: The Factor of Friction change with Local Time at 7L /min. | 91 |
| Fig. 5.20: The Factor of Friction variation for Local Time at 5 L/min. | 91 |
| Fig. 5.21: The Friction Factor Variation Withe Local Time For 3L/min. | 92 |
| Fig. 5.22: The Friction Factor Variation with Local Time For 1.5 L/min. | 92 |
| Fig. 5.23: The Factor of Friction versus with Number of Reynolds to (smooth pipe TT, TTFF, TTOF, and TTS) | 93 |
| Fig. 5.24: The friction factor ratio versus for Number of Reynolds to (TT, TTFF, TTOF, and TTS)..... | 93 |
| Fig. 5.25: Thermal Performance Factor with Local Time for 7 L/min. | 95 |
| Fig. 5.26: Thermal Performance Factor with Local Time For 5 L/min. | 95 |
| Fig. 5.27: Thermal Performance Factor with Local Time For 3LPM. | 96 |
| Fig. 5.28: Thermal Performance Factor with Local Time for 1.5 L/min. | 96 |

| | |
|---|-----|
| Fig. 5.29: The Performance ratio (TPF) versus Number of Reynolds Re for TT, TTFF, TTOF, and TTS..... | 97 |
| Fig. 5.30: The efficiency of solar collector verse with Reynolds number Re for(TT, TTFF, TTOF, TTS, and plain tube) | 98 |
| Fig. A.1: calibration of solar radiation meter..... | A-1 |
| Fig. A.2: calibration of differential pressure manometer..... | A-7 |
| Fig. B.1: temperature distribution between two tubes in flat plate solar collector. | B-1 |
| Fig. B.2: incidence and reflection angles for the irradiance beam from a medium with refractive index n_1 to a medium with refractive index n_2 | B-3 |

LIST OF NOMENCLATURE

| | | |
|----------|---|---------------|
| A_c | The area of solar collector | m^2 |
| A_i | Inside surface area | m^2 |
| A_o | The exterior surface area | m^2 |
| C_p | Coefficient of specific heat | J/kg.K |
| C_{pw} | Coefficient of specific heat for water | J/kg.K |
| D | Nomnail diameter of riser tube | m |
| d_i | Inside diameter of pipe | m |
| d_o | External pipe diameter | m |
| f | The factor of friction | Dimensionless |
| F_R | Removable heat factor | Dimensionless |
| F | The efficiency of straight fin | Dimensionless |
| F' | The collector efficiency | Dimensionless |
| G_T | Global radiation | W/ m^2 |
| h | Coefficient of heat transfer | W/ m^2 . K |
| h_i | Internal convective heat transfer coefficient | W/ m^2 . K |
| h_c | Coefficient of heat transfer by convective | W/ m^2 . K |
| h_r | Coefficient of heat transfer by radiation | W/ m^2 . K |
| h_w | The wind loss coefficient | W/ m^2 . K |
| I_T | Total solar irradiance | W/ m^2 |
| k | Constant of thermal conductivity | W/ m. K |

| | | |
|----------------|--|-----------------------|
| k_e | Thermal conductivity of insulation at edges | W/ m. K |
| k_b | Thermal conductivity of insulation at the bottom | |
| k_p | Thermal conductivity for absorber plate | W/ m. K |
| k_w | \ thermal conductivity for water | W/ m. K |
| K | Extinction coefficient | m^{-1} |
| L | Collector length | m |
| l | Distance between plate and covers | m |
| \dot{m} | The flow rate of mass | kg/sec |
| Nu | Nusselt number | Dimensionless |
| n_1, n_2 | Refraction indices | Dimensionless |
| P | Pressure of water | N/ m ² |
| p | Twist pitch | m |
| Q | Thermal energy | W |
| Q_u | Useful thermal energy | W |
| $q_{loss,top}$ | Thermal loss from collector at the top | W/m ² |
| q_{fin} | Collection heat from fin | W |
| S | Solar radiation absorbtion | W/m ² |
| t | The thickness of the twisted tape | m |
| t_e | Insulation thickness at edges | m |
| t_b | Insulation thickness at bottom | m |
| T_a | Ambient temperature | ° C |
| T_i | Temperature of inlet | K |
| T_p | Temperature of plate | K |
| T_{pm} | Mean plate temperatuer | K |
| T_o | Temperature of outlet | K |
| T_m | The mean temperatuer ($\frac{T_o+T_i}{2}$) | K |
| U_L | Coefficient of overall heat heat loss | W/ m ² . K |
| U_e | Thermal loss coefficient from edges | W/ m ² . K |
| U_b | Thermal loss coefficient from bottom | W/ m ² . K |
| U_o | Coefficient of exterior heat transfer | W/ m ² . K |
| U | speed of water | m/sec |
| u | Wind speed | m/sec |
| W | Distance between two riser tube | m |
| w | Width of twisted strips | m |

| | | |
|----------------------|--|---------------|
| Y | Twist ratio | Dimensionless |
| Greek Symbols | | |
| $(\tau\alpha)_{av}$ | Average transmittance-absorptance product | Dimensionless |
| τ | The transmittance of a single cover | Dimensionless |
| τ_r | Transmittance with only reflection losses | Dimensionless |
| $\tau\alpha$ | Transmittance with only absorption losses | Dimensionless |
| α_n | Absorptance at a normal incident angle | Dimensionless |
| β | The tilt angle of the collector | Degree |
| β' | Volumetric expansion | K^{-1} |
| δ | The declination angle | Degree |
| δ_p | The thickness of the absorber plate | m |
| ΔP | the pressure drop across riser tube | N/m^2 |
| ε_p | The emissivity of plate | Dimensionless |
| ε_c | The emissivity of glass (cover) | Dimensionless |
| η | collector efficiency | Dimensionless |
| η_i | instantaneous collector efficiency | Dimensionless |
| θ_1 | The incidence angle | Degree |
| θ_2 | The refraction angle | Degree |
| θ_e | Effective incidence angle | Degree |
| σ | Radiation constant (5.67×10^{-8}) | W/m^2K^4 |
| ω | solar hour angle | Degree |
| ϑ | The latitude of the city | Degree |
| μ_w | Water dynamic viscosity | Pa·s |
| ρ_w | Density of working fluid(water) | kg/m^3 |
| ν | kinematics viscosity of air | m^2/sec |

ABBREVIATIONS

| Symbol | Description |
|-------------------|---|
| $f(s)$ | Factor of friction for tube fitted with twisted tape |
| $f(\text{plain})$ | Friction factor in a smooth tube |
| N | The number of covers(glass) |
| Nu(s) | Number of Nusselt for tube fitted with twisted strips |
| Nu(plain) | Number of Nusselt for smooth tube |
| Pr | Number of Prandtl |
| Ra | Rayleigh number |

| | |
|------|---|
| Re | Number of Reynolds |
| TT | Typical twisted tape |
| TTF | Twisted tape with curvature vortex generators in front flow |
| TTOF | Twisted tape with curvature vortex generators opposite flow |
| TTS | Twisted tape with straight vortex generators |

Chapter One

Introduction

Chapter One

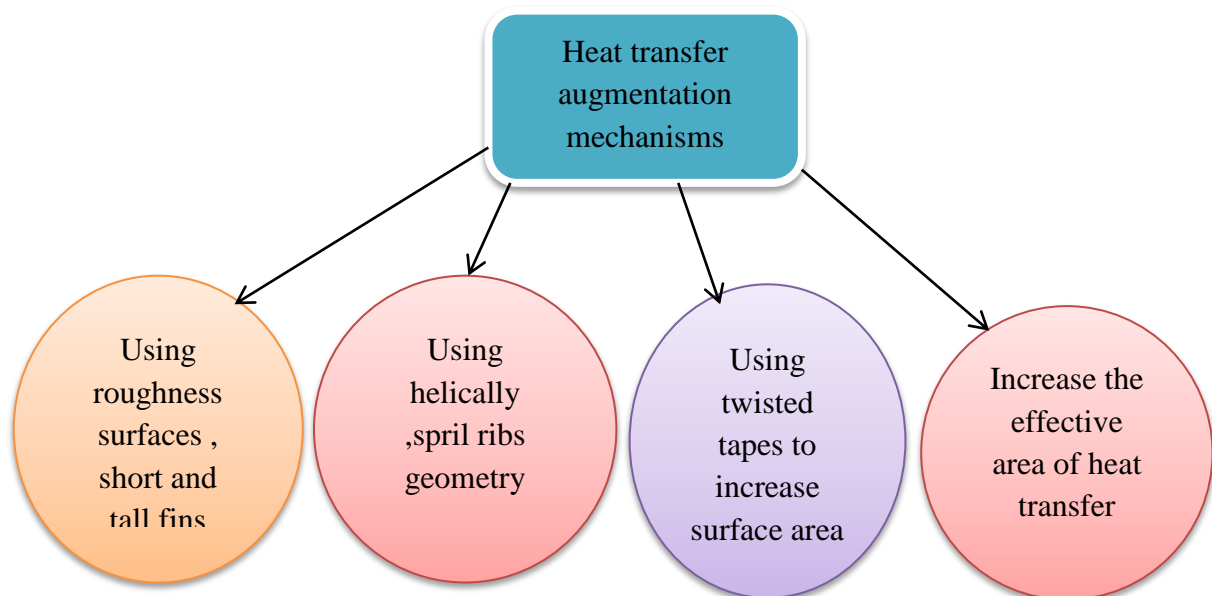
Introduction

1.1 preface

Solar power has converted to a promising source of energy, especially since the industrial revolution, although there are many forms of energy in the world such as oil, natural gas, fossil fuel, coal..etc.. It became a target for many scientists and researchers because it has many advantages as it is one form of renewable energy, environmentally friendly, and low maintenance required compared with the projected high cost of oil and the dangerous emission like CO₂, and CO..., etc.

The fossil fuel, natural gas, coal are source forms of conventional energy where that were created by photosynthetic activity, followed by complicated chemical processes in which decaying under high pressure and temperature. Also wind and tide has a solar origin was created as a result of temperature differences in regains in the earth. There are two forms of energies created from solar energy which are electricity and thermal energy using photovoltaic cells and solar collectors, respectively, also solar energy solves the problem of lack of drinkable water by solar distillation of seawater. Consideration the solar collector as special kind of heat exchanger(Kalogirou 2014) [1] heat device conversion, imposition and recapture heat energy call heat exchanger it is widely used in domestic, mercantile and industrial purpose several prevalent examples as the steam produce in steam plants sensible heating and cooling of viscous media in thermal processing of chemical; agricultural products; air and liquids cooling systems of engines; refrigerant vaporization and intensification in air conditioning and refrigeration....etc. The solar collector receives the solar irradiance and transferred to the internal energy of fluid while the heat

transferred between two fluids in the heat exchanger. Thermal application systems are commonly used in automotive, domestic and physical fields such as for cooling and heating systems, in most all engineering fields, high-efficient thermal equipments are very important in different life applications as well as the need to build an effective heat exchanger was partially utilized by using increased heat transfer rates. The way to improve the rate of heat transfer in the heat systems is done by three mechanisms were classified into, active, passive, and compound (Hallquits 2011) [2] its was divided according to exhausting power or without power and use the both mentioned methods call compound. The heat transfer augmentation mechanisms can be one of the following (Khaled et al. 2010) [3]:



The influence of thermal improvement mechanism in heat exchangers is very important because it is treated with high heat flux handling and reduces the size which also leads to low-cost heat transfer increase methods that are capable of operating heat exchanger at low speeds and with higher heat transfer coefficient (Yousif and Khudhair 2019) [4].

1.2 Solar irradiance

The sun is the source of solar power it is an hot sphere of gaseous matter with a diameter of 1.39×10^9 m, the sun's gross power output is 3.8×10^{20} MW, energy irradiate reach in every directions(Kalogirou 2014)[1], the fig. (1.1) depicted the sun irradiance distributions on earth. The only tiny fraction of the gross irradiance released received by the earth, solar spectral radiation is the wavelength-dependent power reach to the top of the Earth's atmosphere the sunray reaches the ground it electromagnetic short wave absorber and refracted it is visible ray the fig. (1.2) shown the absorption bands with the wavelength.

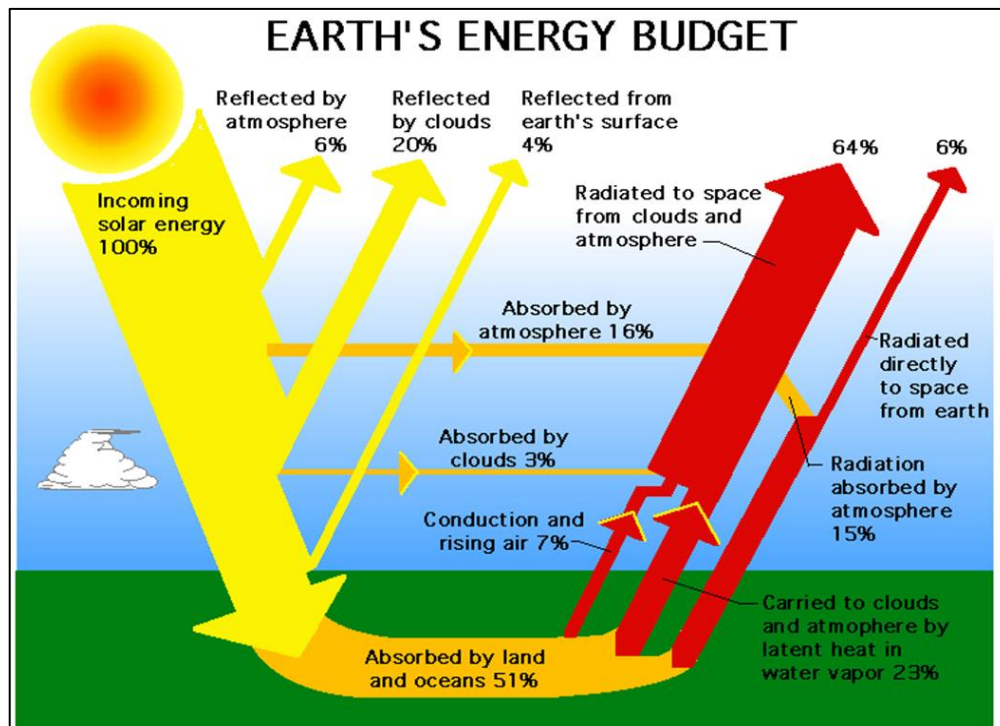


Fig. 1.1 The distribution of solar irradiance on the earth's surface[web site]

1.3 Solar radiation incidence on tilt surfaces

The total quantity of solar power obtained by the Earth call global solar, the radiation as a direct line from the sun is beaming irradiance, while radiation

which scattered out by molecules, aerosols, and clouds represent diffuse irradiance. The sum of direct, spread, and reflected irradiance that reaches to surface is called total or global irradiance. The irradiance components reflected through different surfaces of atmosphere and diffused from the sky represent the amount of a set irradiance sources, like beam of radiation, such that of beam and diffuse irradiance represent incidence radiation on horizontal surfaces and total surface radiation representing the inclined surface (Saraf and Hamad 1988) [5].

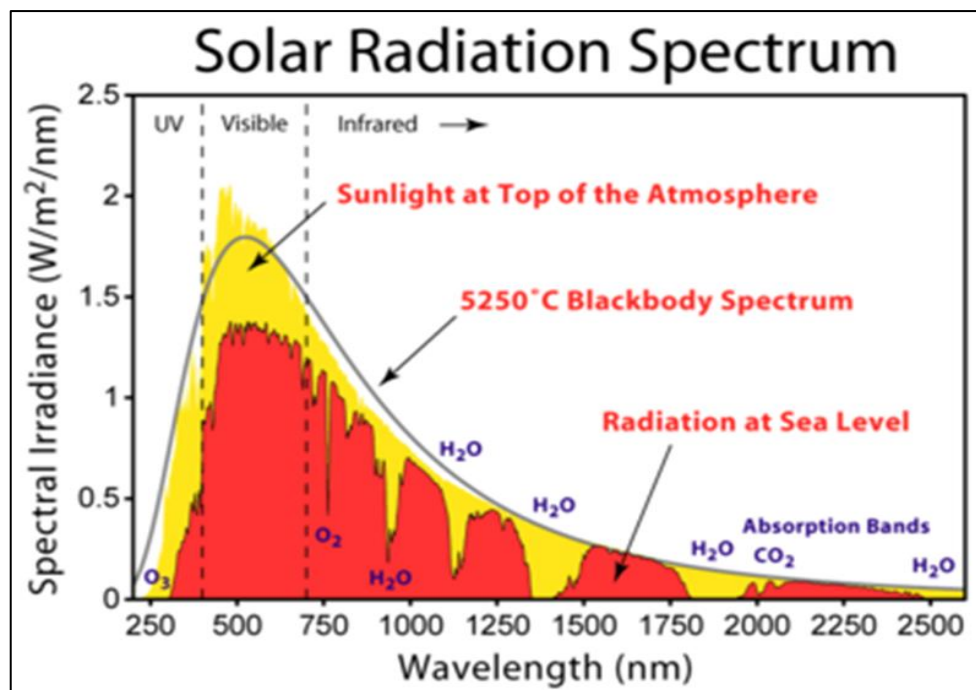


Fig.1.2 The absorption bands with the wavelength[web site].

1.4 Solar collectors:

a solar collector is a device that collects and/or concentrates solar radiation from the Sun.

A. Stationary collectors (Kalogirou 2014) [1]

- Flat plate solar collector(Glazing materials and collector absorbing (plates) shown in fig. (1.3) a and b.

- The evacuated tube collector is shown in fig. (1.4).
- Compound parabolic collector.

B. Sun tracking concentrating collectors:

- Parabolic trough collector is shown in fig. (1.5). Parabolic dish reflector (PDR).
- Heliostat field collector. The classification of solar collectors is tabulated in the table (1.1).



Fig. 1.3: Flat plate solar collector (FPC) [web site].

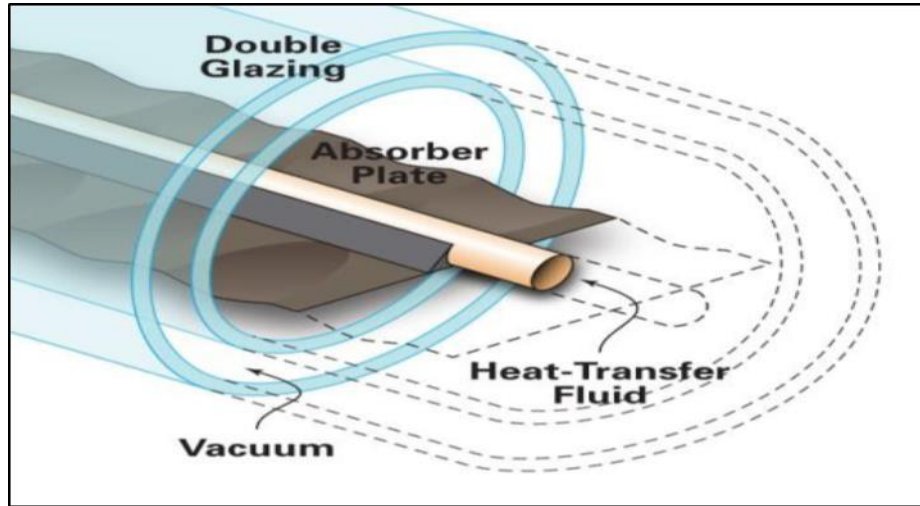


Fig. 1.4: Evacuated tube solar collector[web site].

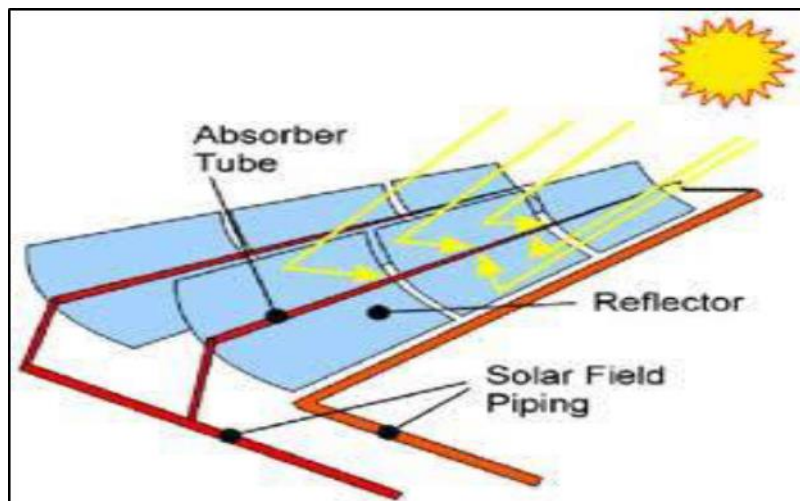


Fig.1.5: Parabolic trough collector[web site]

Table – 1.1: The classification of solar collectors[web site]

| Category | Example | Temperature range, °C | Efficiency, % |
|----------------------|------------------------------|-----------------------|---------------|
| No concentration | Flat-plate Evacuated tube | Up to 80 Up to 200 | 30 – 55 |
| Medium Concentration | Parabolic cylinder | 150 - 500 | 60 – 70 |
| High Concentration | Parabolic dish | 1500 and more | 60 - 75 |

1.5 Flat plate collector

Is a particular form a heat exchanger which absorbs solar irradiance and converts for heat, having different from the heat exchanger in which collectors are transferred heat between two fluids, the main parts of the flat plate solar(Kalogirou 2014) [1]. as follows:

- a) Glassing cover: it may be a single sheet of glass or more some other transmitting - radiation material.
- b) Absorber sheet: this perhaps grooved, waving, or flat, for a tube.
- c) Manifolds or upper and lower Headers: to allow the fluid enters and exit.
- d) Tubes: it performs heat transfer from inlet to outlet, it is made from conducting materials.
- e) Insulation: reducing heat losses from the sides and bottom.
- f) Container: Protecting all parts of collectors from environmental damage, such as moisture and dust. The distribution the solar irradiance over top of the solar collector with flat sheet shown in fig. (1.6).

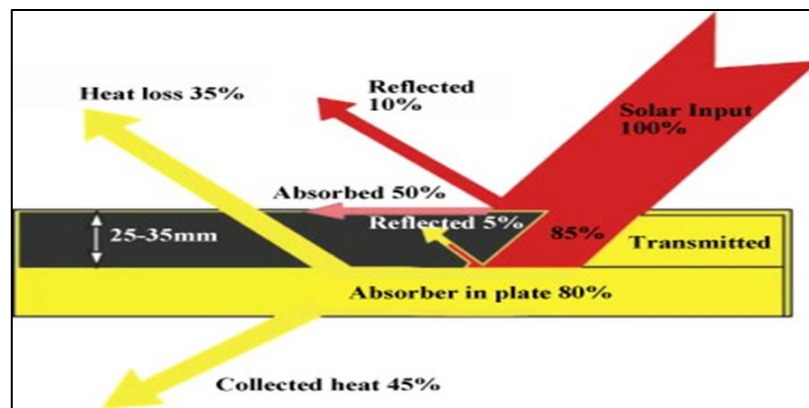


Fig.1.6: Solar irradiance distribution over the flat plate collector[web site].

1.6 Tilt angle for solar flat plate collector

The inclination angle of the flat sheet solar collector is a significant parameter where it is effective on the collector's performance, where both the amount of solar irradiance incidence on absorber plate and the coefficient of top heat loss is affected by variation in the tilt angle(Saraf and Hamad 1988)[5]. A theoretical analysis using three models to measure the optimal tilt angle at any time of the year and at any geographical position The study reveals the optimal inclination an angle for flat sheet solar collectors compute simply from the equation ($\beta_{opti} = \Theta - \delta$) and (β_{opti} is optimal tilt angle, Θ is the altitude of location and δ is declination, it is the function to latitude and declination, the values obtained should be corrected by add 10° (Stanciu and Stanciu 2014)[6].

1.7 Thermal transfer improvement methods

Thermal transfer improvement techniques have been mostly guided toward designing the procedure with standard conditions, in the scope of heat transfer research. More recently, too effective heat transfer devices requirements have led to greater concern with verification of mechanisms that increase or improve heat transfer(A. E. Bergles et al. 1970) [7]. Experimental research into such methods have reached the point of many of them can start to be considered earnestly for use in heat exchangers based on a mercantile principal. These

methods increase the rate of thermal transfer, but commonly at the outlay of extra pumping power, the external power supply to the system increased the cost also weight. Bergles and Morton perform the analysis and evaluation of these techniques(E. Bergles and Morton 1965) [8]. One of the problems is the assurance of general, usable chosen standards for the use of accroissement techniques, due to the big number of parameters interested in the problem of resolution. Numerous of these parameters are economical, including initial expenses, cost of repair and cost of evolution..etc. Heat transfer, enhanced mechanisms which are mostly divided into three groups: active methods, passive methods, and compound methods(Dewan et al. 2004)&(Yousif and Khudhair 2019)[9]&[4] as follows:

1.7.1 Effective Heat Transfer improvement methods

These mechanism are more complicate from layout and use, the method required for certain external power inputs produces the coveted flow amendment and enhancement of the rate of heat transfer due to a greater practical application potency for examples of active heat transfer methods as follows:

- I. Pulsation by Reciprocating plungers or cams
- II. Use of the magnetic field in the flowing stream to disturb the light particle seeded surface vibration and fluid vibration.
- III. Jet impingement.

1.7.2 Passive Heat Transfer improvement methods

Passive methods of thermal transfer increase do not demand any specific input of exterior power to improve heat transfer by taking additional power from the obtainable power in the device, that usually leads to a drop in pressure. The major precept of these methods for increasing the convection thermal rate which can be carried out through the following conceptions (E. Bergles and Morton 1965)[8]:

1. Reduce the thickness of the boundary layer.
2. Increment obstruction in the flowing of fluid
3. Improve the speed gradient near the wall of tube.

Passive methods have a cost problem in manufacturing such as ribbed tubes and finned tubes, or the cost of incorporating components such as wire coils, twisted tape, and helical wire, for examples of passive heat transfer methods:

- I. Treated surface (painting surfaces).
- II. Extended surface.
- III. Rougher surfaces.
- IV. Internally finned tube.
- V. Insertion devices

1.7.3 Compound Heat Transfer Augmentation Methods

This method is a mongrel technique that incorporates the passive and active ways, as these methods have limited application due to their complex design. Below are some forms of the compound method:

- I. Twisted tapes and a rough tube.
- II. Coarse tube with vibration.
- III. A magnetic field with fins.

1.8 Inside Twisted strips Insert Devices

Twisted tapes are the mineral or non-metallic ribbons for several adequate mechanisms in the necessary form and scale, inserted into the flow. The twisted strip inserts are commonly used in heat exchangers for enhancement rate of heat transfer, also twisted tapes improve rate of thermal transfer with lower friction effect for the power of pumping (Elshafei et al. 2008)[10]. However, for the fit is very floating, the ribs action and the swirl effect of fluid is waste. And maybe causing damage to the tube by being frequently struck by the tape. If the fit is

too tight it may be complicated to input the twisted strip into the pipe. The input of twisted strips into a pipe was a easy passive method to increase convection heat rate by swirling into the stream of fluid and shredding the thermal layer near the tube inner surface due to recurrent changes in surface geometry. That is to say, such strips generate disturbance and fabricated eddy motion which produces the weakly boundary layer and lead to better coefficient of heat transfer and best Nusselt number as result to change in twisted strips shaps(Liu and Sakr 2013) [11]. The pressure loss, however, increases across the tube fitting with twisted tape insert, therefore numerical and empirical reserches have been performed to examine the optimum geometry and design to obtain the better thermal efficiency for lower pressure drop.

1.8.1 Major groups of twisted tapes(Man, Wang, and Yao 2014)&(Yousif and Khudhair 2019) [12]&[4]

The most prevalent twisted tapes may be divided into the following groups as shown in fig. (1.7) describing different twisted tapes in geometry and form and used in different operating fluid and flow regimes:

- **Typical twisted tape:** that twisted tape has a an equal longitude of the heat exchanger tubes length as shown in fig.(1.8).
- **changging longitude, twist ratio, and alternate axes:** They vary from the first group in that they do not have the same twist ratio, the tape axes alternate in clock and counter, and the longest tape does not match the length of the heat exchanger tubes...
- **Numerous twisted strips:** more of one twisted tape insert into the tube.
- **Twisted tape with a rod and changing spacer:** helically twisted tapes with spacer and rod to improve the rate of heat transfer.
- **Twisted tapes with attached ribs and baffles:** twisted tape with baffles that connected to strips at some distances to produce more increment.

- **Twisted strips with crevices, holes, notches:** the twisted tape with different holes with diameters and pitch and with different slots.
- **helically left-right twisted strips with twist:** the twisted tape is manufactured in the left-right helical and some time with screw element.
- **Coiled wire with/without rod:** the wire coil with rode used to increase the swirl of fluid and produce enhancement coefficient of heat transfer
- **Twisted tapes inclusive wings:** Wing and winglet twisted tape attached to tape some time in different inclination angles to produce the vortex in the flow with swirl motion.

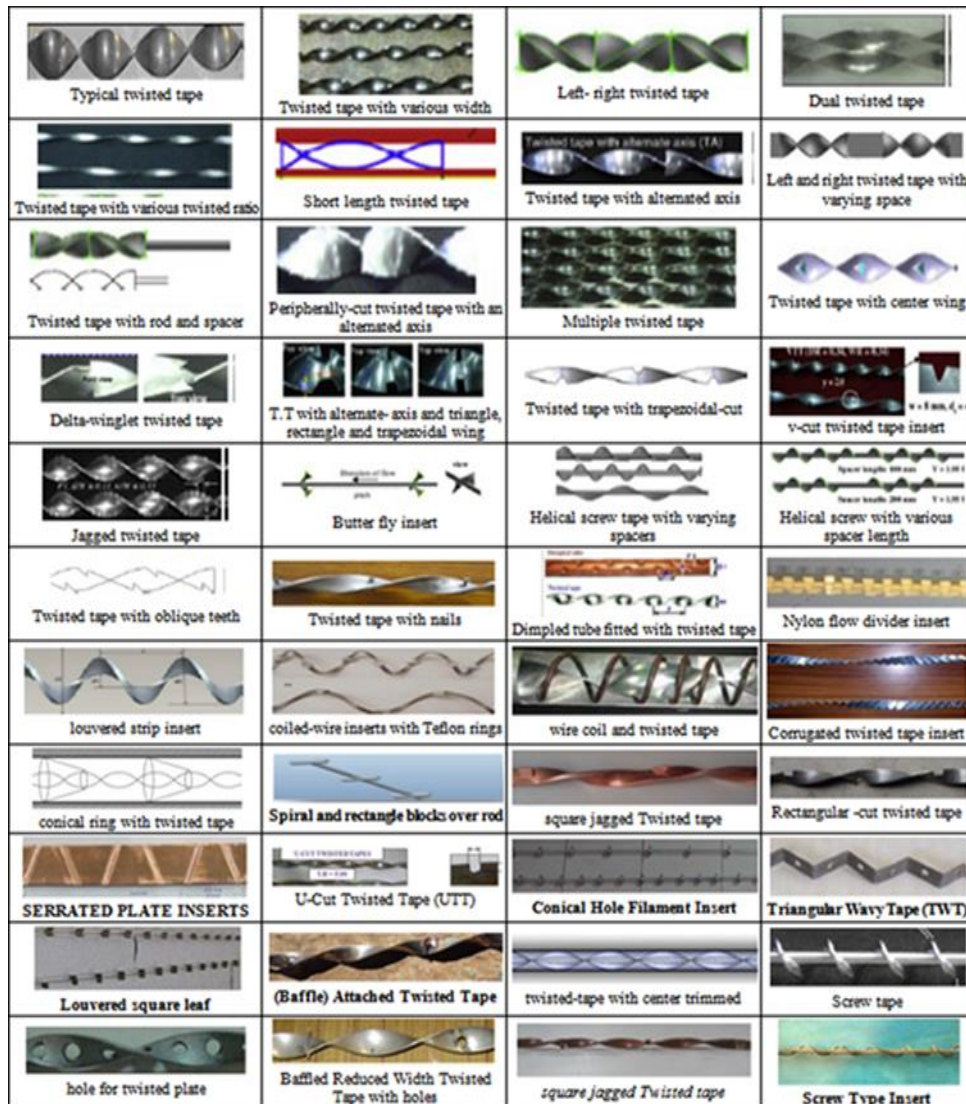


Fig. 1.7: The different categories of twisted tapes [4]

1.9 The goals of the experimental study

The major objective of that study is to promote an experimental research tool to investigate the flowing fluid-structure and the heat transfer characteristic of water in riser tubes for double glass covers flat plate solar collectors equipped with four different twisted tapes, the twisted tapes within front flow curvature vortex generators (TTFF), twisted tapes with opposite flow curvature vortex generators (TTOF), twisted tape with straight vortex generators(TTS)and typical twisted tapes(TT) under laminar flow, this study includes investigating the effect of four different types twisted tapes on the thermal rate in term number of Nusselt, friction parameter, and performance of solar collector, this goal are to achieve through several steps.

The first step involves design, manufacture and installation of the experimental test rig with all necessary instruments required to evaluate the augment in heat and measuring the conditions of the experiment such as (mass flow rate, solar irradiance, pressure difference). The second step is to evaluate the improvement in the rate of heat transfer for riser tube equipped with four types of twistedtapes and compare with plain tube and study, then developing a relationships to evaluate the Nusselt number (Nu), factor of friction (f).

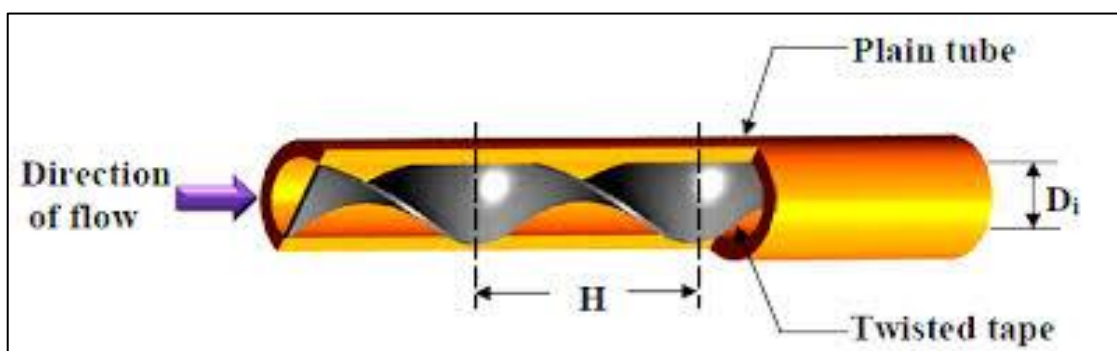


Fig. 1.8: Typical twisted tape insertion into tube

CHAPTER TWO

LITERATURE

SURVEY

Chapter Two

Literature survey

2.1 Introduction

With the required targets as shown in the previous chapter, literature survey progress was achieved by different twisted strip insertion in orbicular pipes in the field of thermal rate increase. To achieve a fruitful literature survey, it is recommended to ensure the historic sight, chosen heat transfer technique for a comprehension of the classification of different types of twisted tape that the research paper is more interested in internal forced convection. The literature in augmenting heat transfer is progressing rapidly, at least more than fifteen present of the heat transfer literature is guide toward the mechanisms of heat transfer enhancement now. A many of studies and experiments have been done in a heat transfer device through using different twisted strips inserts with a different working fluid, both experimentally and numerically. The very common techniques to improve the overall heat transfer coefficient are adding a fins for heat exchangers and use the twisted tape insert. A large number of experimental work has been conducted for this enhancement heat transfer technique of air-side heat transfer.

2.2 The laminar flow

Laminar flow, type of fluid (gas or liquid) flow in which the fluid travels smoothly or irregular paths, in contrast to turbulent flow, It is also of substantial practical importance to expect, generations of scientists have withstand valiantly to understood both the physical essence and the mathematical frame of turbulent fluid flow **Leonardo da Vinci in (1507)** termed the event observed in eddying flow “la turbolenza” (Ecke 2004)[13]. In general, thea systematic study

of turbulence had initialized with Osborne Reynolds' work in (1883). Reynolds had been studying the classic problem of flowing through long straight pipes and the annular cross-section has a constant diameter.

Using his "color band method," he was the first person to prove that the flow for velocities below a certain critical velocity will be orderly (laminar) for a given fluid and pipe. Reynolds found that the criteria for the transition from laminar to turbulent flow could be uniformly expressed in terms of the value assumed by the dimensionless group(Re) called Reynolds number.

2.3 Twist tapes as turbulence promoters

Twisted tapes are generally one of the passive techniques applied to increase heat transfer rate in thermal devices such as (heat exchanger, solar water heater, boiler... etc.), many researchers have conducted methods that are widely used to improve thermal performance, so in that chapter, describe the studies concerned with using twisted tapes to enhance heat transfer rate(Manglik and Bergles 2003)[14]. For measurement of the thermal performance factor or performance ratio that describes the increase in heat transfer over traditional thermal rate and this parameter also indicates the increase in heat rate. To benefit from previous studies converted by twisted tapes as passive ways to increase thermal efficiency, the classification of analyzes for previous studies as indicated below:

2.4 Effect of twist ratio

Experimental investigation study was conducted by(Zhang et al. 2019) [15], to examine the heat rate and friction factor features of the heat exchanger tube by experimenting insertion of self-twisted strips with various twist orders ($Y=2.2, 3, 4$ and 6) shown in fig.(2.1 a ,b) and comparison with stationary twisted tapes under turbulence flow ($12000 < Re < 45000$) heat

performance factor with pressure loss were found the increase with lessening twist ratio, maximum performance ratio of 1.03, 0.9444, 0.924, and 0.898 for to twist ratio $Y= 2.2, 3, 4$ and 6 respectively (Taylor, Patil, and Babu 2014) & (Vijaybabu 2012). [16] & [17] conducted an experimental study for square duct equipped for twisted strips of various twist ratio shown in fig. (2.2 a, b) to show the effect of rising and decreasing twist order on the heat transfer rate and friction factor under laminar flow ($100 < Re < 1200$).

The results displayed a slight increment in heat transfer rate in both the increase and decrease twist ratio. The (Nu) increased from 1.33 to 4.27 and from 0.9 to 3.46 times for increased and decreased twist order, compared to plain ducts. (Smith Eiamsa-ard, Wongcharee, and Promvonge 2012) [18] An experiential study was performed to state the effect of successional, frequently and intermittently twisted strips for increment detraction twist ratio. Results showed the average TPF in the repeated tapes that were tested for slowly decreasing twist ratios about 1.3.

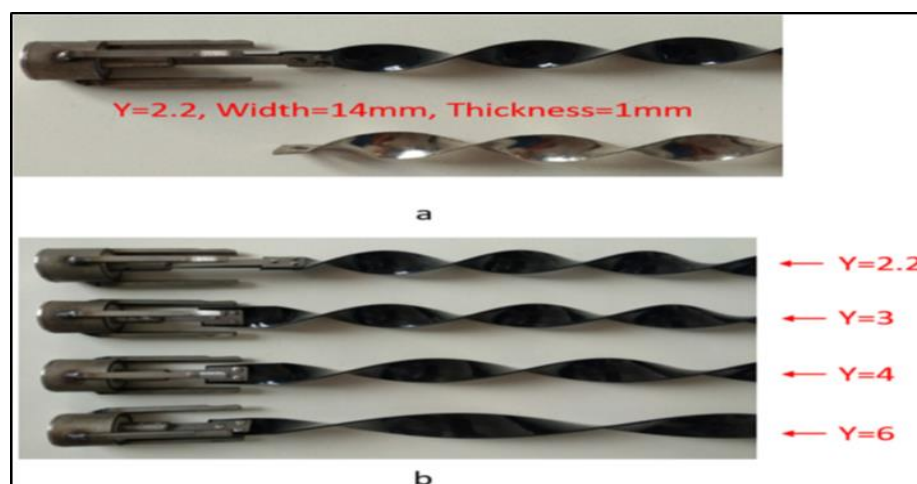


Fig. 2.1 :(a) SRTT and STT & (b) pictorial view of SRTT for different twist ratio [15].

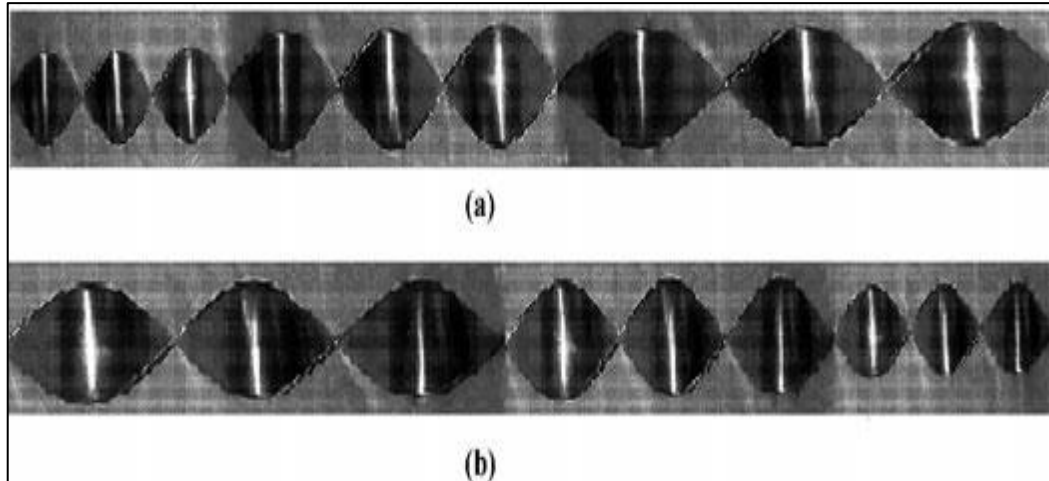


Fig. 2.2:(a) Twisted tape with increase twist ratio&(b)-with decrease twist ratio[16].

2.5 Effect of modulated twisted tape

The (CFD) investigations were conducted by (Rahimi, Reza, and Abdulaziz 2009) [19] for detect the effect of modified, twisted tapes on the heat transfer rate, pressure drop, this experiment performed using simply twisted strips as ruptured, cribriform and notched twisted strips. The results shown, the best TPF was about 1.21.

(Shabanian et al. 2011)[20] The CFD and experimental study aimed to inspect the impact of three different kinds of twisted strips insertion were conventional, butterfly, and shredded twisted stripe shown in fig(2.3) on improving air cooler heat transfer. The outcomes revealed the butterfly had alargest Nusselt number (Nu) with an increment in the(Re) compared to an jagged and classic twisted strips and and the TPF was changed between (1.2-1.62), (1-1.23) and (0.88-1.03) in butterfly, shredded and imitative twisted tapes respectively. (Sheikholeslami, Li, and Moradi 2018)[21] CFD simulation analysis to show the effect of twisted tapes has an alternative axis shown in fig. (2.4) on the heat transfer and revolution angle and Reynolds Re, the results showed that temperature gradient rises with an increment in revolution angle

because of excess in secondary flow but an accretion in pressure falling at increment in revolution angle. The CFD research in this review indicated that at insert twisted tape of alternative pivot improved the thermal performance and increasing an angle of revolution (β) lead to higher temperature difference.

(Murugan et al. 2019)[22] An experiential survey performed using four different twisted tapes, including central pins finned (CFTT) convolute strips and typical twisted strips (TT) at two various twist order ($Y=3&6$) to show the effect of these twisted tapes on the performance of solar collector of flat plate .For same twist ratio, the experimental result for(CFTT) with minimum twist ratio ($Y=3$) gave the highest thermal efficiency of 11.08 % compared to (TT).

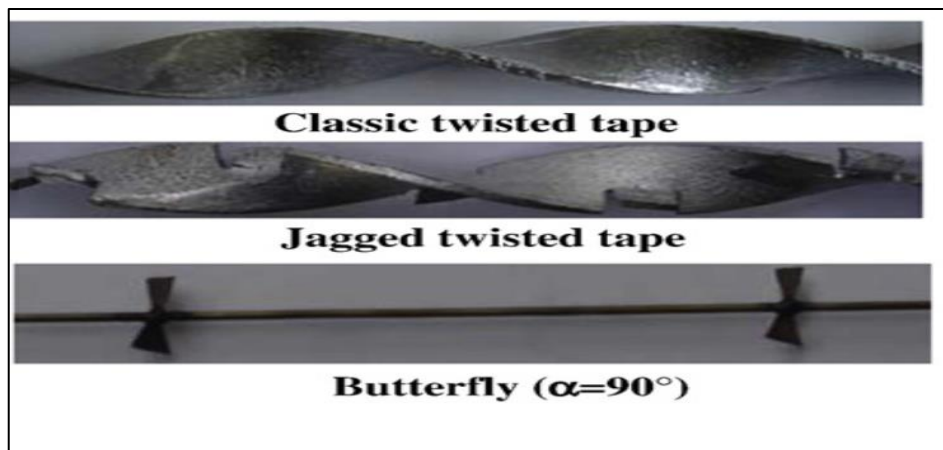


Fig. 2.3: Three different twisted tapes[20].

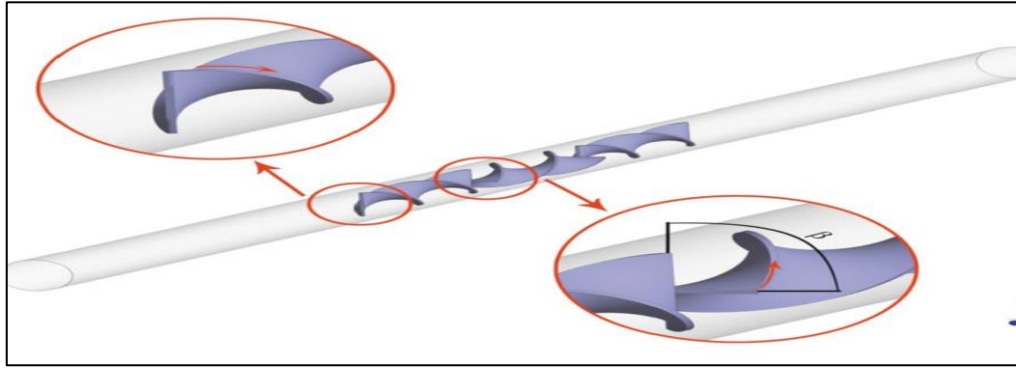


Fig. 2.4: Twisted tapes with an alternate axis [21].

2.6 Effect of helical strips

The helical configuration insert has a large action on thermal rate also friction factor. (Sivashanmugam and Nagarajan 2007)&(Sivashanmugam and Suresh 2007)[23]&[24] Experimental studies were conducted using the helical spacer length and full length with different twisted ratio shown in fig. (2.5) with unequal and equal length with a right to left twist. The results of the tests appeared promote the heat rate over to a smooth a maximum TPF of up to 3 could be obtained.

Experimental work was done on the thermal rate and friction effect features of elliptic tubes equipped by multiple helically strips [25], for laminar flow twist ratio $Y=0.22$ and pitch ratio $S=1$, the outcomes showed the spiral screw elements at specific twist ratio (y) and pitch ratio (S) have an influence on the heat transfer rate and pressure drop, for maximum TPF was 1.2. The influence of multiple helical tapes at different helix angles (9° , 13° , 17° and 21°) for turbulent flow was achieved by (Bhuiya et al. 2012)[26], the reduction in the helix angle with ($22000 < Re < 51000$), the power of blower increased from 2 to 3 times and the TPF improved from 1.08 to 1.30.

A (CFD) survey conducted by (El et al. 2017) [27] to research the output of heat exchangers with double pipes fitted with helical baffles inserted in the

annual side, the baffle spacing values was (0.025–0.1 m), the analysis results were found because of large pressure falling in entry part the TPF in all cases was less than one compared to the simple double-pipe exchangers.

An analysis of three dimensions of the CFD was conducted by(K. Ahmed et al. 2019) [28] for annular channel consideration, used wire warped helical insert with a 1.92 twist ratio for single-phase and Re ($200 < Re < 2300$). The outcomes of the simulation revealed the Nusselt number and the friction effect raised from 1.34 to 2.6 also from 3.5 to 8 times respectively, for wire-wrapped tube compared to a plain tube, the thermal performance ratio $TPF= 3.79$.

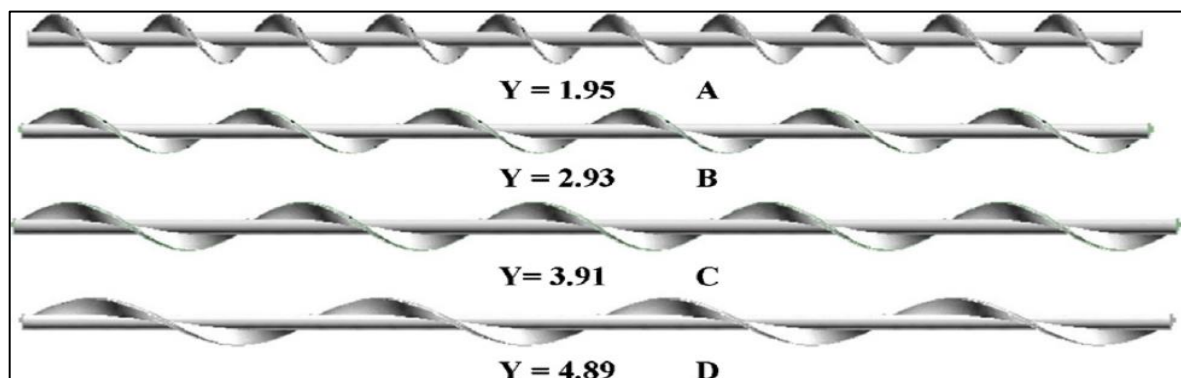


Fig. 2.5: Spril device inserts with various twist orders [24].

2.7 Effect of twisted tapes dimensions

An experimental study, conducted by(Saha, Dutta, and Dhal 2001) [29] the author used regular splay twisted strips with different widths and rod diameters and different twist ratio with space ratio to study an action of regular spaced involuted tape for laminar regime and constant heat flux characteristic at the test section, . The outcoms showed the reduction of twisted tapes width lead to low thermal rate for increased of phase angle more than zero created complexity in tape manufacture more than increased heat transfer.

(Smith Eiamsa-ard, Thianpong, and Promvongse 2006) [30] experimental analysis of the thermal rate and action of friction effects normal twisted tapes with diverse twisted ratios ($y=6$ and 8) for regular spaced twisted tapes of different distance ratios ($S=1, 2$ and 3) for two convolute strips at thickness= 0.001m with longitude of 1.5 m , An outcomes indicated for increase of the open distance rate with reduction of the twist rate lead to increase of thermal rate.

(Smith Eiamsa-ard et al. 2009)[31] was investigated an effect of both short-length and the full length of twisted strips insert in to circular pipe under constance heat flux for fixed twisted ratio. The experimental results showed for shortend strips at $R = 0.3, 0.4$ and 0.6 show least heat flow and friction factor, the maximum TPF of $Re= 4000$ was 1.04 . An influence width for twisted strip was investigated by (Sarada et al. 2010)[32] plain tube experiments with/without convolute tape for various mass flow rates for constant heat flux, and twisted tapes at five varied width shown in fig. (2.6). The conclusions revealed the width for the torsion tape had a powerful effect in the heat rate, the heat increase was observed as the width increased.

Experimental research performed by(Esmaeilzadeh et al. 2014)[33] to investigate the thermal flow rate and effect of friction featuers for annular tubes equipped for different thicknesses of torsion tapes for same twist ratio of $Y=3.21$ and conestance heat, the tests were performed with the laminar order ($160 < Re < 1600$) for twist tapes thickness was adjusted by three values ($1/2, 1$ and 2) milimeter. An experimental results indicated that the nanofluid has the best heat transfer rate with higher tape thickness and increased friction factor with increased twisted tape thickness. Finally, the increased thickness of the twisted tape contributes to increased thermal rate and efficiency.

(Piriyarungrod et al. 2015)[34] showed a twisted tape inserts influence with four different taper angles 0.3° , 0.6° , and 0.9° as shown in fig. (2.8). All twisted tapes were tested at each taper angle under turbulent flow regime ($6000 < Re < 20000$), the experimental results has confront for a smooth pipe and indicated the heat rate improved and pressure loss increment for detracton angle of taper and torsion rate. Increased thermal efficiency with rising angle of taper and lessening the twist proportion. the best TPF of 1.05 was achieved with twisted tape at angle of taper (almost) of 0.9° and twist ratio of $Y=3.5$ yielded at $Re = 6000$.



Fig. 2.6: Twisted tapes in five different twisted ratios and width [32].

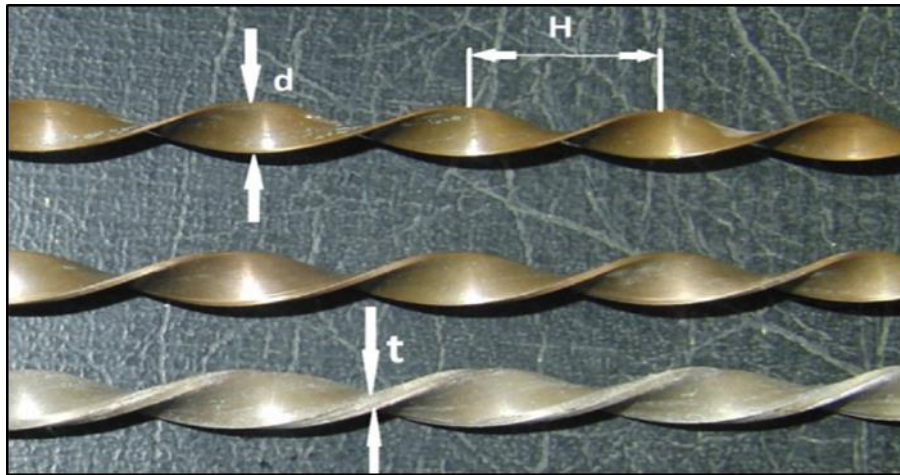


Fig. 2.7: Schematic layout of different thickness twisted tapes [33].

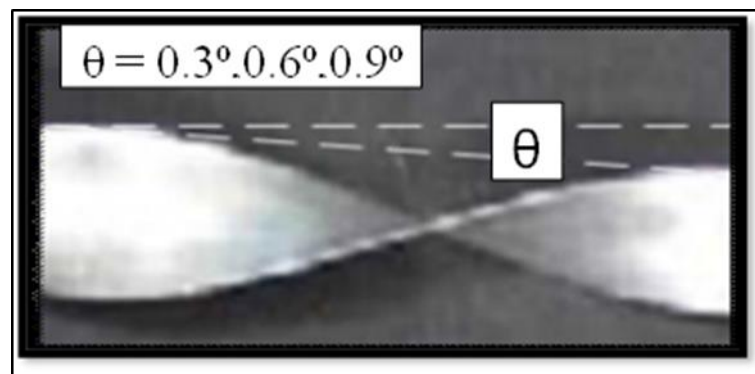


Fig. 2.8: Taper twisted tape with different taper angles (Θ) [34].

2.8 Effect of multiple twisted tapes

Some experimental work was done using multiple convolute strips instead having a changes for a convolute tapes. (Smith Eiamsa-ard et al. 2010)[35] the experiment study to improve thermal rate was carried out by insertion of three various types of convolute strips with fixed torsion strip, orderly - diverged dual and entire lengths torsion strips in circular heat exchanger tubes. , torsion strips entire length at three different twisted rates (3,4 and 5) for spaced regular convolute strips at three diverse spacing rates ($s/d = 0.742, 1.48$ and 2.24), that investigation involved a turbulent flow regime under the Re at a range from

4000 to 19000 with a stationary wall thermal flowrate. The results for the experiments showed the thermal rate for pipe fitted with the convolute strips was largest than smooth pipe with or without single convolute tapes, the Nusselt number and pressure loss for singular and full-length double convolute strips rised for lower twisted ratio and the thermal rate of regular twisted tapes decreased with higher space ratio, the regular- spaced dual twisted tape also delivered lower heat transfer rates than full-length dual twisted tape.

An experimental research was conducted by by (Eiamsa-Ard and Wongcharee 2013) [36] to study the effect of the pressure drop, heat transfer, and thermal efficiency parameter for double torsion strips put in to a micro-fine pipes, the convolute tapes are shown in fig. (2.9) were the twisted tapes inserted in different configuration arrangements, the opposite direction for counter-double twisted tape, and micro-fin pipes include single convolute strips in parallel and opposite arranging for comparison, the tests were performed at turbulence flow the numbers of Reynolds range from $5650 < Re < 17\ 000$. An empirical outcome indicates the convolute strips created stronger swirl/turbulence flow in opposite directions for counter swirls, The outcome displayed for a double inverse twisted strips with twisted ratio 3 the TPF was more than one

.An Influence of inserting triple convolute strips on thermal rate, thermal performance, also pressure loss was achieved by (Bhuiya, Chowdhury, Shahabuddin, et al. 2013) [37] for the turbulence flow for Re range of 7200 until 50200, for mild steel triple convolute tapes appears in fig. (2.10) at four different twisted ratios (1.87, 2.78, 4.88 and 6.87), were used. The results concluded that the Nusselt number and friction factor for utilize the triple twisted tapes inserts was rised for 3.87 and 4.33 times respectively, and largest thermal rate comparison with smooth tube, the performance was be 1.44. New twisted tape geometry architecture used in the study of numerical simulation

was presented by (Li et al. 2015) [38] named central hollow narrow twisted tape to detect an influence for tube under laminar regime on the enhancement of thermal flow and thermal efficiency. Two variable parameters were studied which were hollow width and clearance and then the concept of a unilateral twisted tap was compacted as shown in fig. (2.11). The results appeared that the gross heat transfer performance for tube contain a cross hollow torsion strips inserts is better with different hollow widths compared to conventional convolute strips., the new form of twisted tape increases overall heat transfer performance by around 28.1%.

(Promvong 2015)[39] was an experiment presenting research to detect the action of the increase in thermal rate under a turbulent regime of the combined insertion of 30° V-fins and quadruple counter-twisted tape in a square duct, for ($4000 < Re < 30000$) and the uniform heat flux, the V-fin counter twisted tapes obtained by inserting V-fins inside the brims of fourfold convolute strips for constant convolute proportion of $Y=4$, furthermore the effect of relevant V-fin parameters such as four R_B (0.16,0.21,0.32 and 0.42) fin height ratio and four R_P the pitch ratio (4,8,12 and 16) was tested. The outcomes of the tests showed the increased fin height ratio R_B on the V-fin counter, convolute strip increased the number of Nusselt Nu and friction action, but reversed action for an increased pitch ratio R_P . thermal performance for the v-finned converse - convolute strip was larger than of the single quaternary torsion tapes also the maximum $TPF=1.75$.

The experimental research work carried out by (Vashistha, Patil, and Kumar 2016) [40] in that study, several twisted tapes put in to a annular pipes were used to research the impacts of heat rate and frection effect, multiple twisted tape inserts for single, twin and four convolute strips arranged in a co-eddy and converse-eddy tendency and for three different torsion rates (2.5 ,3 and 3.5)

shown in figure (2.12) with turbulence flow regime number of Reynolds range from 4000 to 14000. For single, twin, and four convolute strip inserts, the empirical conclusions showed the thermal rate improved by using redoubled convolute strips with a torsion prportion of 2.5 for synchronous raised in friction factor comparsion with the plain pipe. Increases in thermal rate also pressure loss has the values of 2.3 and 6.8 times respectively over a plain pipe and 1.26 for twist ratio 2.5 is found to be the best thermal performance factor for a group of four twisted converse eddy strips. (Kumar et al. 2019)[41] the numerical analysis study showed the influence of two convolute strips in counter-swirl and co-swirl arrangements on thermal flow enhancement and pressure drop, simulation of laminar regime conditions under number of Reynolds ranging of (1000 - 2000). The outcoms showed that to the smooth tube the thermal efficiency of annular pipe fitted with two strips would be rise.

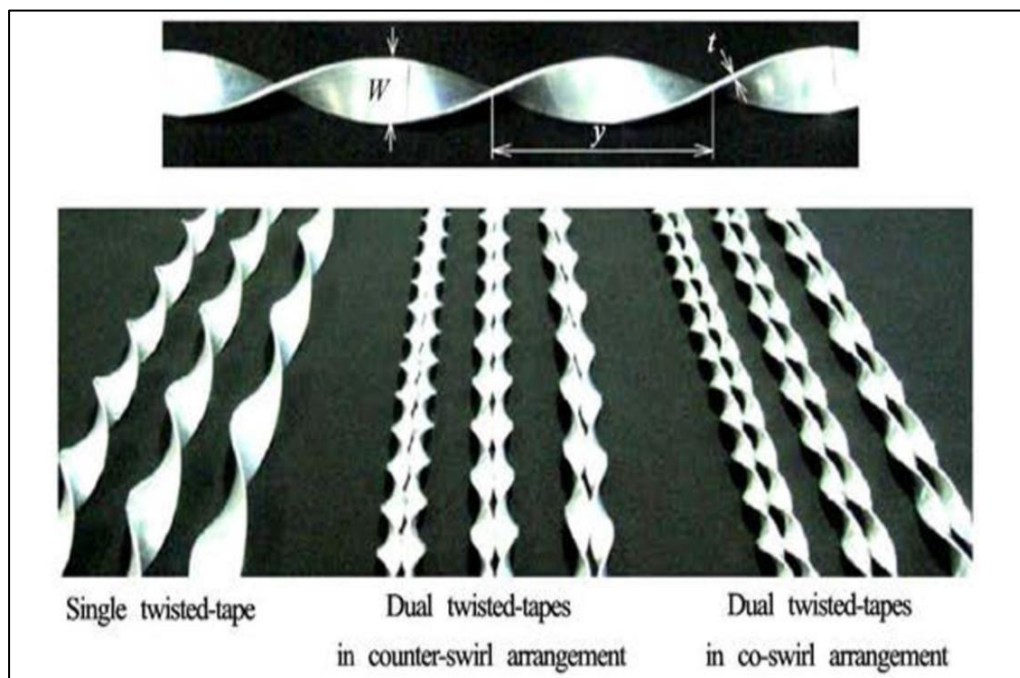


Fig. 2.9: The counter coupling, co-coupling and single twisted tapes [36]

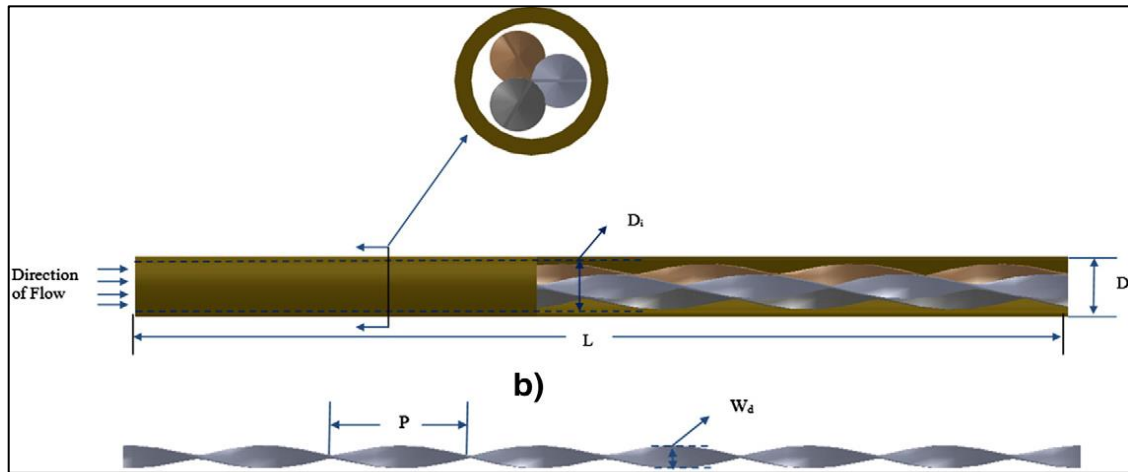


Fig. 2.10: Triple twisted tapes with four different twist ratios [37].

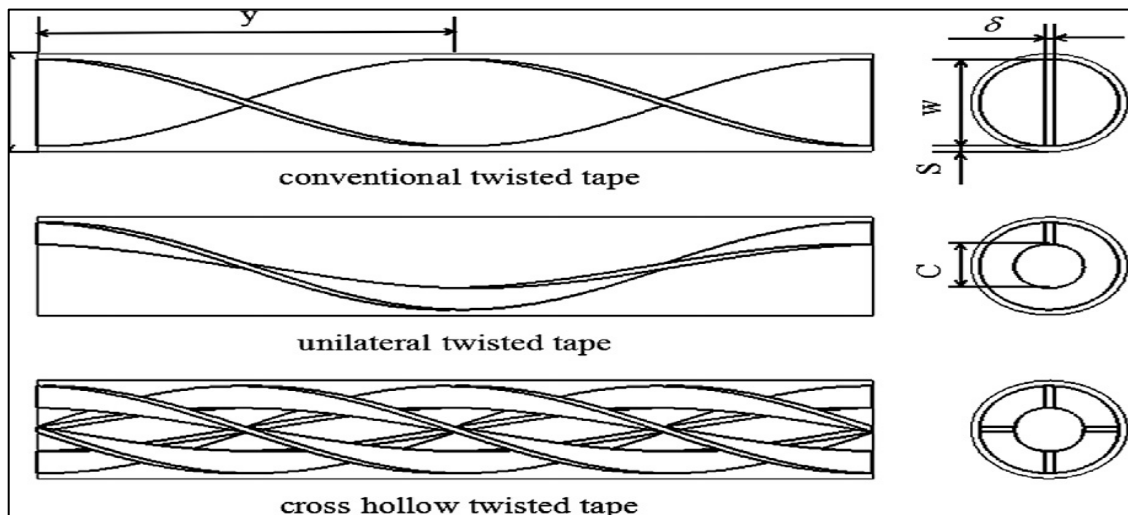


Fig. 2.11: Typical, unilateral and cross hollow twisted tapes [38].

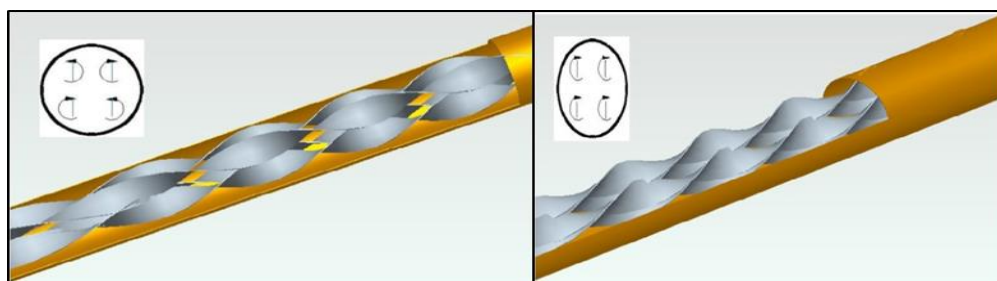


Fig. 2.12: The annular pipe fitted with co / counter swirl convolute strips [40].

2.9 Effect of the wire coil

The experimental studies were performed by (Gunes, Ozceyhan, and Buyukalaca 2010a), (Gunes, Ozceyhan, and Buyukalaca 2010b) and (Gunes et al. 2011) [42],[43] and [44] to investigate the effect on heat transfer, pressure drop, and the performance ratio for the wire coil insert. (Gunes, Ozceyhan, and Buyukalaca 2010a) [42] used wire coil has an equilateral triangular cross-section for three various pitch rates ($p/\text{dia} = 1, 2 \text{ and } 3$), the inserted wire coil distanced away from the pipe wall at a distance of 1 mm at two different ratio ($a / \text{dia} = 0.0734, 0.0887$), the experiments performed for ($3500 < \text{Re} < 27000$) the working fluid was air. The data of the test indicated that the wire coil insert increased the heat transfer rate and friction effect comparison to the plain tubes. Wire coil insert yielded the best 36.5 % enhancement performance.

(Gunes, Ozceyhan, and Buyukalaca 2010b) [43] An empirical work to investigate the heat rate and friction action in tubes fitted with wire coil inserts distanced from the pipe wall at two various spaces (1 and 2) mm for a stationary thickness of wire at 0.006 m with three pitch ratio p / dia (1, 2 and 3) under turbulent flow with Re from 4105 to 26,400 and constant wall heat flux. The experiment results were collected and compared with the smooth pipe, the maximum total improvement performance was fifty percent was accomplished with the wire coiled at $P/\text{dia} = 1$, space = 1 mm at $\text{Re} = 4220$.

(Gunes et al. 2011) [44] an experimental study carried out the definition of the best amounts of layout parameters in tubes for wire coil with equilateral triangle cross-section, the effect of design factors like the pitch ratio (P / D), the ratio of the triangle side length to pipe diameter (L / dia), the ratio of the space between the coil wire and the pipe wall to the pipe size (s / dia), and the number of Reynolds (Re) were checked for thermal rate and friction factor, the higher thermal rate and maximum thermal efficiency and minimum pressure

drop that was obtained with $s / d_{ai} = 0.0349$, $pitch / d_{ai} = 1$ and $a / d_{ia} = 0.0744$, for $Re = 20000$. (García et al. 2012) [45] the study introduced an experimental review, presenting a comparison between three artificial heat transfer improvement mechanisms. The distinction was made from the three best samples selected from the large variety of geometries investigated. This test was achieved with three systems of flow: laminar, transitional, and turbulence regimes. The result found the wire coil more effective over artificial roughness surfaces for laminar flow ($200 < Re < 2000$), but for (Re) greater than 2000, the utilize of dimpled and corrugated pipes was preferred due to the minimize loss of pressure at equivalent heat rate.

(Selvam, Thiyagarajan, and Suresh 2012)[46] the experimental work used three different bonding wire coils with three different 0.005m, 0.01m, and 0.015 m pitch ratios and without sticking to the pipe wall as shown in the fig. (2.13). The results showed that the thermal flow increases with reduction the pitch of the wire coil and coil matrix tabulator with sticking and that the best enhancement ratio for the 5 mm pitch coil wire with boding was 42 %.(Rout and Saha 2014) [47] An empirical analyses of thermal flow and falling of pressure for a circular pipe fitted with two heat-enhanced techniques; coil wire and helical screw at constant heat flux with laminar regime. The combination of wire-coil and sprial screw strips inserts accomplish the best for the individual improvement mechanism behaving alone.

(Suresh 2012)[48] An empirical study was conducted to detect the influence of wire coiled-coil matrix tabulators with different pitch (P) to diameter (D) ratios(0,23,0,45 and 0,68) to research the impact of coiled wire bonding with turbulent flow and constant wall temperature. The collected data of the tests were comparsion with a smooth tube for all the tapes revealing a large thermal rate and factor of friction over the empty pipe, the best enhancement

ratio was 42 %. An experimental work was conducted by (Martínez et al. 2014)[49], the thermohydraulic behavior of a annular pipe equipped with two different wire coils with various pitch rates (pitch /dia= 1 , 2) was characterized by the use of both Newton and non- Newton fluids for laminar and transitional regimes. The empirical data were obtained comparison with the smooth tube and results shown for up to $Re = 500$ were normally ignored for the impact of the wire coil insert for non-Newton fluid with minimum number of Reynolds, that head to the coild wire insert is not a reasonable choice to increment the thermal rate with non-Newton fluid.

(San, Huang, and Chen 2015) [50] An empirical reserch was achieved to examine the action of the insertion of wire coils into a annular pipe on thermal rate and the association of fluid friction with air and water as working fluids. Used coil insert with coil diameter to pipe inner size ratio (e / dia) vary from 0.0712 to 0.128, and pitch of wire coil to pipe inner size($pitch / dia$) vary from 1.304 to 2.319, the test data showed that the Nusselt number enhanced for increase the ratio (e / dia) and the pitch to the inner size rate ($pitch / dia$) of the pipe decreased, the efficient heat transfer improvement was achieved with the ratios for air working fluid e / D and p / D being 0.101 and 2.319 respectively, and 0.101 and 1.739 for water as test fluid.

(Roy and Saha 2015) [51] examined the impact of two inserting devices on the thermal rate and factor of friction for laminar flow in the circular channel, coiled wire and helically screw strip are used in the experiment work, the experimental results showed that the Nusselt number and friction factor for spiral screw tapes and wire coils increased. A numerical study conducted by (Feng et al. 2017) [52] characterizes the thermohydraulic activity of the rectangle cross – section small channel thermal basin fitted with coiled wire insert for water as test fluid under laminar flow and stasionary wall thermal flow. the result

indicated thermal flow and pressure falling increased because of the longitudinal eddies due to intercalation of coiled wire into microchannels. The maximum performance factor changed to $400\text{W} / \text{m}^2$ from 1.4 to 1.8 and the results showed the best thermal performance for wire coil inserts achieved at low Reynolds number.

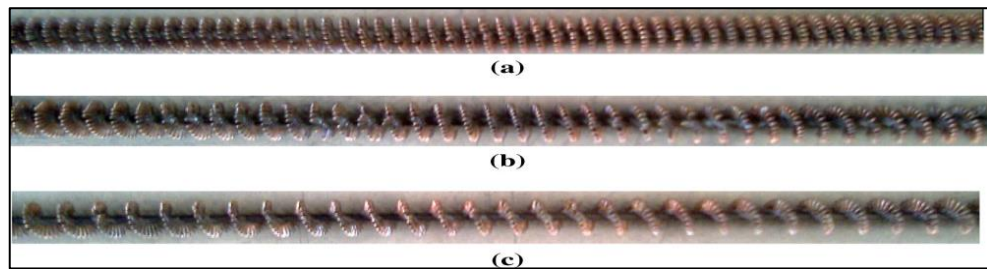


Fig. 2.13: Wire coil with three different pitch ratio Coiled Wire template Coil tabulator of pitch: (a) 5mm (b) 10mm (c) 15mm [46].

2.10 Effect the perforation

An investigation of an experiment carried out by (S. Ahmed 2013)[53] used a twisted tape with holes at different diameters for $1300 < \text{Re} < 5200$. The results showed the heat transfer and friction effect compare to plain tube enhanced., the best heat rate was 4.6%. (C. T. P. Eiamsa-ard and Eiamsa-ard 2012)[54] experimental work carried out in uniform heat flux condition and with perforated twisted tape at $l/m = 2.9, 3.9$ and 4.9 , $\text{dia}/m = 0.13, 0.15$ and 0.18 , also $\text{pitch}/m = 0.4, 0.6$ and 0.8 as shown in fig. (2.14). experiment data showed the rate of heat increased in with decreased both (pitch/m) and (l/m) for increased (dia/m) over plain tube. The beter transfer of heat around 28.2% and 89%, with respect to the pipe with normal convolute strip and plain tube respectively that yielded Compared to the typical torsion strips and smooth tube, the best transfer reat of heat was 27.4 % and 86.7 % respectively for perforated

twisted tape at pitch / $m = 0.5$, $\text{dia}/m = 0.18$, and $1/m = 2.9$. (Thianpong et al. 2012)[55] experimentally investigate was presented Research on thermal flow and falling of pressure advantages of a circular pipe fitted for punched parallel wing torsion strips (PTT) shown in the fig. (2.15) for turbulent flow regime in the Re at range of 5500 to 20500 and constant heat flux. The study tested perforated twisted tapes (PTT) with three different punch size ratios ($\text{dia}/m = 0.12$, 0.29 and 0.49) at three different depth of wing ratios (d/m 0.1 , 0.2 and 0.3), and a normal torsion strip (TT). An experimental data showed up to 208 %, and 190 % increased the transfer of heat rate for pipes equipped with (PTT) and (TT) for $\text{Re} = 5500$ respectively, and the maximum TPF was 1.32 for tubes fitted with (PTT).

(Bhuiya, Chowdhury, Saha, et al. 2013)[56] an experimental work was presented to study the impact of twisted punched strips at four various porosities (R_p) on transfer of heat, drop in pressure and performance ratio (TPF). The experiments were conducted with $R_p = 1.6$, 4.5 , 8.9 , and 14.7 % perforated twisted tapes for turbulence regime for Re in 7000 to 50000 utilized air as the working fluid for stable flux of thermal. The empirical data showed that the thermal transfer, as well as the pipe friction factor fitted with perforated convolute strips, were larger than of plain tube. The tube equipped with perforated twisted tubes had a number of Nusselt, a factor of friction, and a heat performance ratio of 110 % to 340 %, from 110 % to 360 % and from 28 % to 59 % over a plain tube respectively.

(Nanan et al. 2014)[57] perforated helical twisted tape (H-PTT) was used in experimental investigation research appear in fig. (2.16) to study the performance of thermal and the pressure loss effect. The experiment was conducted using (H-PTT) for three diverse diameter rates (dia/w) (0.22 , 0.41 and 0.59 for three various perforations pitch ratios (pitch/w) of 1.1 , 1.4

and 2 to insertion, and fixed the helical pitch proportions ($\text{pitch}/\text{dia} = 2$) and the twist ratio ($Y = 3$) for the turbulent flow regime, the Re varies between 6000 and 20 000 under constant heat flux. The outcomes revealed that the insertion of perforate torsion strips into the tube cause to reduction in pressure falling compared to that of spiral strips, in addition to rise in transfer of heat, and performance ratio of thermal at pitch/w increases for dia/w decrease, the higher TPF yielded by perforate spiral strip with $\text{dia}/w = 0.21$ and $\text{pitch}/w = 2.1$ was found to 1.28 at $Re = 6000$.

(Skullong et al. 2016)[58] experimental research has been carried out to characterize the thermohydraulic activity of a annular pipe provided with staggered-winglet perforated strips (wpt) shown in fig. (2.17) for stable thermal flow and the number of Reynolds range $Re = 4100$ to 26000 for turbulent flow regime. The goal of utilize the (wpt) was for generate a linear eddies flow for increase disturbance of the boundary layer near the wall of pipe and to achieve a efficient blending of fluids. The tube under test fitted with (wpt) has angle of wing of 30° at three wing pitch proportions ($pr = 0.5, 1.1$ and 1.6) for five separate wing blocking rates ($br = 0.11, 0.13, 0.22, 0.24$ and 0.31). The test data revealed an increase in the (Nu) number of Nusselt, friction impact, and TPF in pipe fitted with (wpt) for reduction of pr and br the best performance ratio was found to yield 1.75 in tubes fitted with WPT has $br = 0.14, pr = 1.1$ with number of Reynolds $Re = 4180$ comparison with normal non-punched staggered-winglet (WTT) tapes.

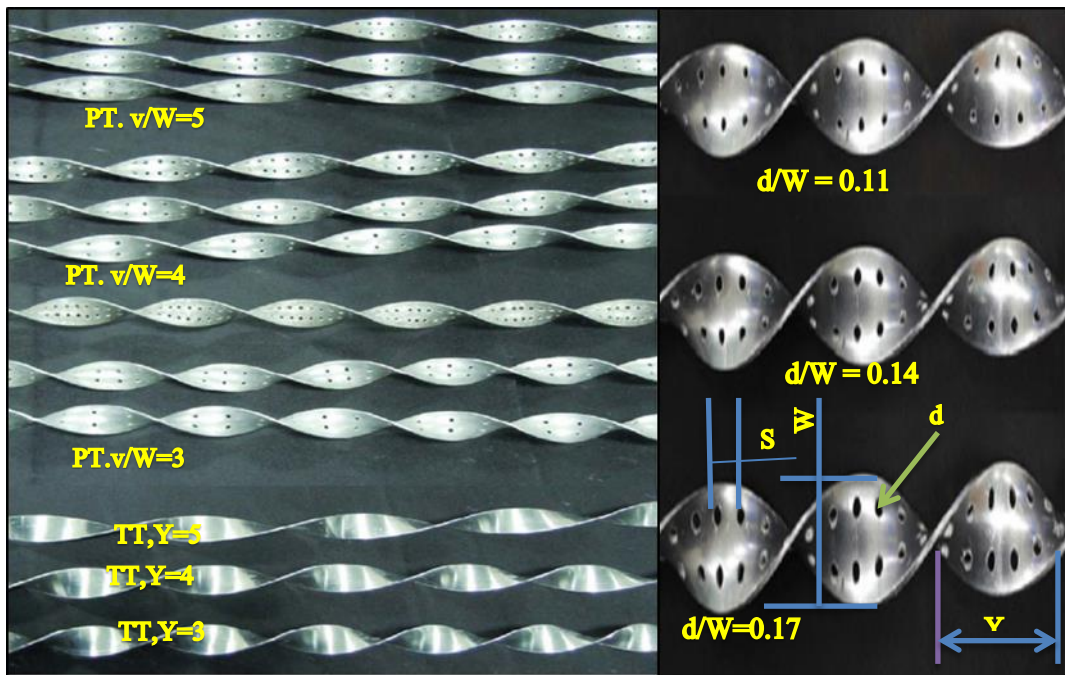


Fig. 2.14: Perforated torsion strip with punches in diverse size [54].

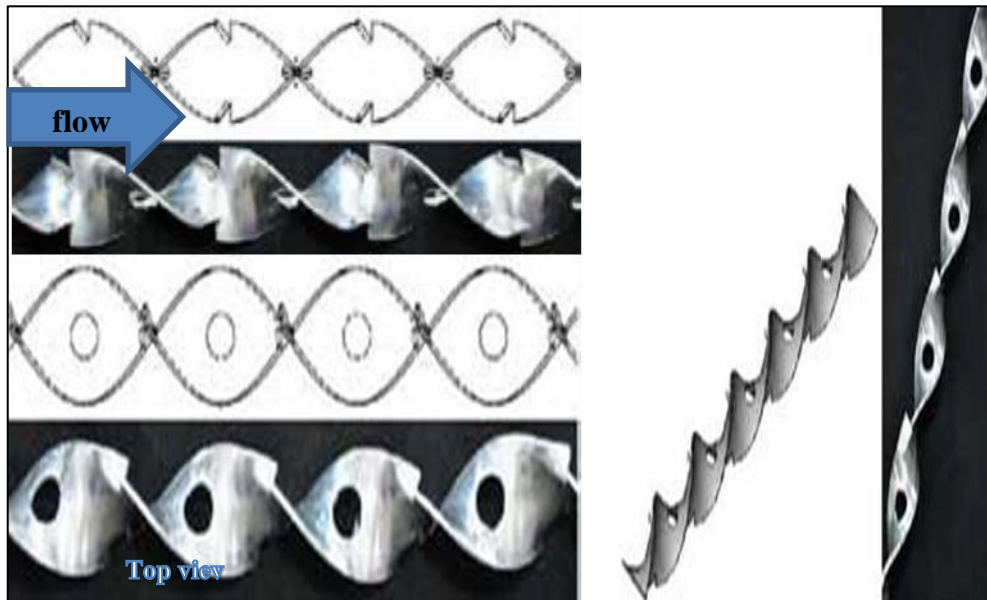


Fig. 2.15: Punched convolute strip with wings in parallel array (PTT)[55].

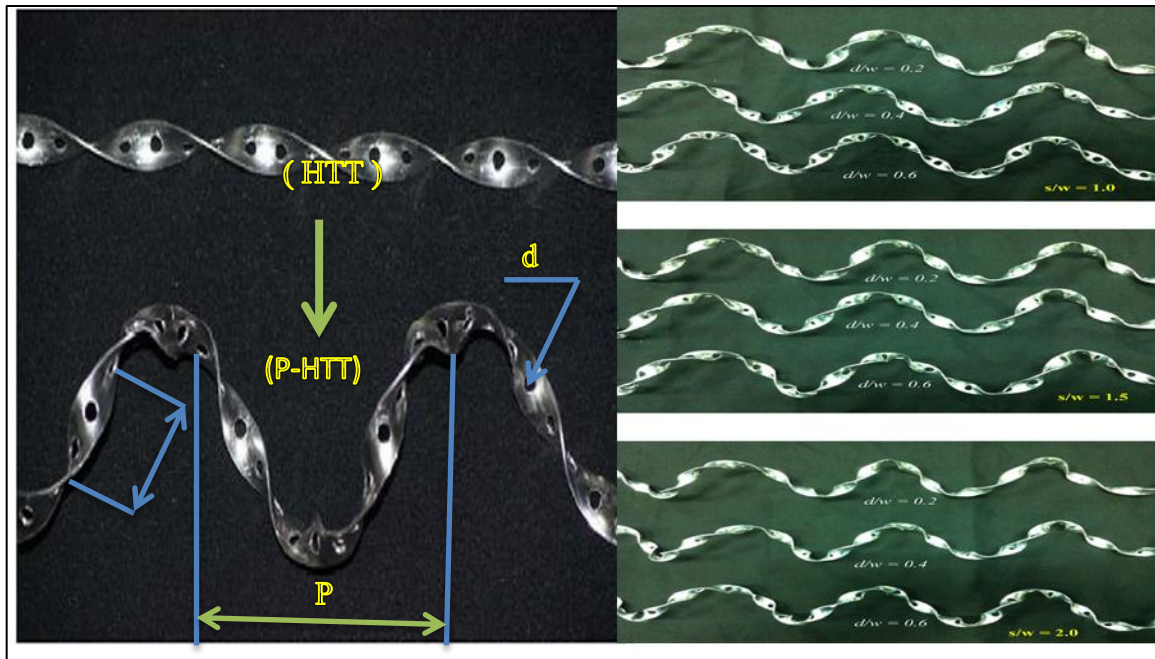


Fig. 2.16: Perforate-helical twisted tapes (P-HTT) [57].

2.11 Effect of winglet twisted tape

Experimental research was undertaken by (S Eiamsa-ard et al. 2010a)[59] to detect the influence on thermal flow, pressure drop, and the performance ratio of winglet convolute strips put in to the pipe. An experiment was performed using two types of twisted winglet tape: incline-triangle convolute wings strips with upright-triangle twisted wings strips shown in fig. (2.18) for three diverse twist proportions ($\gamma=3.0, 4.0$ and 5.0) at three diverse cut rates of wing depth ($d_r = \text{dia} / w = 0.12, 0.23$ and 0.34), for turbulent flow and uniform heat flux, water utilized as test fluid with number of Reynolds range of 3000 to 27000. The results of the experiment reveal the number of Nusselt (Nu), effect of friction and performance ratio (TPF) rised for increment the depth of wing cut ratio (d_r) and decrease twist tape rate (γ), also the incline-triangle wings strip more efficient than upright- triangle strips wings was indicated to enhance the thermal flow. The Nusselt number, the performance ratio and the drop of

pressure in tube fitted with incline-triangle strip were found 1.02–1.7, 1.04–1.13 and 1.08–1.87 times over the normal convolute tapes. (S Eiamsa-ard et al. 2010b) [60] an empirical survey was achieved to characterize the thermohydraulic activity in tubes equipped with convolute strips with wings at center for alternate-pivots (WT-A) shown in fig. (2.19), the Reynolds number from $5200 < Re < 22000$. The experiment used four types of convolute strips at constant twist ratio ($y / d=3$) that involved: (1) the convolute strip for alternating axes alone (T-A), (2) the convolute strip at wings alone (WT) also (3) the normal convolute tapes (TT) to compare with (WT-A), the wings attached to the centerline of tapes at three different attach Angles ($\beta = 43^\circ, 53^\circ$ and 74°).

Results showed that the thermal flow rate, thermal performance ratio and friction effect at tubes equipped with (WT-A) were largest than that in tubes fitted with WT, T-A and plain tubes and the best thermal performance factor was found 1.4 in a tube fitted with (WT-A) with attached angle ($\beta=74^\circ$). The notable efficiency of the (WT-A) over those of the other twisted tape because it requires three combinations as in the below steps: (1) a normal eddy flow by torsion tapes, (2) wings that exist as vortex generators and (3) a heavy disturbance of streams due to alternative axes. (Wongcharee and Eiamsa-ard 2011)[61] an empirical search was carried out to illustrate the effect on thermal rate, drop of pressure, and the efficiency ratio of convolute alternate-axis strips with wings, at rectangle, triangle and trapezoid shapes. Twisted tape for three various Wing shapes was used for the experiments; rectangle, trapezoid, and triangle, for three diverse wings-tendon rates (dia/w) of 0.11, 0.21 and 0.32 at a fixed torsion ratio of $Y = 4$ for the angle $\beta = 60^\circ$.

The best TPF of 1.42 was yielded in tubes fitted with convolute strip include alternate pivots and wings at trapezoid shape at $dia/w = 0.3$. The twisted strips with twin wings in delta shape have an influence on thermal transfer and impact

of friction indicated by (Taylor et al. 2015) [62] twisted tapes used in that experiment contained three different twin-delta wing configurations: (1) the twisted tapes with twin wings at delta shapes at inverse the fluid flow (ttw-up, the tips of wings forming at upstream of flow), (2) the convolute strips with twin wings in delta shapes wings in a co-flow (ttw-down, the tips of wings forming at downstream of flow) and (3) the twisted tapes with twin wings at delta shape in opposite flow direction (ttw-o, the tips of wings forming in opposite direction), with three diverse angles of wing-strip of 62° , 43° , and 21° and used water as working fluid for turbulent flow regime ($5000 < Re < 15000$) under constant wall heat flux. The experiment indicated the (ttup) twisted tapes were more effective to generate maximum heat rate., the maximum TPF of 1.26 in a tube with (wtt-up) with wing-tip angle 20° .

The numerical investigation study was carried out by (Lin et al. 2016)[63] to show the effect twisted tapes with parallelogram winglet insert on friction factor and heat transfer rate. The study was used parallelogram winglet as vortex generators with four different attack angles α ($\alpha = 27.2^\circ$, 21.5° , 17.62° , and 14.32°) and four diverse pivotal distances St ($St = 0.85d$, $1.1d$, $1.1d$ and 0.69) in laminar flow and constant wall heat flux. From the simulation results, the PWVGs (parallelogram winglet twisted tapes) can effectively enhance heat transfer under the constant pumping power condition comparison with smooth pipe. The thermal flow rate rises with PWVGs for large attack angle α and small St .

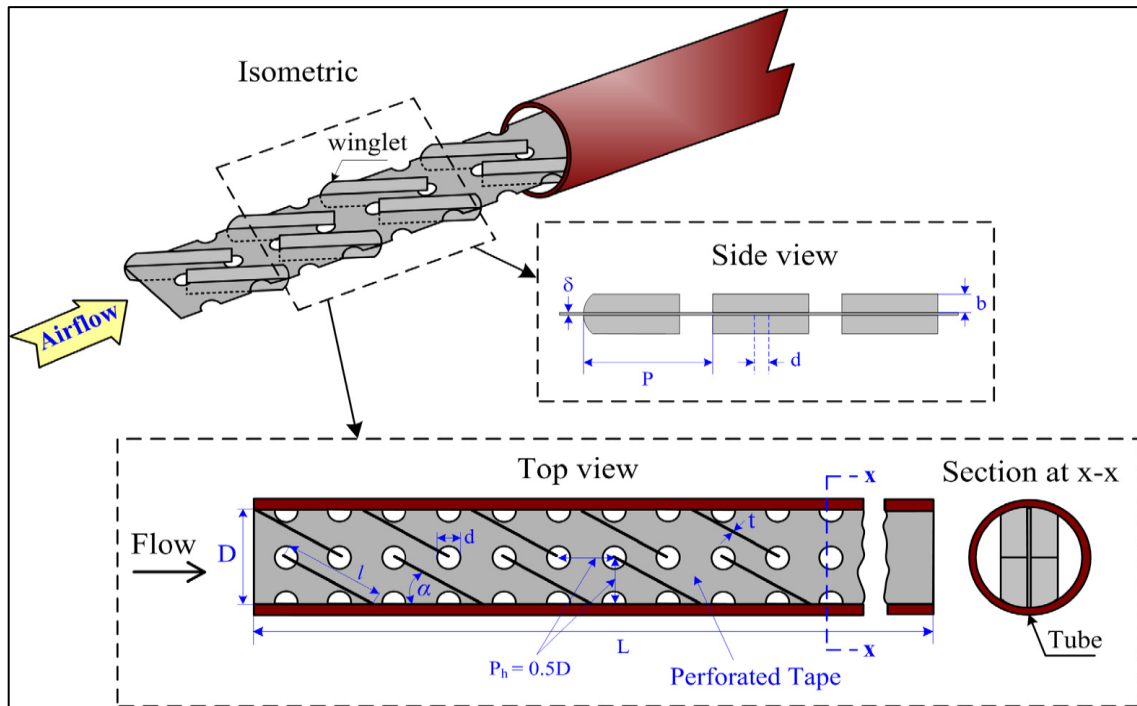


Fig. 2.17: Staggered-winglet typical tapes [58].

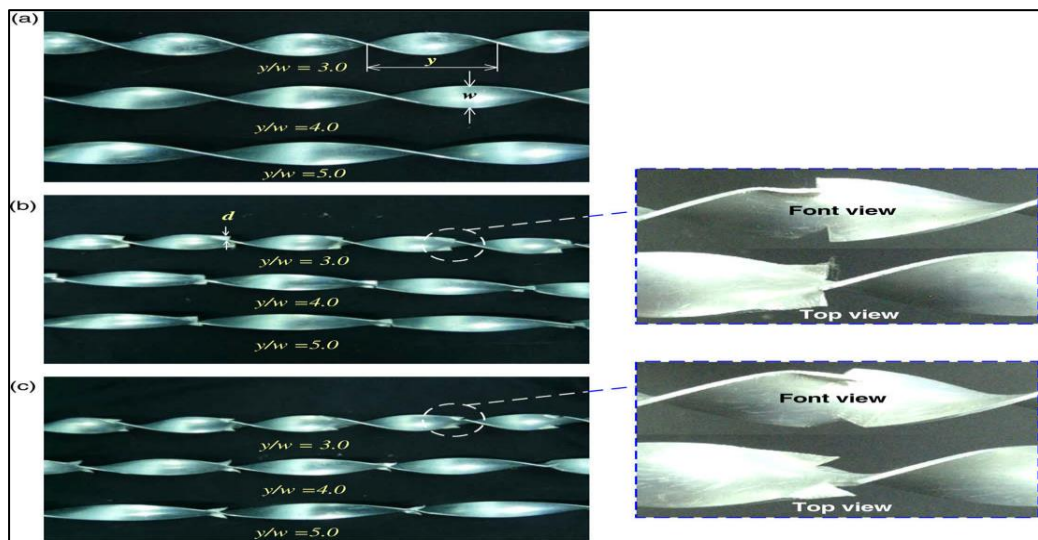


Fig. 2.18: Triangle-wing convolute strip (a) normal convolute strips (b) upright triangle-wing torsion strips (c) incline triangle-wing convolute strips [59].

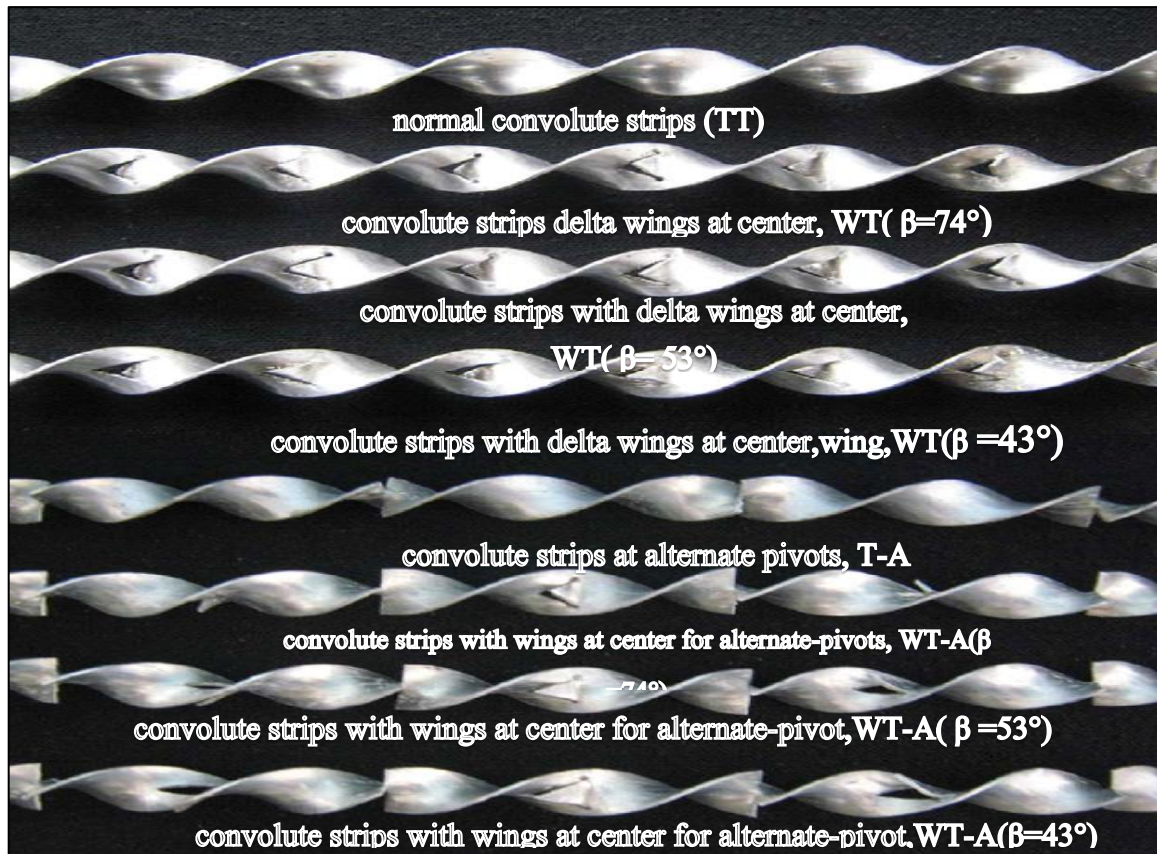


Fig. 2.19: Normal convolute strips (TT), convolute strips with delta wings at center (WT), convolute strips at alternate pivots (T-A), convolute strips with wings at center for alternate-pivot (WT-A)[60].

2.12 Effect of twisted tape with ribs

The effect of the twisted strips with 30° V-shaped ribs, as clear in fig. (2.20) on transfer of thermal and drop of pressure carried out by (Tamna et al. 2016) [64], the experiment used convolute strips with ribs at V-shaped with four varied blockage ratios ($br = b/dia = 0.06, 0.08, 0.013$) with fixed the pitch of rib ($pr = pitch/dia = 1.8$) and twist ratios = 4 at a rib angle of attachment $\alpha = 30^\circ$ for turbulent flow the number of Reynolds Re range from 5300 to 24,000 with stable wall flux of heat. The experimental outcomes showed the the thermal flow in term Nusselt number and drop of pressure in term parameter of friction appears to increase for increment of number of Reynolds (Re) and blockage

ratios(pr) over the conventional convolute tape without ribs, the best The thermal enhancement ratio for V-ribbed convolute strip is around 1.4 compared to typical twisted tapes with $br = 0.09$. The experimental research was carried out by the(Tarasevich et al. 2017) [65] An experimental work to investigate the effect of convolute strips with ribs on thermal rate and behavior of friction inside a annular pipe for two-phase fluid (air-to-water) flow, the experiment used wounded wire twisted tape in twisting direction and in the opposite twisting direction shown in fig. (2.21) at turbulence regime of flow, the number of Reynolds(Re) range from 8000 to 80000. The experiment results showed that thermal transfer, thermal efficiency ratio, and effect of friction in a tube equipped with twisted tapes with ribs were increased over the typical twisted tape, the best rate of heat rate produced in to tube with convolute tape with wounded wire against twisting direction. Table (2.1) represents the summary for an important twisted tapes that were applied to enhance the thermal flow and the effect of friction .

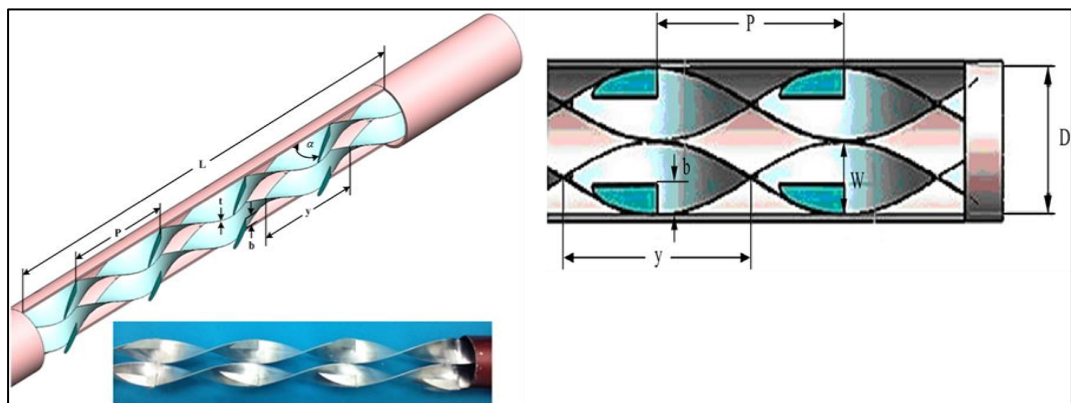


Fig. 2.20: Convolute strips with 30° v-ribs [64]

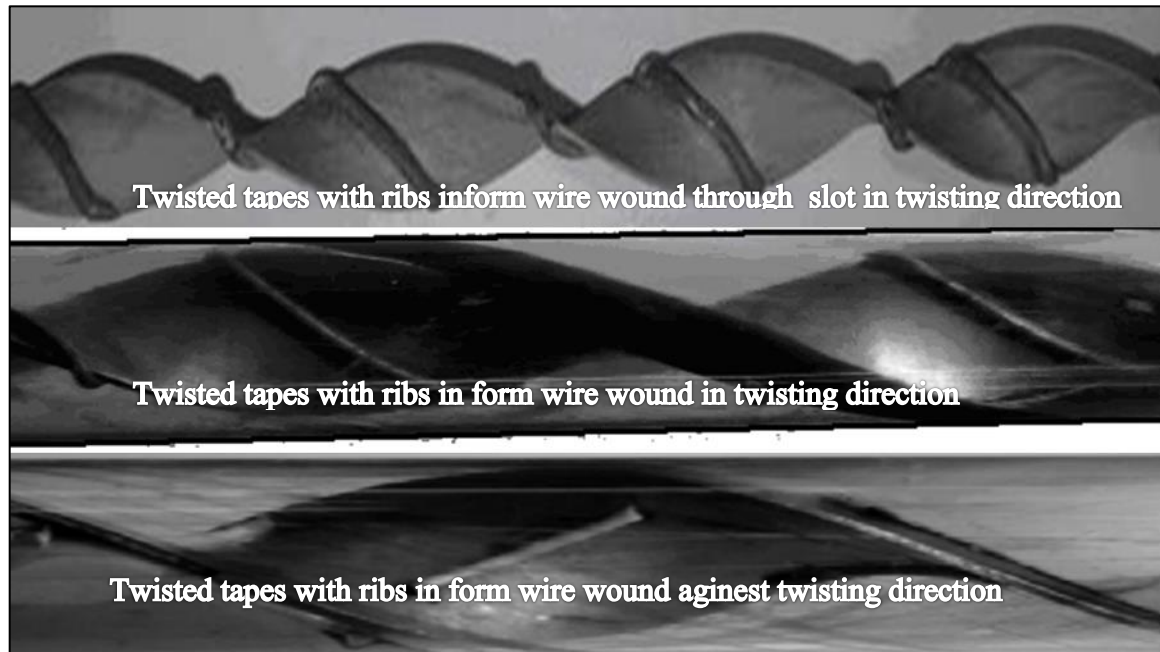


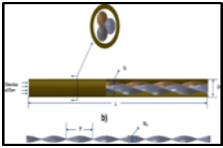
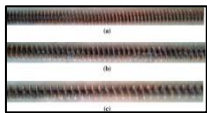

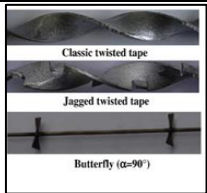
Fig. 2.21: Twisted tapewith ribs[65].

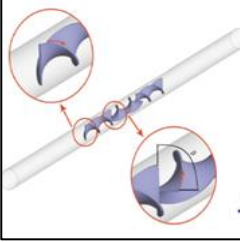
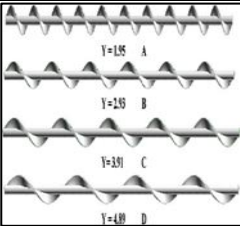
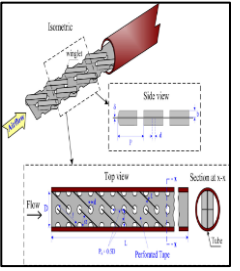
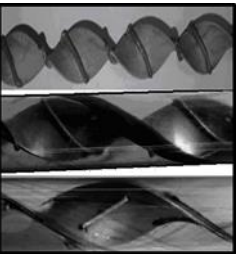
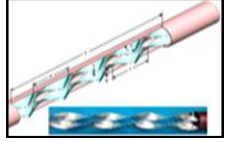
2.13 Scope of present work:

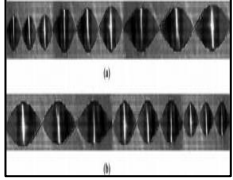
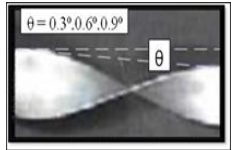

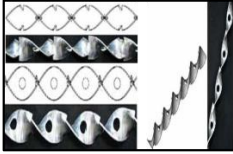
The objectives of this article is to investigate the effect on the thermal performance dueto equipped the riser of solar collectoe by four types of twisted aluminum tapes include curvature and straight vortex generator (CVGs&SVGs), and show that action on heat transfer in term of the Nusselt number (Nu), pressure drop in term of friction factor (f), thermal performance factor (TPF) and the efficiency (η) of a simple flat plate solar collector.

During the experiments ,investigate five cases of thermohydraulic bahaver for risers of flat plate solar collector include insertion twisted tapes with curvature vortex generator in front flow (TTFF)into riser(tubes) of collector, also twisted tapes with curvature vortex generator in opposite flow (TTOF) and straight vortex generator (TTS) and comparsion with typical twisted tapes and smooth tube in close system forced flow with four flow rates(7,5,3 and 1.5) L/min for laminar flow $300 < Re < 2000$.

Table- 2.1: The summary

| Author | Working fluid | Configuration of twisted tapes | Type of investigation | Observation | Image |
|--------|---------------|---|---|---|---|
| [37] | Air | Triple twisted tapes with different twisted tape 1.92, 2.88, 4.81, and 6.79. | Experimental study | Re (5000-55000) TPF enhanced. Compare to the plain tube was around (1.10-1.44) |  |
| [46] | Water | The center core rod of wire coiled-coil with Three different twisted ratios (0.23, 0.45 and 0.68 | Experimental Study | Re(9000-24000) TPF was around 1.42 |  |
| [60] | Water | convolute strips with wings at center at three various attach angles, ($\beta = 43^\circ, 53^\circ,$ and 74°) and alternate-axes | Experimental Study | Re(5000-25000) Th performance ratio of up to 1.39 at attache ($\beta = 75^\circ$) |  |
| [20] | Air | Three different twisted tapes <ul style="list-style-type: none"> ➤ Classic twisted tapes ➤ Notched twisted tapes ➤ Butterfly with ($\alpha=90^\circ$) twisted tapes | Experimental and Computational Fluid Dynamics (CFD) | For Re(14,000&10,000and 6000) TPF were various as = (1.28 - 1.62), (1 - 1.23) for the butterfly and jagged twisted tapes respectively |  |

| Author | Working fluid | Configuration of twisted tapes | Type of investigation | Observation | Image |
|--------|---------------------|---|------------------------------------|---|---|
| [21] | CuO–Water nanofluid | Alternate axis twisted tapes with different revolution angle ($\beta= 0 - 1.57$) | Computational Fluid Dynamics (CFD) | Re(5000-20000) With an increase of revolution angle Pressure drops increased Nusselt number enhanced Thermal performance increased |  |
| [24] | Water | entire - longitude spril screw twisted tapes for diverse twist ratio ,and spril screw devices | Experimental Study | Re (6000-14000) Nu decrease for the helical twist tapes with subsequent increase in spacer length, (f)for entire - longitude screw is higher than spril screw inserts with various lengths of spacer |  |
| [58] | Air | Staggered-winglet perforated tapes (WPT) | Experimental Study | Re from 4180 to 26,000 The performance ratio in tube fitted with (wpt) was higher than the Staggered- winglet tapes without punches(wtt) |  |
| [65] | Air&water | Twisted tapes include wrapping ribs in the counter direction of twist | Experimental Study | Re from(8000-80000) Ribs installed against twisting showed the highest heat transfer rate and hydraulic efficiency until |  |
| [64] | Air | convolute strips with v-ribs for attach angle 30° | Experimental work | TT with ribs at blockage ratio $br = 0.09$ produced the maximum thermal rate and higher performance ratio about 1.4 |  |

| Author | Working fluid | Configuration of twisted tapes | Type of investigation | Observation | Image |
|--------|---------------|--|-----------------------------|--|---|
| [16] | Water | a) Twisted tape insert of increasing twist ratio; (b) twists tape insert of decreasing twist ratio | Experimental investigations | Re(100-10000) Decreased twist ratio lead to Nusselt numbers were found to be 2.46–5.73 and 1.28–4.03 times a plain square duct |  |
| [34] | Air | Tapered twisted tapes with different taper angle ($\theta=0.0^\circ, 0.3^\circ, 0.6^\circ, 0.9^\circ$) | Experimental investigations | Re(6000-20000) TPF tended to increase with θ and decreasing tape, twist ratio, max. TPF 1.05 at $\theta=0.9^\circ$ and twisted ratio 3.5 |  |
| [32] | Air | The twisted tapes are of three different twist ratios (3, 4 and 5) each with five different widths (26-full width, 22, 18, 14 and 10 mm) | Experimental investigations | Re range from 6000 to 13500 The improve of thermal flow with convolute strips and comparsion with smooth tube changed from 35% to45% for entire width and 32% to 37% in minimize of width |  |
| [55] | Water | Perforated twisted tapes (PTT) with three various punch size ratios (dia/m =0.12 , 0.29 and 0.49) | Experimental investigations | The maximum performance ratio 1.32yielded for the PTT at dia/m = 0.12 and d/m = 0.37 at Reynolds number of 5500 |  |

Chapter Three

MATHEMATICAL BACKGROUND

Chapter Three

Mathematical Background

3.1 Introduction

Enhanced thermal flow at a heat exchange is vastly used at domestic and industrial applications, because of the require for too integrated heat exchanges, depress running costs, power savings and environmental benefits, the application of twisted tape in various shapes and geometries is another popular solution, and twisted tapes are widely utilized as thermal transfer improvement instruments in heat exchangers, that simply aimed to mix the flow to control the thermal layer growth also to increment the exchange of heat near surface of tube (Yousif and Khudhair 2019)[4]. Using twisted tapes with vortex generators (VGs) in a large variety from numbers of Reynolds may provide preferable thermal efficiency for limited rise infalling in pressure comparsion with other VGs, the regions of tangency between the convolute strip and the working fluid is wide for a conventional twisted tape, resulting in a significant drop in pressure(Lin et al. 2016) [63].

Due to its abundance, power of solar as the most hopeful source of energy, this power of solar can be transformed for usable power either by photovoltaic cells as electric energy or by solar collectors and solar ponds as thermal energy. One of the simplest and most commonly solar collectors is a solar collector of type flate plate, the thermal flow and effect of friction in the solar collector's riser pipe, equipped with modification of the convolute strips geometry raise due to extra turbulence along with the twisted tapes induced swirl flow that would increase the volumetric rate, it helps to increase the thermal rate between the fluids which flows through the riser tubes and receiver sheet(Murugan et al. 2019)[22], the process industry is working actively to integrate enhanced heat

Transfer rate in both heat exchanger and practically for the solar collector at the same time each solar collector is a potential candidate for enhanced collector efficiency resulting in enhanced heat transfer, initially, a solar collector was designed to use plain (smooth) surfaces for heat transfer.

3.2 Twisted Tapes

Most swirl-flow mechanisms have been found to promote argumentation about excess heat transfer, but a penalty is often imposed for the resulting raise in drop of pressure. The increment in transfer of heat in tubes equipped with a swirl-flow device is largely due to fluid disruption and mixing induced by the secondary flow resulting from the swirl fluid motion, in the case of twisted tape inserts, apart from their longitudinal vortex-generating features, tape thickness, the direction of helical flow and surface finishing effects often affect the thermal-hydraulic efficiency, perhaps the most attractive characteristic of twisted tapes is the relative ease with which a convolute strips schematic diagram within a pipe. It could be generated using fig. (3.1), the twisted tapes are knowed geometrically via the strip thickness (δ) also the torsionl order (twist ratio) (Manglik and Bergles 2003)[14]. The twisted order (Y) is specify as the pivotal longitude represent pitch (p) for 180° which is twisted tape angle, over the tape width (W), then the twist ratio is $Y=P/W$.

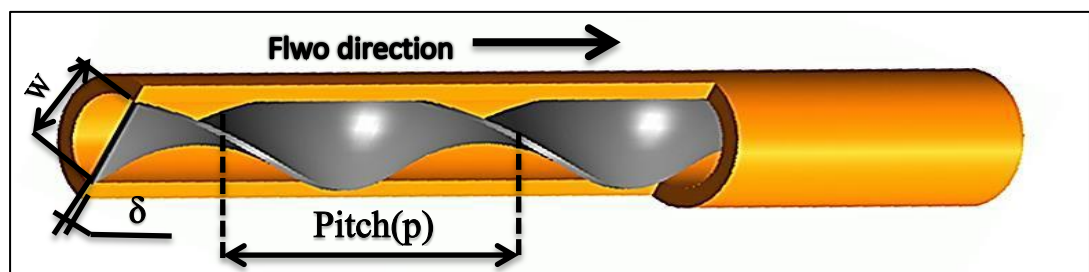


Fig. 3.1: Schematic of twisted tape inside a tube.

3.3 Twisted tape with vortex generators

The ribs attached to the twisted tape shown in fig. (3.2) are used as a vortex generator to help increase disruption of the thermal boundary layer to obtain a thinner layer than typical twisted tape, also ribs on a tape facilitate the fluid motion from the tape toward tube thermal transfer regions to achieve maximum transfer of heat rate and higher thermal efficiency (Tarasevich et al. 2017)[65].

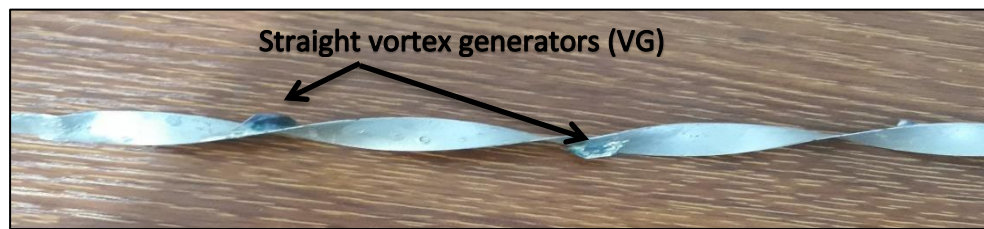


Fig. 3.2: Twisted tapes with vortex generators.

3.4 Transfer of heat and flowing of fluid into circular pipes

Turbulent regime commonly used in practice, in order to the correspondingly maximum coefficient of thermal flow and because of the complexity of turbulent flow theoretical treatment as long as the most heat rate parameter correlations and turbulent flow friction depend on experimental studies, the effect of friction into empty annular tube at turbulence regime of flow can be calculated either from first Petukhov (Petukhov 1970)[66].

$$f = (0.79 \ln Re)^{-2} \quad (3.1)$$

or the friction factor calculated from the well-known Darcy-Weisbach equation which calculates the pressure drop (Jf et al. 1992)[67]

$$\Delta P = f \frac{L}{d_i} \frac{\rho u^2}{2} \quad (3.2)$$

And

$$f = \frac{\Delta P}{\frac{L}{d_i} \frac{\rho u^2}{2}} \quad (3.3)$$

The following equation evaluates the Nusselt number from the common correlation of coefficient for the transfer of heat by convection (h_i), (K_w) and, the internal riser tube diameter (d_i)

$$Nu = \frac{h_i d_i}{K_w} \quad (3.4)$$

3.5 Physical and thermal properties of working fluid (water)

The properties of water can be calculated from the following equations and these equations can apply in the range ($0^\circ\text{C} \leq T_w \leq 100^\circ\text{C}$) (Azmi et al. 2012) [68]

Thermal conductivity

$$K_w = 0.56112 + 0.00193T_w - 2.60152749e^{-6T_w^2} - 6.08803e^{-8T_w^3} \quad (3.5)$$

Density

$$\rho_w = 1000 \times \left[1 - \frac{(T_w - 4)^2}{119000 + 1365 \times T_w - 4 \times T_w^2} \right] \quad (3.6)$$

The Specific heat

$$C_{pw} = 4217.629 - 3.20888T_w + 0.09503T_w^2 - 0.00132T_w^3 + 9.415e^{-6T_w^2} - 2.5479e^{-8T_w^5} \quad (3.7)$$

Viscosity

$$\mu_w = 0.00169 - 4.25263e^{-5T_w} + 4.9255e^{-7T_w^2} - 2.0993504e^{-9T_w^3} \quad (3.8)$$

3.6 The performance of a solar collector

At a steady-state, the energy balance indicated the distribution of solar energy incidence description of the solar collector efficiency, the division of solar power incidence to beneficial power gains, optical losses also heat losses.

The difference between solar irradiance incidence and optical losses represents solar radiation, which is absorbed by the solar collector (S), thermal losses in collectors at conductive form, infrared irradiance and convective, exemplified by the coefficient of heat transfer U_L , thermal losses equal the product U_L by the temperature difference of mean absorber plate temperature T_{pm} and ambient temperature T_a thus the term represents thermal energy, loss from the collector is $U_L(T_{pm} - T_a)$ per meter square of collector area A_C , therefore The difference between the solar irradiance absorption and the losses of heat represent the solar collector's useful energy or energy output in steady-state:

Useful energy $Q_u = A_C [S - U_L(T_{pm} - T_a)]$, the predicament of that equation of the mean temperature of the absorption plate T_{pm} is difficult to predict because it related with three parameters, collector layout, fluid condition, and solar irradiance incidences which create a problem for beneficial energy equations.

The collector performance represents the solar collector output, which is known as a proportion of the beneficial power gain from solar power incidence over the same interval (John A. Duffie 2013)[69] :

$$\eta = \frac{\int Q_u dt}{A_C \int GT dt} \quad (3.9)$$

And for stable condition-state, the collector efficiency becomes as

$$\eta = \frac{Q_u}{I_{TAC}} \quad (3.10)$$

The provision of minimum cost energy is too important factor for construction of a solar power device so that this design of an efficient collector can be beneficial, less than is technically feasible if the expense reduction significantly, including the expectation that the solar collector output will in any event occur. Several simplifying assumptions will make the simple physical condition the assumptions as follows model the condition in fig. (3.3) without opacity:

1. Performance is steady conditions.
2. The structure is in parallel form and surface-plated.
3. The header cover areas are limited and small thus could be ignored.
4. The headers supply steady flow risers.
5. Solar irradiance does not absorb by a cover which causes extra heat losses.
6. In one dimension the heat flows through the cover.
7. Ignored the temperature decreases over the cover.
8. Glass covers are opaque for solar irradiance.
9. In one dimension, thermal flows through the bottom insulation.
10. Consider the sky like a black body at equivalent black body temperature.

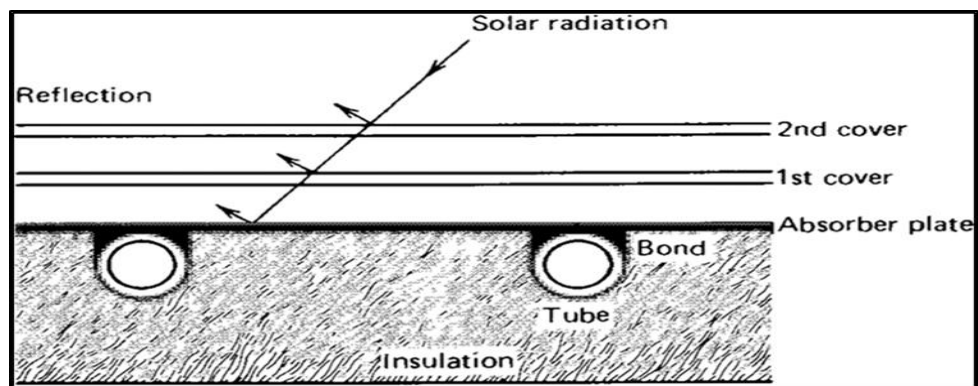


Fig. 3.3: Distribution of solar irradiance over solar collectors [69].

3.7 The gross coefficient of heat loss for flat plate collector U_L

Itemized analyses to solar collectors is a complex issue, and a comparatively easy analyses can yield very accurate results, this outcomes reveal significant factors, how they are related, and how they affect the performance of the solar collector.

To clarify this fundamental concepts, a collector of liquid heat, as clear in fig. (3.3) the following developments will be tested first, it is hoped that the division of temperature in a construct solar collector will be understood, an area between two tubes should be attached together with the plate to the tube area, in which some of the solar energy absorbed by the plate, and in between the tubes at halfway the temperature is larger than near the tubes, while the temperature above the tubes is approximately uniform due to the pipe and metal of welding relationship.

Power transported to the fluid heats the fluid, which causes a temperature progress in the trend of flow, since the local temperature at every area of the collector was governed by the generic temperature scale, having defined the temperature distribution over the flat plate collector, revealing the idea of a total loss coefficient U_L for a solar collector is useful for mathematical

simplification, consider the flat plate collector thermal network for the two covers that absorb energy S divided to heat losses through the upper and back side and beneficial energy gain, simplifying calculation of the overall coefficient of heat loss by converting the losses to the top thermal network, the loss of thermal energy resulting from convective and irradiation within parallel plates. In stable conditions, the transfer of thermal energy between the first cover of T_{c1} temperature and the absorber plate T_p is like any other two neighboring covers, and is therefore equivalent to the power loss from the upper parallel plates to the environments as showing in the fig. (3.3), loss of heat from the upper is similar to the transfer of heat from the absorption plate to the first glass(cover) (John A. Duffie 2013)[69] where :

$$q_{loss,top} = h_{c,p-c1}(T_p - T_{c1}) + \frac{\sigma(T_p^4 - T_{c1}^4)}{\frac{1}{\epsilon_p} + \frac{1}{\epsilon_{c1}} - 1} \quad (3.11)$$

The subscript($q_{loss,top}$) symbolize the thermal losses from the upper of the collector and term $h_{c,p-c1}$ represents the coefficient of thermal transfer by convective between absorption plate and glass1 (cover1), also radiation between the plate at a temperature T_p and cover 1(glass1), and between glass 1 and cover 2 (glass2) at temperatures T_{c1} and T_{c2} respectively and between cover 2 and sky at a temperature T_s as illustrated in follow:

The radiation heat transfer coefficient h_r express in the following equation [69]:

$$h_{r,p-c1} = \frac{\sigma(T_p + T_{c1})(T_p^2 - T_{c1}^2)}{\frac{1}{\epsilon_p} + \frac{1}{\epsilon_{c1}} - 1} \quad (3.12)$$

Where $h_{r,p-c1}$ represent the radiation coefficient of thermal transfer between the absorption plate and glass1 (cover 1), then the thermal is lost from top of collector to ambient for one glass cover can be expressed as follows:

$$q_{loss,top} = (h_{c,p-c1} + h_{r,p-c1})(T_p - T_{c1}) \quad (3.13)$$

Now the resistance R_3 in fig. (3.4) which represent thermal resistance analysis for a solar collector can express as:

$$R_3 = \frac{1}{h_{r,p-c1} + h_{c,p-c1}} \quad (3.14)$$

In the same way, R_2 is the resistance between the covers (glass1 and glass2) given by

$$R_2 = \frac{1}{h_{c,c1-c2} + h_{r,c1-c2}} \quad (3.15)$$

The (R_1) represent thermal loss of the top to ambient shown in the fig. (3.4), where

$$R_1 = \frac{1}{h_w + h_{r,c2-a}} \quad (3.16)$$

Where h_w and $h_{r,c2-a}$ represent the convective thermal transfer loss coefficient due to wind also irradiation thermal transfer loss coefficient from top collector to ambient respectively where

$$h_w = 2.8 + 3.3V_w \quad (\text{Ong, K.S. 1995}) \quad [70] \quad (3.17)$$

Where V_w represent wind speed (m/sec) .

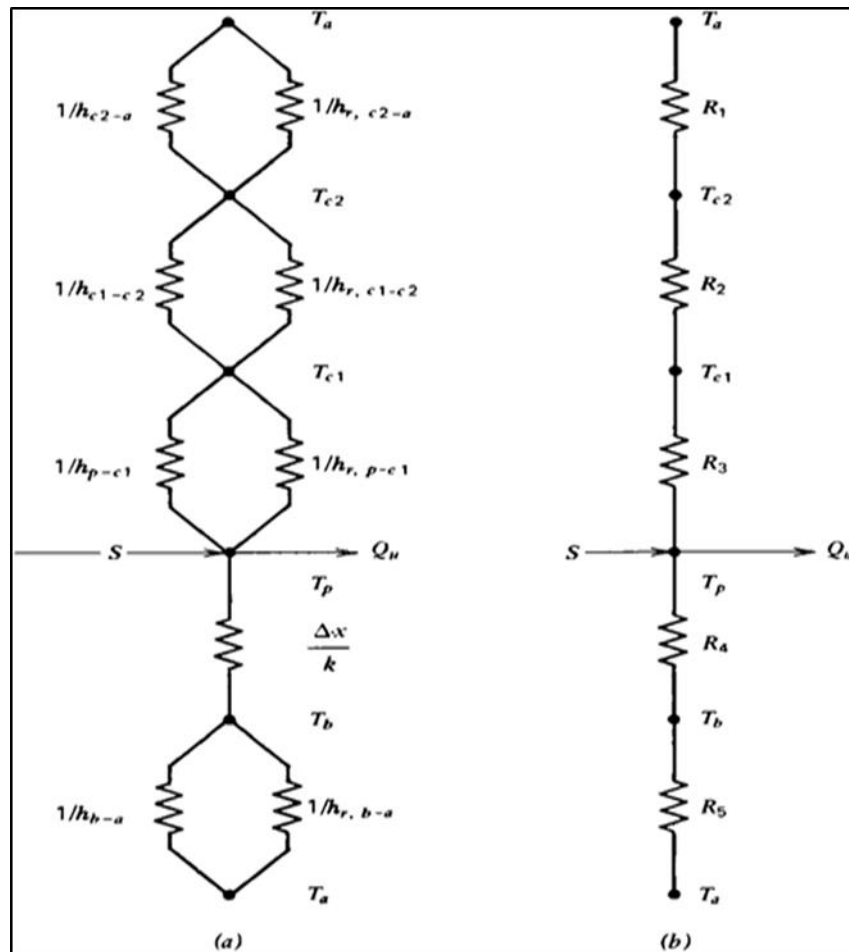


Fig. 3.4: Thermal resistance network for a solar collector with two covers [69].

In this two-cover solar apparatus, the upper loss parameter from the collector plate to the surrounding is

$$U_t = \frac{1}{R_1 + R_2 + R_3} \tag{3.18}$$

From the fig. (3.4) the resistances R_4 and R_5 both represent the energy loss from the bottom (U_b) and edges (U_e) of the solar collector to ambient. The bottom loss coefficient U_b can experiences in the following equation:

$$U_b = \frac{1}{\frac{t_b}{k_b} + \frac{1}{h_{c,b-a}}} \tag{3.19}$$

Where the (t_b) , (k_b) Represent the thickness (m) and thermal conductivity (W.K/m) of insulation at the back side within the collector, $h_{c,b-a}$ represent the coefficient of thermal lose by convective between the bottom of the collector and the enviroment usually is equivalent to (h_w) .

In the same way the coefficient of thermal losses from the edges of the collector U_e can be symbolize in the following equation [69]:

$$U_e = \frac{1}{\frac{t_b}{k_e} + \frac{1}{h_{c,e-a}}} \quad (3.20)$$

Thus the coefficient of gross thermal losses U_L within solar collector represente in the following correlation(Baqir .S. A. et al. 2019)[72]& (Khwayyir. S. H. et al. 2019)[73]:

$$U_L = U_t + U_b + U_e \quad (3.21)$$

The coefficient of heat transferby convective between the absorbetion plate and cover (glass1) $(h_{c,p-c1})$,and between the covers (glass 1&glass2) $(h_{c,c1-c2})$ evaluate from the following formula:

$$h_c = \frac{k}{l} \left(1 + 1.446 \left[1 - \frac{1708}{Ra \times \cos(\beta)} \right] \left[1 - \frac{1708(\sin(1.8\beta))^{1.8}}{Ra \times \cos(\beta)} \right] + \left[\left(\frac{Ra \times \cos(\beta)}{5830} \right)^{-0.333} - 1 \right] \right) \quad (3.22)$$

Where (β) inclination angle of the collector, k is the thermal conductivity of air between (plate-glass 1) and (glass1-glass2) the (Ra) represent the Rayleigh number evaluated from the following equations:

$$Ra_{(p-c1)} = \frac{g\beta' pr(T_p - T_{c1})L^3}{\nu^2} \quad (3.23)$$

$$Ra_{(c1-c2)} = \frac{g\beta' pr(T_{c1} - T_{c2})L^3}{\nu^2} \quad (3.24)$$

Where: (L) is the distance between (plate-G1) and (G1-G2) in meter(m), g- gravity (m/sec^2), ν - viscosity of air (m^2/sec), pr- Prandtl number of air and β' volumetric coefficient where $\beta' = \frac{T_p+T_{c1}}{2}$ and $\beta' = \frac{T_{c1}+T_{c2}}{2}$ and T_p , T_{c1} , T_{c2} are plate, glass 1, and glass 2 temperature in $^{\circ}$ K.The properties of air in the gap between(plate-glass1) and (glass1-glass2) taken at $\frac{T_p+T_{c1}}{2}$ and $\frac{T_{c1}+T_{c2}}{2}$ respectively.

3.8 The internal convective coefficient of heat transfer for water flow (h_i) into riser pipe

$$Q_u = \dot{m}C_p(T_o - T_i) = U_oA_o(T_p-T_m) \quad (3.25)$$

The heat balance for solar collector riser tube where

$$\frac{1}{h_oA_o} = \frac{\ln\left(\frac{d_o}{d_i}\right)}{2\pi\alpha k_w L} + \frac{1}{h_iA_i} \quad (3.26)$$

To compute the internal convective coefficient of heat transfer (h_i) combined eq (3.25) &eq (3.26) the Nusselt number Nu calculated from eq (3.27) (Murugan et al. 2019)[22]&(Al-Shamkhi H. M. D. 2016)[71]

Where:

$$Nu = \frac{h_i d_i}{k_w} \quad (3.27)$$

3.9 The efficiency of collector and useful energy

The terms of the consumed energy within plate and losses of energy from absorber represent the useful energy where can be calculated from (John A. Duffie 2013) [69]:

$$Q_u = A_c F_R [I_T(\tau\alpha) - U_L(T_i - T_a)] \quad (3.28)$$

The Heat removal factor is given by

$$F_R = \frac{\dot{m}c_{pw}}{A_c U_L} \left[1 - e^{\left(1 - \frac{A_c F' U_L}{\dot{m}c_{pw}}\right)} \right] \quad (3.29)$$

And (F') is efficiency of collector where:

$$F' = \frac{1}{\frac{w}{D+(w-D)F} + \frac{wU_L}{\pi D i h i}} \quad (3.30)$$

F is a factor representing the efficiency of straight fin in rectangular shape expressed as:

$$F = \frac{\tanh[m(W-D)/2]}{m(W-D)/2} \quad (3.31)$$

The calculation F in appendix (B)

Here, the parameter m is given by:

$$m = \sqrt{\frac{U_L}{K_p \delta}} \quad (3.32)$$

Where the δ the thickness of absorber plate in m ($\delta = 0.00005\text{m}$), K_p Thermal conductivity of absorber plate.

The instantaneous collector efficiency relates the gross incident irradiation to useful energy, where can be calculated from:

$$\eta_i = F_R \left[(\tau\alpha) - U_L \frac{T_i - T_a}{I_T} \right] \quad (3.33)$$

Transmittance-absorbent product ($\tau\alpha$) = 0.87 (Murugan et al. 2019) [22] calculated in the appendix(B).

3.10 Thermal performance factor (performance ratio) (TPF)

Performance ratio for constant pumping is defined as in the following equation (Sivashanmugam and Nagarajan 2007) [23]& (Majeed. A, et al. 2020)[74]

$$TPF = \frac{(Nu_{twist}/Nu_{plain})}{(f_{twist}/f_{plain})^{0.1666}} \quad (3.34)$$

Where the Nu_{twist} is the Nusselt number within pipe fitted with convolute strip, Nu_{plain} Nusselt number in a plain tube, f_{twist} factor of friction in a tube fitted with twisted tape, f_{plain} parameter of friction in empty pipe.

Also all above equations used in calculation by (Shandal. J, et al. 2020)[75]to evaluated the efficiency of solar collector that used both air and water used in solar collector as working fluid.

Chapter Four

Experimental Work

Chapter Four

Experimental work

4.1 Introduction

In this chapter the description includes the information and details relating to the experiment work and measuring devices used in the experiment, the experimental system is designed to examine the influence of the different kinds of twisted tapes inserted on the efficiency of flat plate collector and to investigate the rate of heat transfer, drop of pressure also the performance ratio (TPF) into pipes equipped with four types of twisted tapes and to compare them with plain tubes, for laminar flow regime with the insertion of four kind of convolute strips; typical twisted tape (TT), twisted tapes with curved ribs in front of the flow (TTFF), curved ribs opposite of the flow (TTOF) and twisted tape with straight ribs (TTS), also describe the manufacturing steps of the twisted tapes and the experimental working method of the flat plate type collector. The distilled water is the experiments fluid in the closing system, and experimental work is carried out in the AL- Kefil district, Babel governorate.

The investigational work was performed in the this study of the following cases:

1. The flat plate collector facing south has been installed with 45 ° according to the optimum tilt angle web site and same study in the university of ALanbar facultat of engineering.
2. Riser tubes without twisted tape insertion with distilled water.
3. Riser tubes with typical twisted tapes (TT) insert.
4. Riser tubes with twisted tapes with curved ribs in front flow insert (TTFF).

5. Riser tube with twisted tapes with curved ribs opposite flow (TTOF) insert.
6. Riser tube with twisted tapes with straight ribs (TTS) insert.

4.2 Experimental Test Rig Description

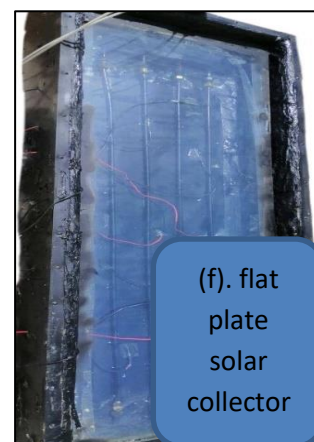
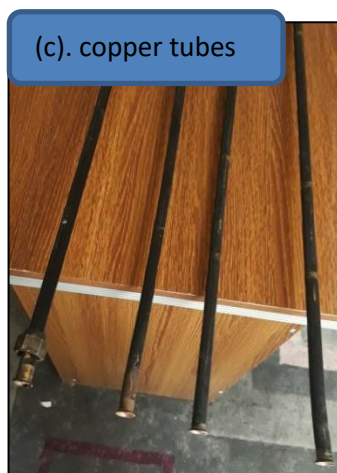
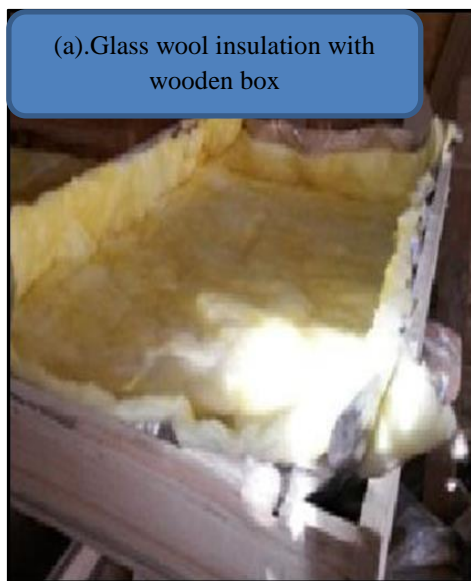
The experimental apparatus consists of the following parts:

- a) Flat plate solar collector.
- b) Four different types of twisted tapes.
- c) Water pump.
- d) Pipes.
- e) Valves.
- f) Measuring devices.

4.2.1 Specifications of Flat Plate type solar collector

The following steps illustrate the construct of solar collector as shown in the figure (4.1), the first step is the preparation of the riser tubes which are the copper tubes divided into four tubes of inside diameter 1.15cm and diameter of outside 1.25cm with a length of 1.6 m fastened on the absorber plate by welding in a parallel arrangement, the distance between the center line and the other is 100 mm, the lower and upper headers are copper tubes of the same inner and outer diameter of risers connected by 1/2 inch screw net size to the risers. The absorber plate was made of aluminum metal with a length of 160 cm and a width of 40 cm and a matt black paint coating with absorption (0.92-0.98) to increase the fraction of available solar power received by the plate and to minimize the loss of long-wavelength radiation from the absorbing surface, the absorber plate was mounted in a wooden box and separated from the bottom and side by 4.5 cm and 2.5 cm glass wool insulation thickness respectively to

minimize the conductive loss, Also to minimize convection leakage at upper side for solar flat plate collector the box closed by two covers with 4 mm thick ordinary window glass sheet due to glass has the high property of transmitting around 90 percent of short-wave radiation incidence and preventing longwave irradiance released from the receive plate to escape into the atmosphere, the distance between the plate and the glass¹ is 4.5 cm while the distance between the glasses is 2 cm, thickness of absorber plate was 0.5mm and the stand manufactured from carbon steel for the purpose positioning and the solar collector is tilted to the south-facing with 45°.



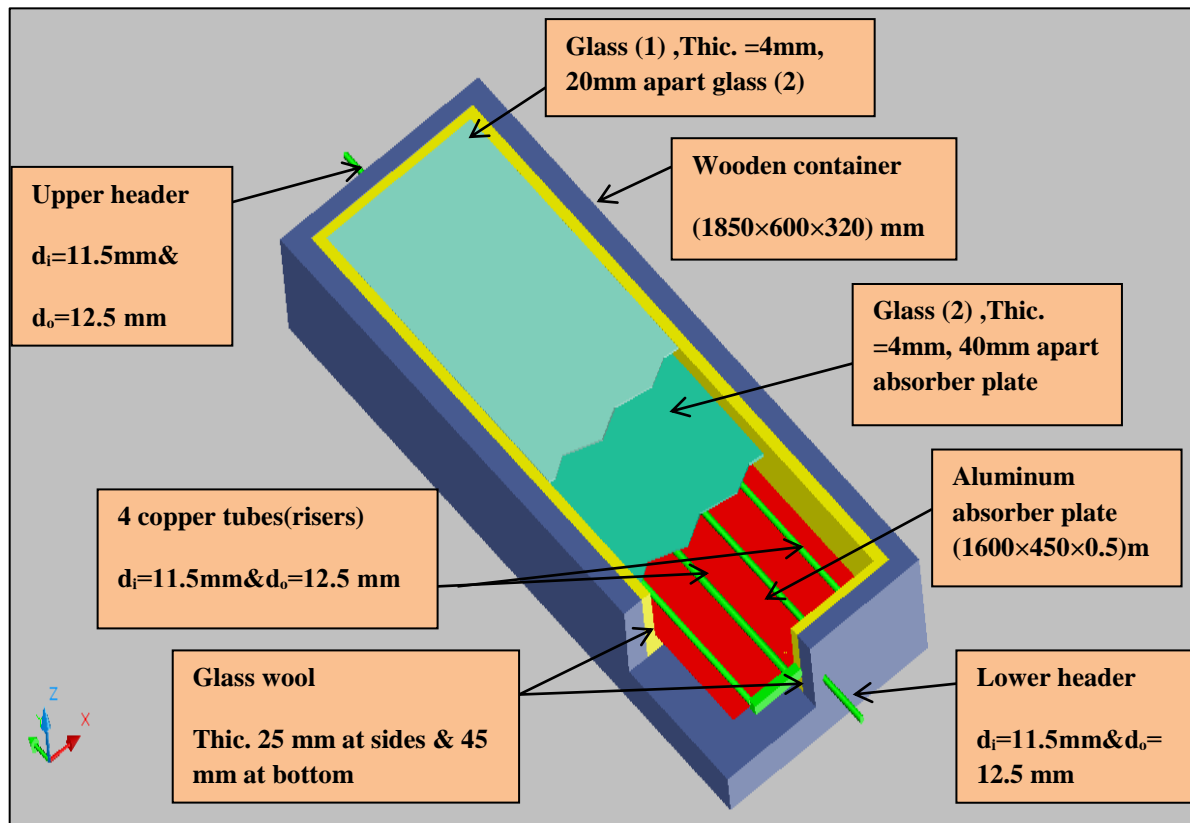


Fig. 4.1: Flat plate solar collector.

4.2.2 Experimental setup of the system

The figures (4.2) and (4.3) respectively show the solar collector of flat plate type and schematic diagram of experimental setups, the specification for the collector is given in table (4.1), as solar irradiance incidence passes across a cover of glass and hits particularly absorbent at black end receiver surface, the plate absorbs a large part of solar energy and conversion solar power into thermal power, thus heat is transferred to fluid tube conveying medium for use or storage, the pump helps the working fluid circulate in a close system. The performance of solar collectors in the district of AL- Kefel, Babil, has been experimentally investigated at that location of ((latitude 32°,13', 27' N and longitude 44°, 22',36' E), the data are recorded under transient conditions and with 45° tilted to the south.

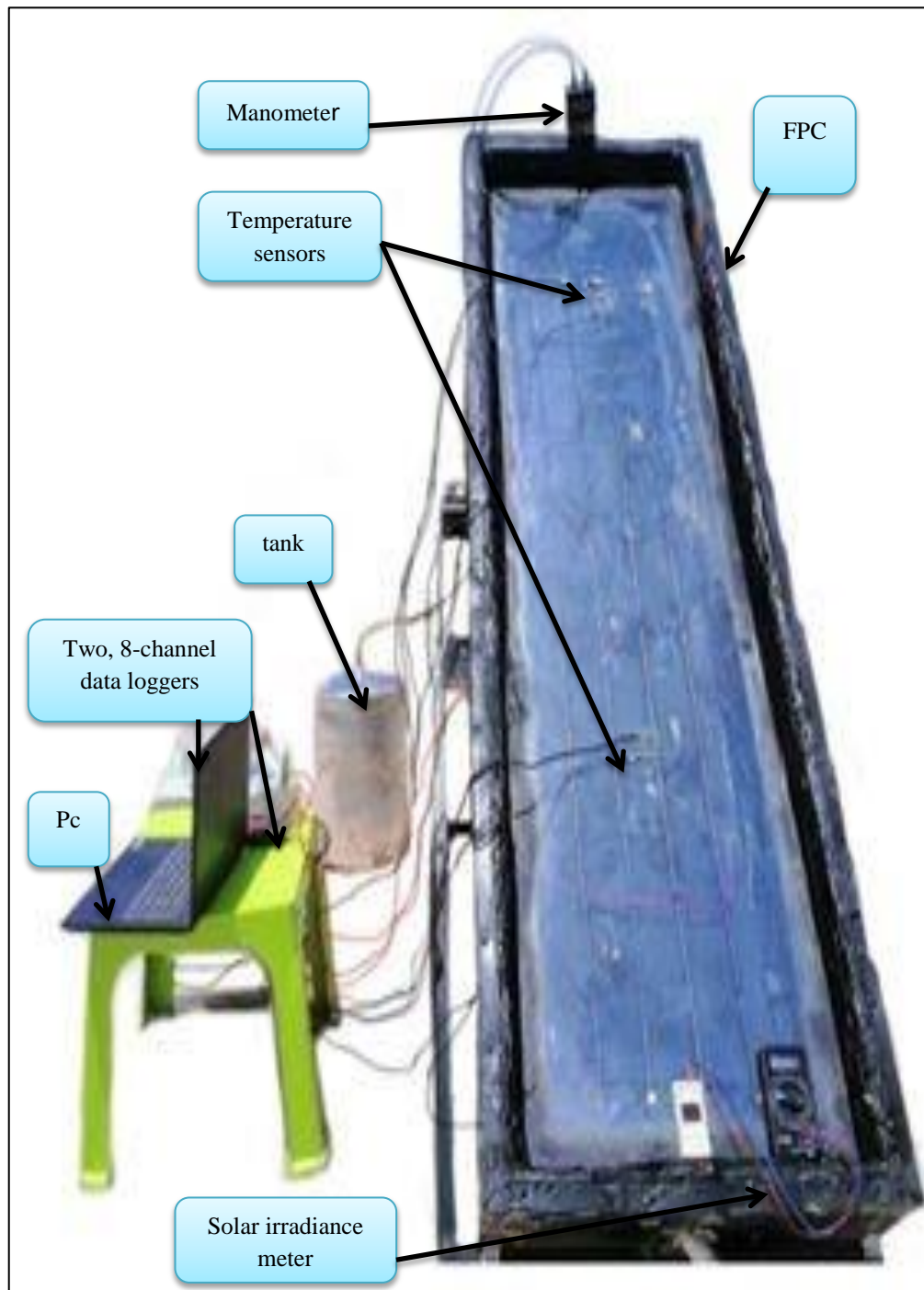


Fig. 4.2: The main parts of the flat plate solar collector and measurement devices.

Table- 4.1: The specification of flat plate solar collector

| Component | Dimension(mm) | Remark |
|-------------------|--|---|
| Collector | 1850mm*600mm*320 mm | |
| Absorber plate | 1600mm*400mm*0.5mm | Material: black painted Aluminum |
| Riser tubes | The inner diameters is 11.5mm ,outer diameters is 12.5mm, length 1600mm The tube center to center distance 100 mm | Material: copper Number of tubes: four |
| Header pipes | Inside and outside diameters 11.5mm , odiameter 12.5mm , with length 400mm | Material: copper Number of tubes: two |
| Bottom insulation | 450m m thickness | Material: glass wool |
| Edges insulation | 250m m thick | Material: glass wool |
| Tilt angle | 45° | |

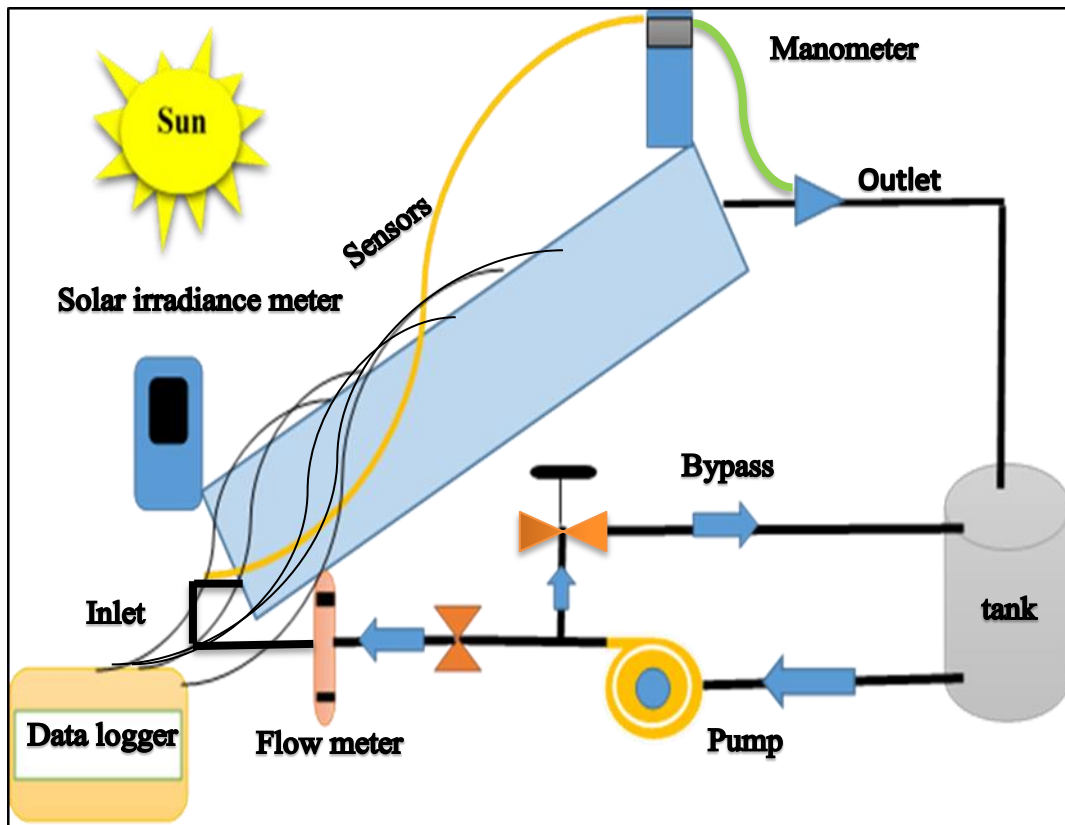


Fig. 4.3: Schematic of test rig construction and the measurement devices.

4.2.3 Twisted tapes geometrical configuration and dimension

Four different convolute strips inserts for twist order $Y=2$, which there are a typical twisted tape and ribbed twisted tapes were used as illustrated in the figures (4.4) and (4.5) and during the experimental study of change the rib geometric shape through insertion different twisted tapes. This tape was manufactured from Aluminum material strips with the following dimensions:

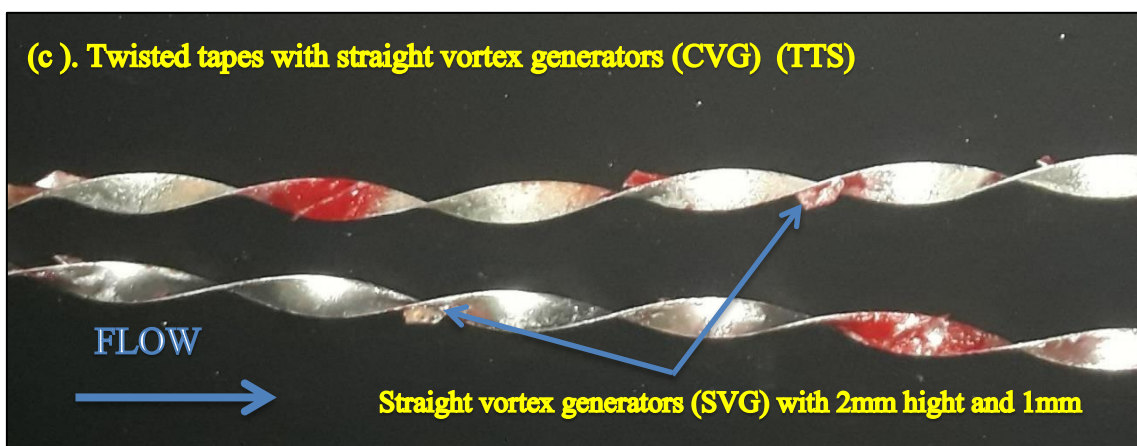
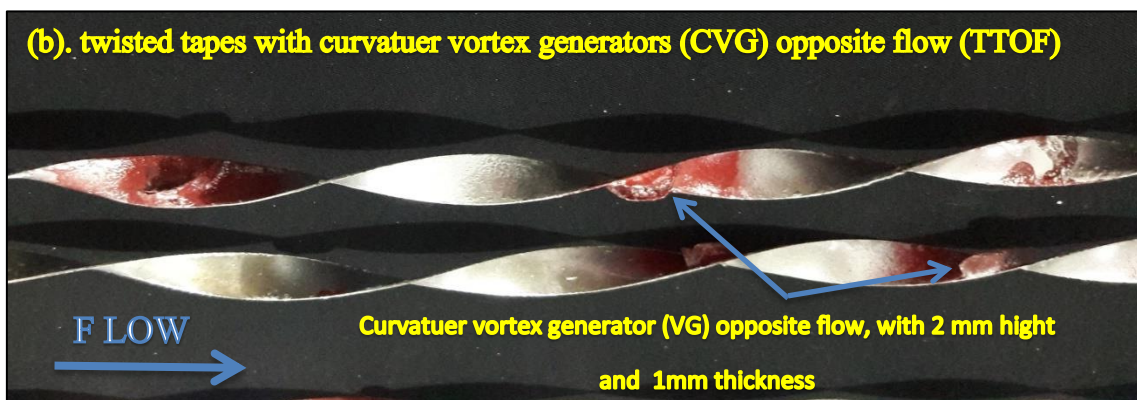
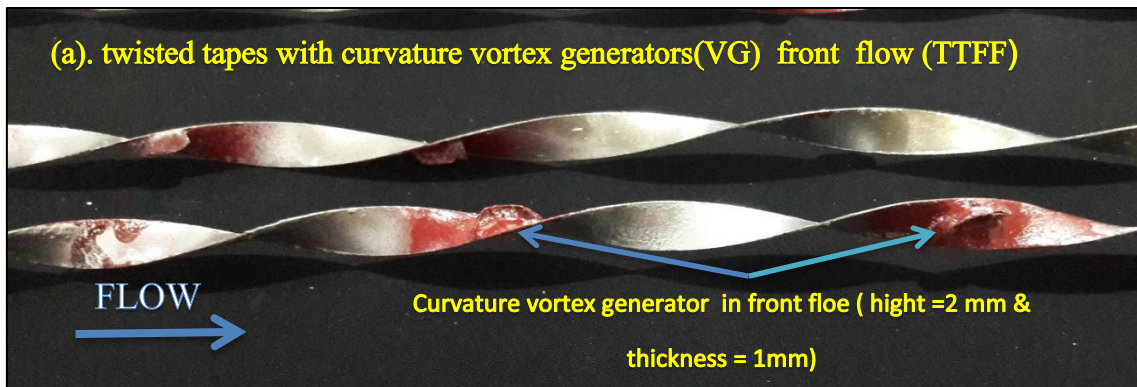
1. The twisted tape has tape width ($w=11.5\text{mm}$), thickness ($t=1\text{mm}$), length ($L =1600\text{mm}$), and twist ratio $Y=2$ at which the twist ratio is defined as the pitch length of twisted tape (P) to the tube inner diameter (d_i). Pitch is defined as the distance, length of one twist in the twisted tape for rotation angle 180° where $Y =P/ D$.

2. Twisted tapes with vortex generator as curvature aluminum rib attached to tapes by solder welding the rib dimensions are thicker =1mm and high = 2mm) the curve ribs attached to a twisted tube in front of the flow (TTFF).
3. Twisted tapes with curved ribs (the curved ribs opposite)(TTOF).
4. Twisted tapes with straight ribs (TTS).

The rib attaches to twist tape working as vortex generator in the region between and tube wall and the edge of the tape.



Fig. 4.4: Four different twisted tapes (TT, TTFF, TTOF, and TTS)



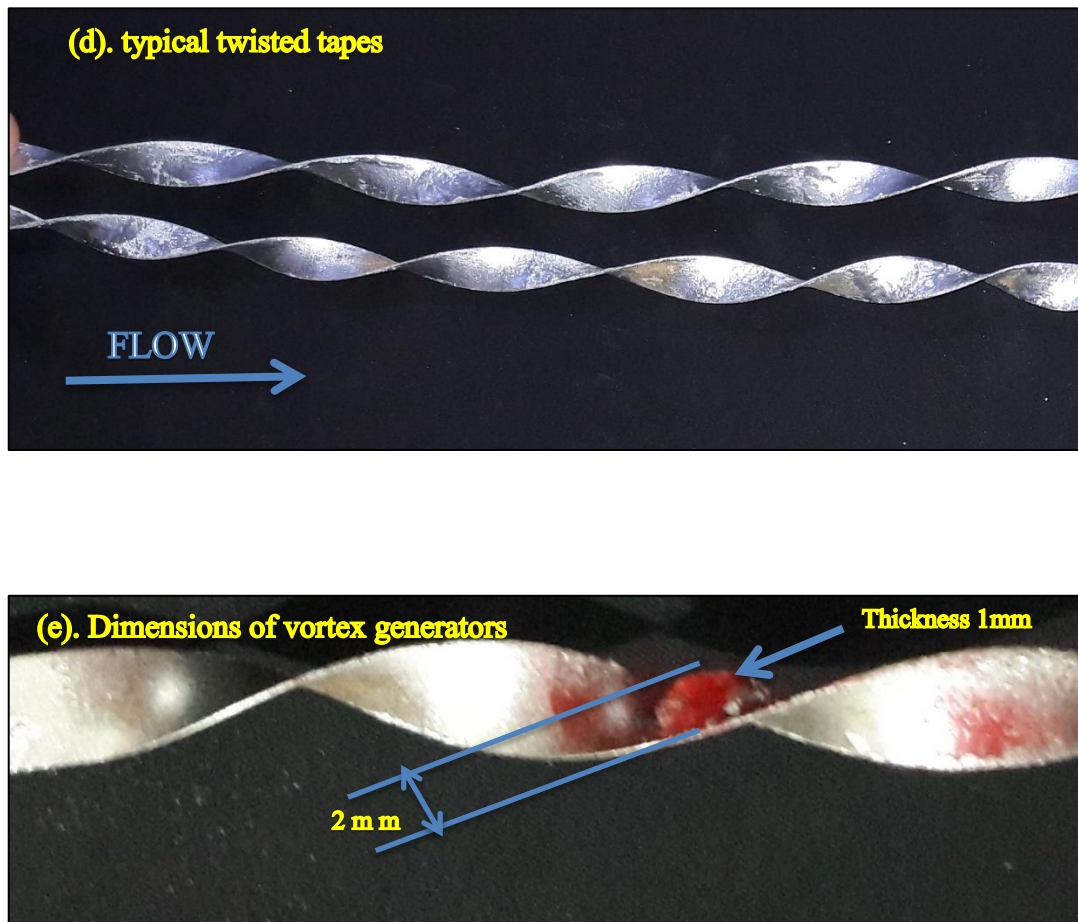


Fig. 4.5: Types of twisted tapes and dimensions of vortex generators.

4.2.4 Water pump

The centrifugal pump powered by an electric motor was used to rotate the water via the experimental test device. The specifications of the water pump illustrate in table (4.2).

4.2.5 Pipes

Plastic 12.5mm (1/2 inch) tubes are utilized for joining all the main sections of the test system, the pump with the storage tank and inlet collector and the outlet collector storage tank.

Table- 4.2: the specification of the centrifugal pump

| Electrical data | | | speed | Q max | Power |
|-----------------|----|-----|-----------|----------|----------|
| V | Hz | A | | | |
| 220 | 50 | 1.8 | 2850r.p.m | 30 L/min | 0.370 KW |

4.2.6 Valves

Two ball valves were used to regulate the volumetric flow rate of water in the close system, one on the mainline between the pump and collector inlet and other as a bypass between tank and pump.

4.2.7 The measuring devices

There is a variable parameter that has been measured during the experimental test rig is listed below:

- Temperatuers of water at enterance and at exit
- Fallin of pressure within tubes.
- A volumetric flow rate of water.
- The surface absorber plate temperature.
- Incidence of Solar irradiance.
- Wind speed.
- Ambient temperature.

The devices were used to measure these variables are discussed in details in the next section:

1. 8-channel temperature data loggers V2 module HC-02

The Device specification as follows:

- Measuring 98mm×82mm×30mm
- Digital temperature sensors based on DS18B20 chip.
- Can be controlled from a PC via controlling commands.
- Easily connected to the Android device via Bluetooth.
- Power circuit from USP power supply.

That device used to display the measured temperature value for each of the 8 sensors connected as clear in fig. (4.6), the range of temperature to be evaluate from 125 °C to - 55 °C with an error ± 0.5 ° C, two devices used for these experiments

a. Temperature sensors

The numbers of temperature sensors were 16, The fig. (4.7) showing the 8- stainless steel waterproof sensors to monitor the temperature at diverse places for test rig with dimension 6×50mm the sensor cable can be extended up 10 meters and connected to 8-channel data logger mentioned.

b. Digital thermometer

The fig(4.8) showing the digital thermometer model excel – 3208 and the sensors used to measure the temperature, four sensors used with that device, the range of temperature from -50 °C to 950 °C.

Positions of temperature sensors

The positions and distribution of sensor are shown in the fig (4.9) and fig (4.10) were fixed as the following positions:

- Twelve sensors fixed on the absorber plate surface to measure the temperature of the absorber plate.

- Two sensors fixed in at entrance and exit of collector to evaluate temperature of water at the inlet and outlet respectively.
- Two sensors fixed on the glass 1 cover the to measure surface temperatures of glass.
- Two sensors fixed on the glass 2 to measure surface temperatures of glass.
- One sensor the ambient temperature and one to measure the tank temperature.

2. Water volumetric flow meter

One flow meter with range (1 to 10 liter/minute) installed at the delivery pipe of test rig to measure volumetric rate circulates into the system. producer and scheme of calibration for water flow meter are shown in Appendix (A).Fig. (4.11) shown the flow meter.

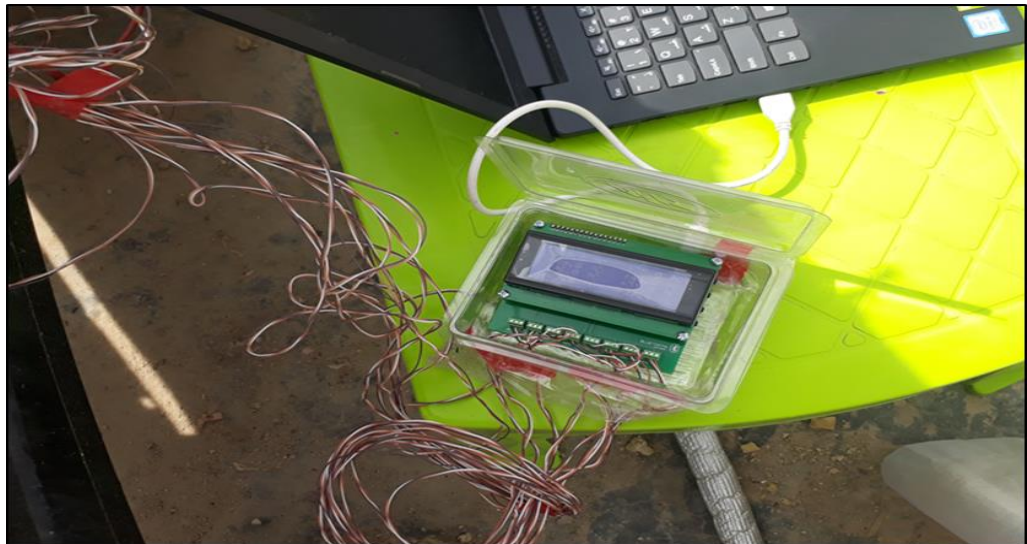


Fig. 4.6: 8-Channel data logger.



Fig. 4.7: Eight temperature sensors.



Fig. 4.8: Digital thermometer.

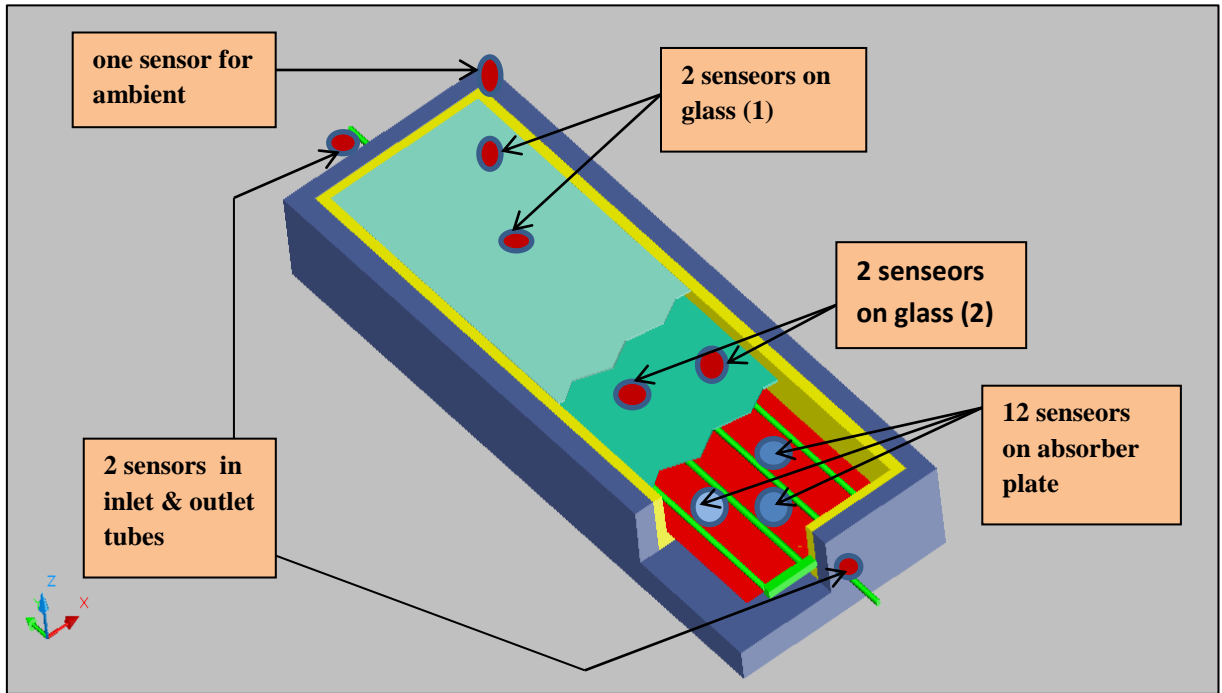


Fig. 4.9: Positions and number of sensors.

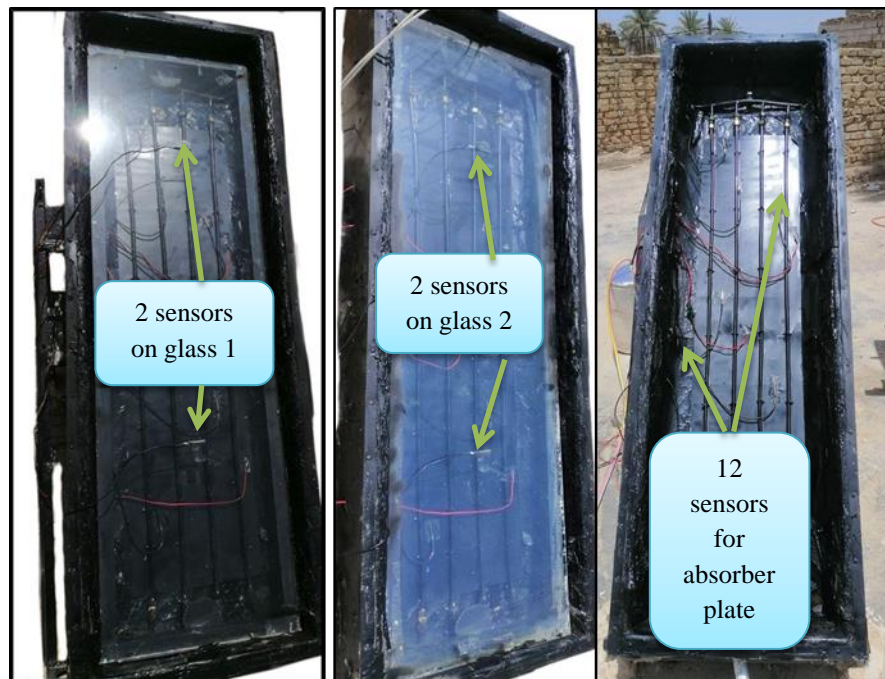


Fig. 4.10: Number and positions of sensors.



Fig. 4.11: Volumetric flow meter.

3. Pressure measurement

Manometer of range (from 5 mbar to 7000 mbar), Model PCE-917 shown in the figure (4.12) uses to display the variation in pressure between the entrance (p_1) and exit of the collector (p_2) through connected the tubes of inlet and outlet respectively.

4. Solar irradiance meter

Protek model DM-301 shown in figure (4.13) used to measure solar irradiance incidence, that device consists of the solar cell (solar panel) and an ohmmeter to measure solar cell DC voltage in m installed at 200 m volt-2000 m volt and converted to solar irradiance w / m^2 For, calibration of the device shown in Appendix (A).

5. Wind speed

To measure the wind speed used the website and weather conditions to evaluate the speed wind instantaneously according to the location of the test rig.

4.3 Experimental procedure

The tests are conducted in five cases by using four different twisted tape insertions furthermore the plain tube and use distilled water as the working fluid.

The following steps have been done for each case:

- a. Fill an insulated tank with 20 liters of fresh distillate water for each working day.
- b. Prepare the measuring instruments to read and record data from the experiments.
- c. Operating the data logger to record the temperature reading and setting for taking the data for every (10 minutesby data logger).
- d. Operating the water pump and setting the flow meter on the wanted
- e. Turn on the soler irradiance device and setting at range 2000 mvolte.

The experimental work was conducted for eight hours from 9:00 AM to 4:00 PM.

That procedure was repeated with the four flow rates (7,5,3and1.5) liter/minute for every five cases (plain tube and four different types of twisted tapes).



Fig. 4.12: Manometer



Fig. 4.13: solar radiation meter.

Chapter Five

RESULTS AND DISCUSSION

Chapter Five

Results and Discussion

5.1 Introduction

This chapter discusses experimental results and provides detailed explanation of them, the experimental work involves water flowing at four volumetric flow rates (7,5,3 and 1,5 LPM) into the manufactured flat plate solar collector, and evaluate the collector performance by inserting four types of twisted tapes with curved front-flow vortex generator (TTFF), twisted tapes with curved opposite-flow vortex generators (TTOF), twisted tapes with straight vortex generators (TTS), and traditional twisted tapes (TT), the experiments were performed during the period (January, February and March)/2020 to compare the effect of using four different twisted tapes on thermohydraulic activity of solar collector with different mass flow rates for water as the working fluid, all experiments were performed at four working fluid mass flow rates (0.11,0.0833,0.05 and 0.025) kg / sec for eight hours from (9:00AM to 4:00PM) in Babal, Iraq, with the temperatures, solar radiation, differential pressure, and wind velocity registered every sixty minutes and three times for each volumetric flow .

The experimental work involves the performance of collector of flat plate type represented by transfer of heat (Nuseelt number) and effect of pressure (factor of friction) within solar collector tubes equipped with four different twisted tapes and compared with smooth tube at four mass flow rates ,the drinkable water used as test fluid at the laminar regime of flow for number of Reynolds (Re) range from 400 to 2000.

5.2 The solar irradiance results

The amounts of irradiation were measured from atmosphere at winter months and for eight hours from 9:00 am to 4:00 pm as shown in figures (5.1) to (5.3), it found that solar radiation was oscillating due to a few days containing few clouds although the days of the experiments were chosen in a situation that could be sunny days, besides, it found that in winter months the diffuse components of solar radiation are more than beam components of solar radiation due to the slope of the northern hemisphere 's rotation axis far from the sun.

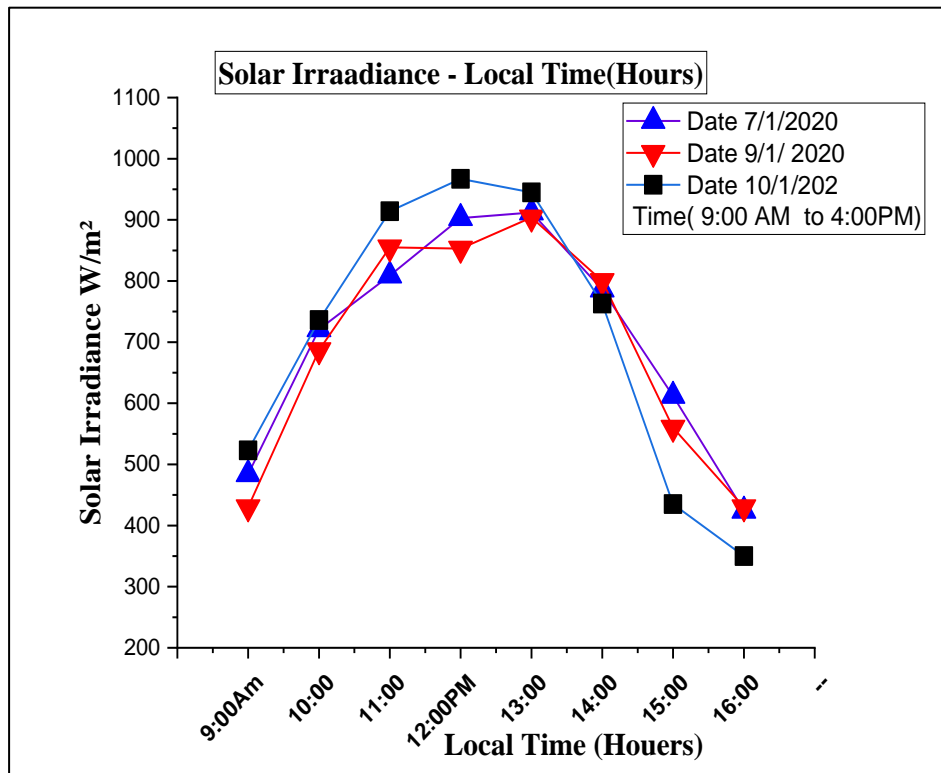


Fig. 5.1: Solar radiation for(7,9,10)/1/2020.

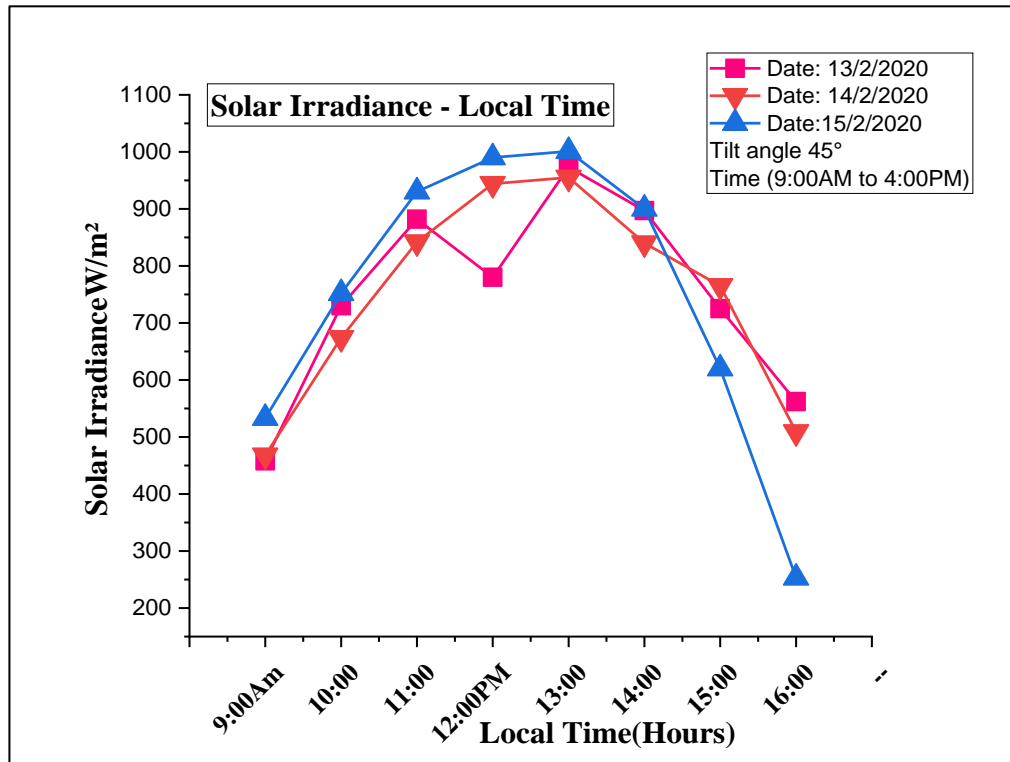


Fig. 5.2: Solar radiation for(13,14,15)/2/2020.

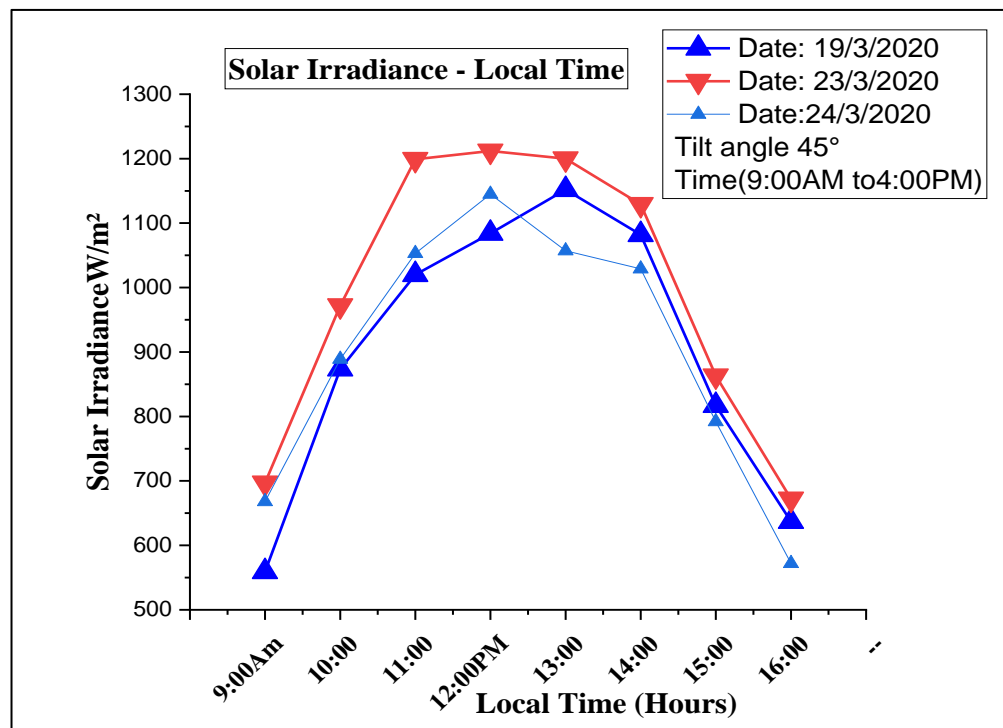


Fig. 5.3:Solar radiation for(19,23,24)/3/2020.

5.3 The results of temperature difference

The water temperature variance between the entrance and the exit influenced by the rate of flow of the working fluid, figures (5.4) to (5.8) show the water inlet -outlet temperature difference with four volumetric flow rates (7, 5, 3, and 1.5) L / min. The decrease in the flow rate has been found to increase the water temperature variation between the exit and the entry, because of the transfer of thermal from the pipe to the water, it is not instantaneous, but takes more time and the duration in small flow rates is large, and the low volumetric flow rate leads to low fluid velocity and therefore to the absorption of more solar energy to increase the temperature. The maximum temperature difference was (18.3 ° C) for 1.5 L / min, as illustrated in fig. (5.7), the temperature difference increased to (11:00 AM) and decreased. The figures (5.4) to (5.8) indicate the outlet and inlet temperature differences for tube fitted with (TTS), (TTFF), (TTOF), (TT) and the smooth pipe for volumetric rates from 7 LPM to 1.5 LPM, the maximum temperature difference was (18.3 ° C, 18.7 ° C, 15.2 ° C, 17 ° C and 14 ° C at (1.5 L / min) within pipe equipped with (TTS), (TTFF), (TTOF), (TT) and for the empty pipe respectively.

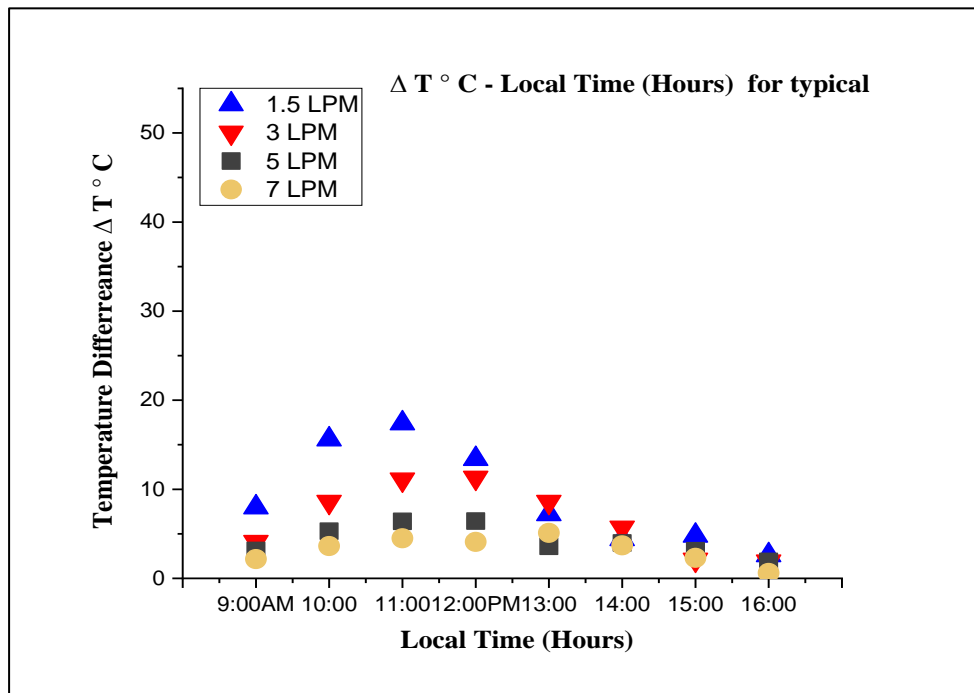


Fig. 5.4: Temperature difference for typical twisted tapes(TT).

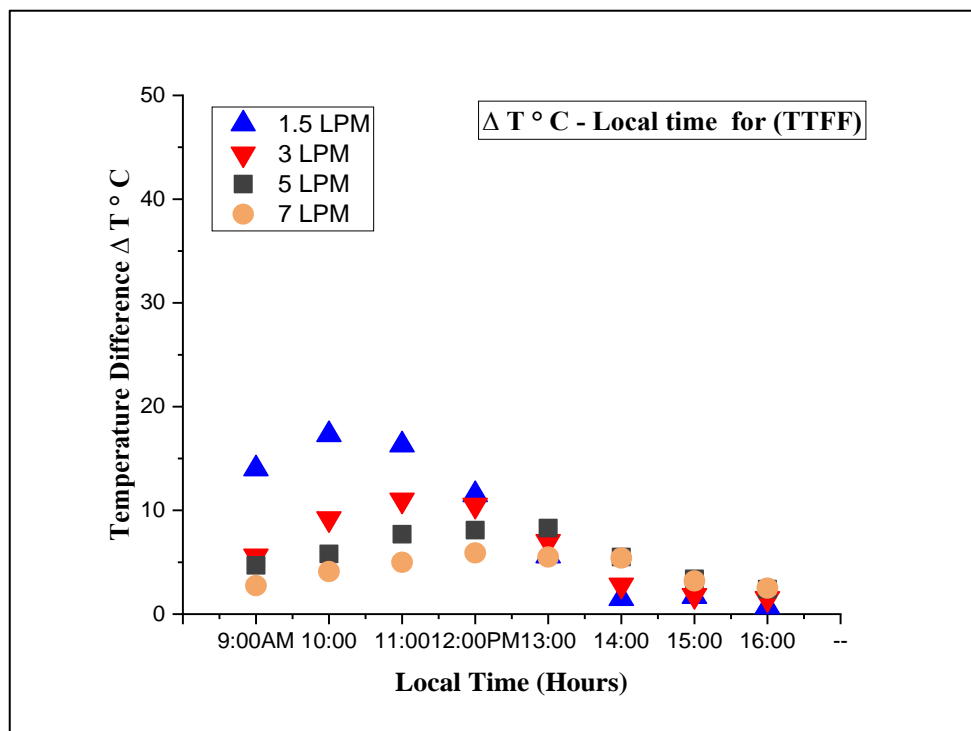


Fig. 5.5: Temperature difference for (TTFF).

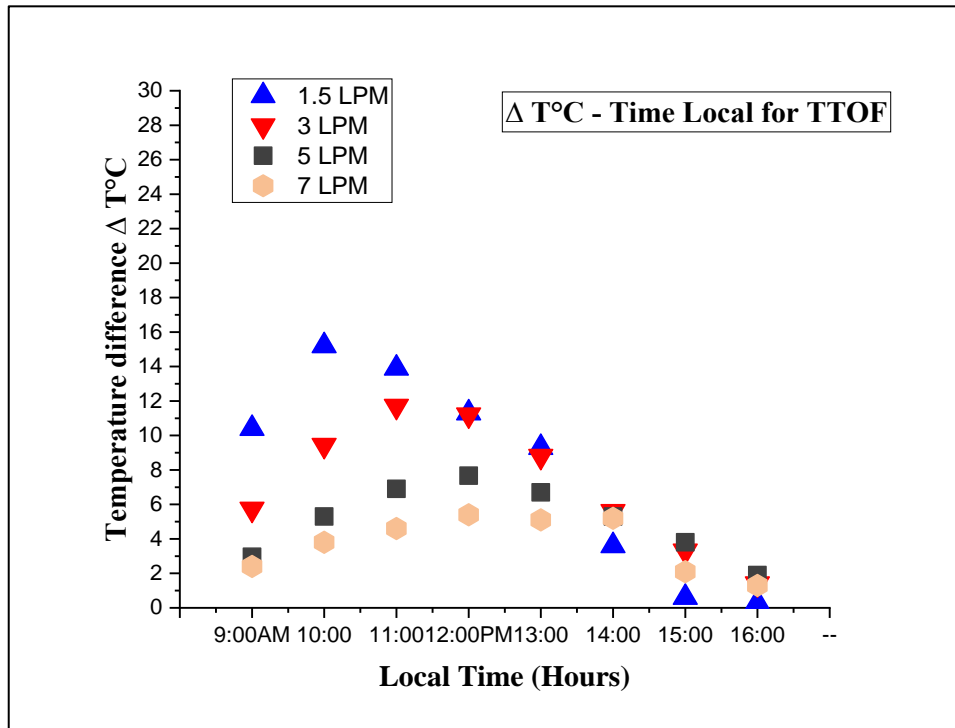


Fig. 5.6: Temperature difference for (TTOF).

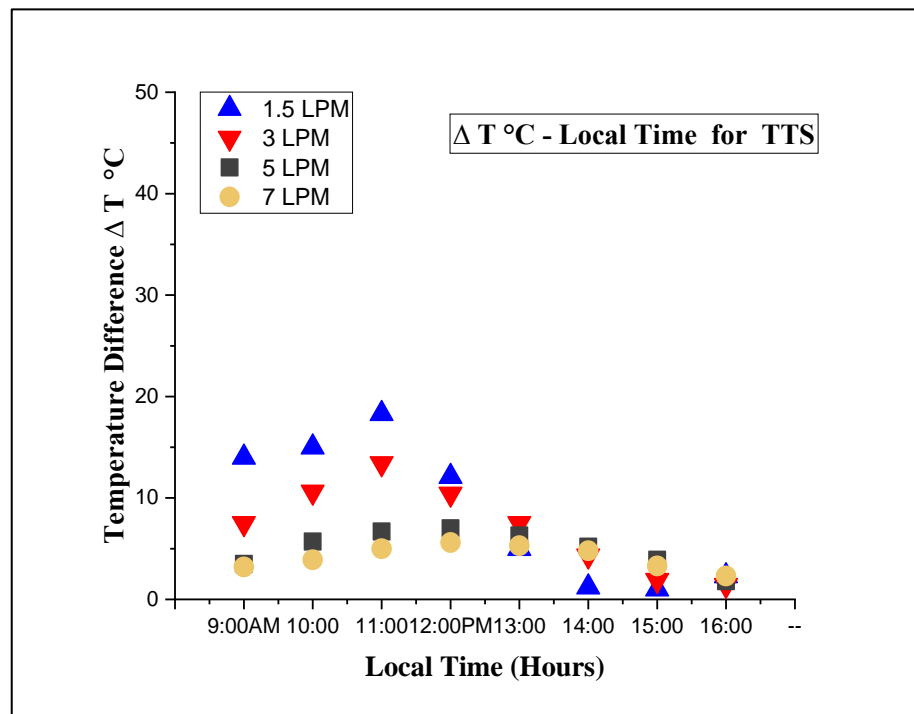


Fig. 5.7: Temperature Difference for (TTS).

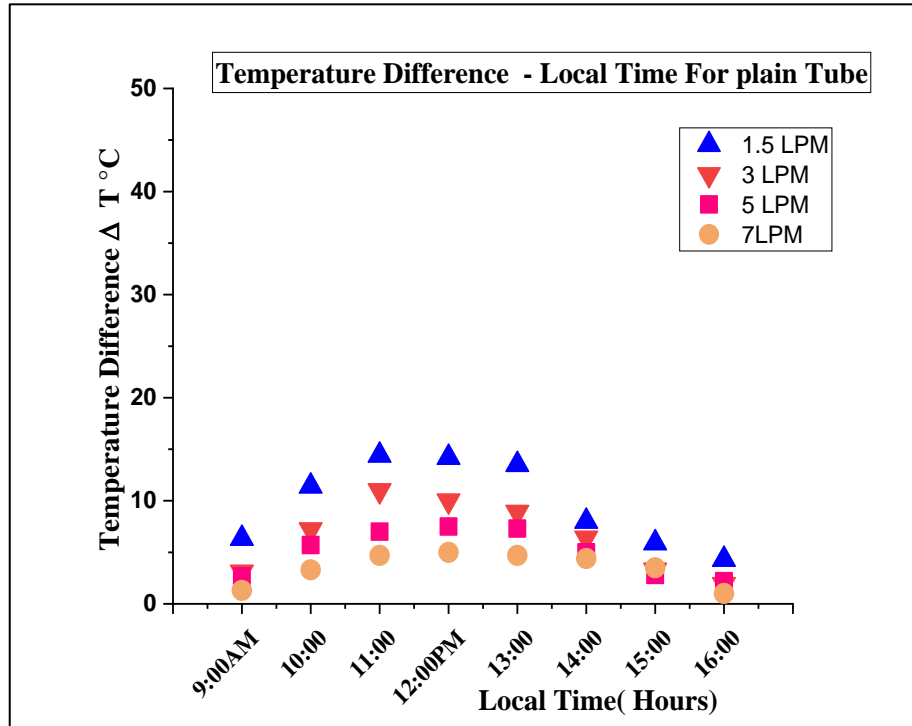


Fig. 5.8: Temperature Difference for the plain tube.

5.4 The result of outlet temperature

Figures (5.9) to (5.12) show the effect of four different twisted tapes (TTFF), (TTOF) and (TTS) at four volumetric flow rates (1.5,3,5 and 7 LPM) on the riser tube outlet temperature (T_{out} °C). The figures (5.9) to (5.12) indicate the maximum outlet temperature within pipe fitted with (TTFF) comparison with other convolute strips and plain pipe. The maximum outlet temperature of the tube equipped (TTFF) was 98 ° C for 1.5 L / min compared with typical twisted tape alone and a smooth tube. The (TTFF) produced stronger and more efficient eddies near the tube wall than other twisted tapes with vortex generators which result in a higher outlet temperature than the other (TTOF, TTS) over typical twisted tapes alone and plain tube. Besides the existence of vortex generators in the front flow helps to increase the disturbance in boundary layer with increase the transfer of heat via region adjacent with tube wall and fluid increasing the outlet temperature in the tube fitted with (TTFF) (Taylor et al.2015)[62].

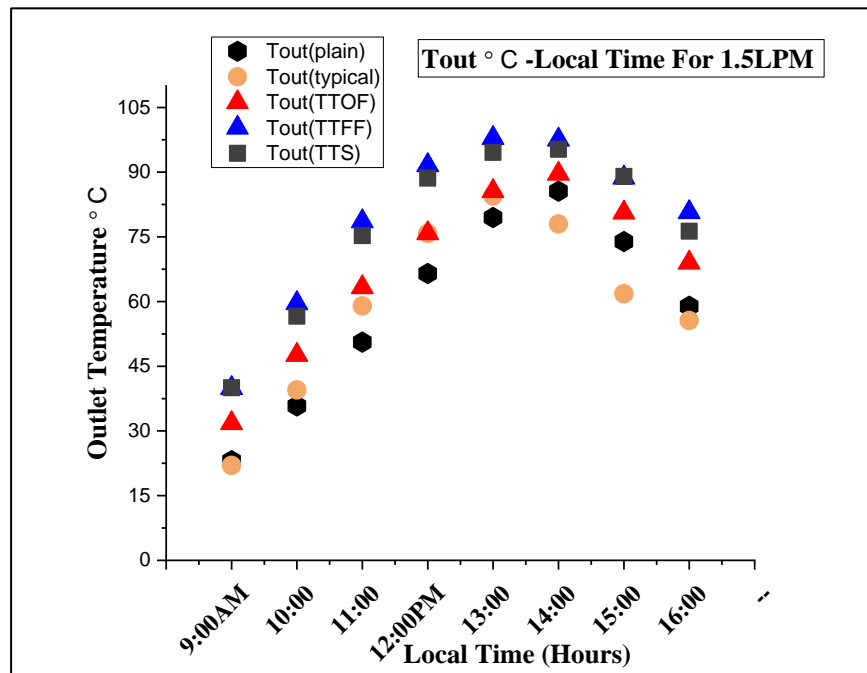


Fig. 5.9: The outlet Temperature for 1.5 L/min.

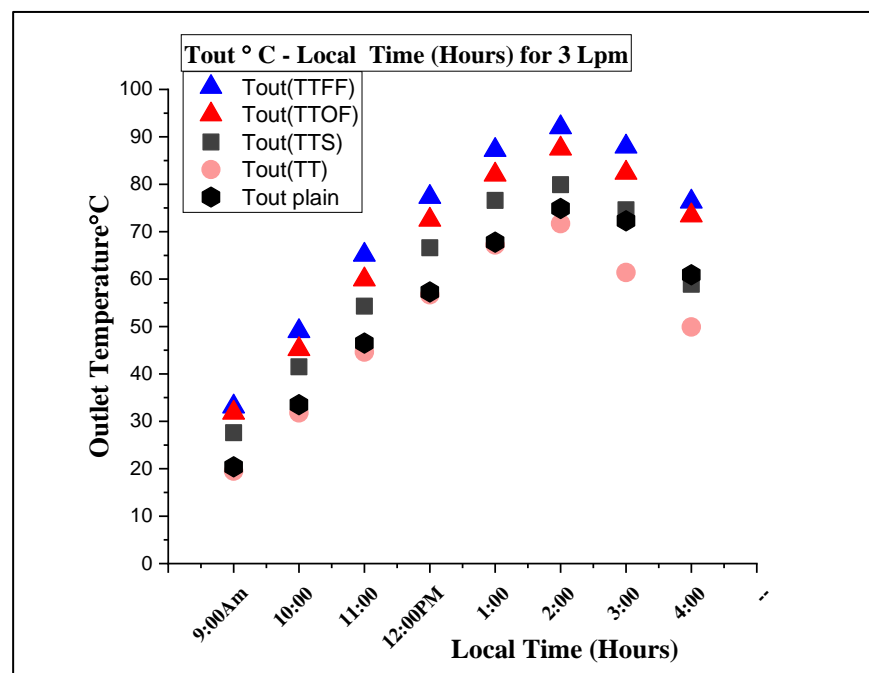


Fig. 5.10: The outlet Temperature for 3L/min.

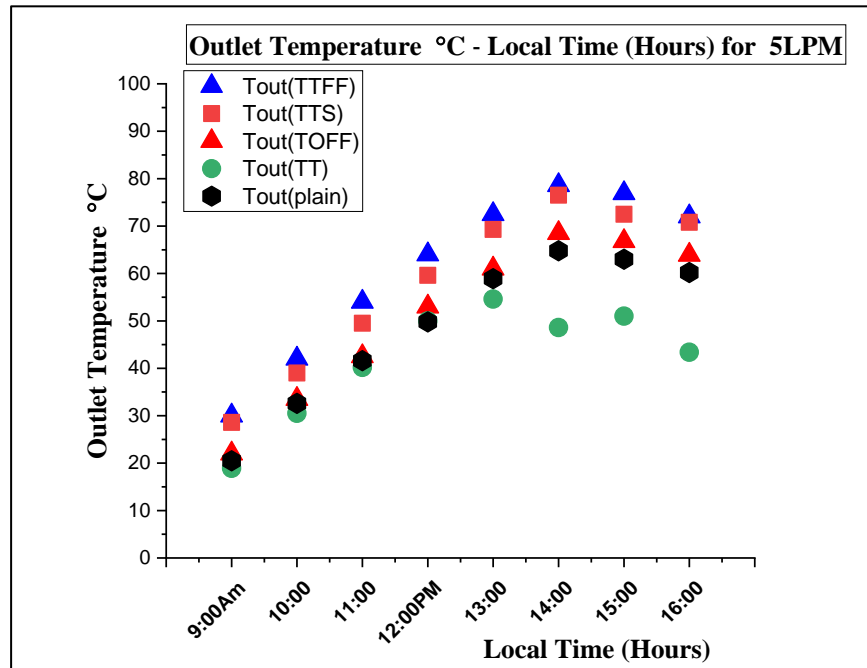


Fig. 5.11: The outlet Temperature for 5 L/min.

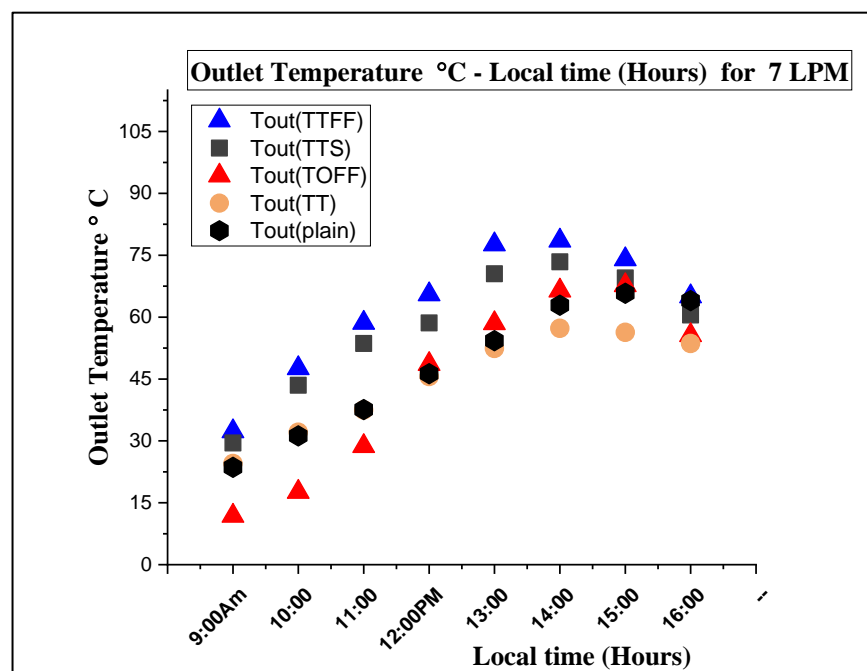


Fig. 5.12: The outlet Temperature for 7L/min.

5.5 The thermal rate variation

At this part, the alteration of thermal flow represented by Nusselt number (Nu) with Local Time also change of number of Nusselt and ratio of Nusselt $Nu(s)/Nu(p)$ against number of Reynolds (Re) is shown to reveal the impact of diverse kinds of twisted tapes on transferd of heat in term Nusselt Number. The figures (5.13) to (5.16) show the Nusselt Number alteration in pipe fitted with four different convolute strips against local time, the maximum thermal rates within pipe provided with curvature vortex generators in front flow twisted tapes (TTFF) compared with twisted tape alone and plain tube at four flow rates (7,5,3 and 1,5LPM).

The figures (5.17) and (5.18) show the disparity for both Number of Nusselt (Nu) and Nuesselt Ratios versus Reynolds Number, the fig. (5.17) shows that the (Nu) obtained from the tube fitted with (TTFF) tends to be larger than that gained from the typical twisted strips (TT) and the plain pipe alone, the Number of Nusselt in pipe equipped with (TTFF) enhanced to 31%,38.2%,40%, and 54.2% compared to the smooth pipe. Figure(5.18) depicts the diversity of Nusselt number in pipes fitted with four various tapes $Nu(s)$ to Nusselt Number in plain tube $Nu(p)$ as a ratio of $Nu(s)/Nu(p)$ with Reynolds Number Re, showing a slight increase in the $Nu(s)/Nu(p)$ ratio with the increment in Re. In pipe fitted with twisted strip with vortex generation, the heat transfer rate was larger than the typical convolute strip alone and smooth tube since the vortex in the twisted tape gives this help to the additional disturbance produced by the typical swirl flow. This behavior directly increases the rate of heat transfer over that provided by the eddy flow alone(S Eiamsa-ard et al. 2010b).[60]. As result to exist these types of convolute strip with front-flow vortex generator, the maximum Nusselt Number supplied in a tube fitted with (TTFF) mixes the bulk flow very well with the additional action of vortex generators in the laminar flow(Yousif and Khudhair 2019) [4].

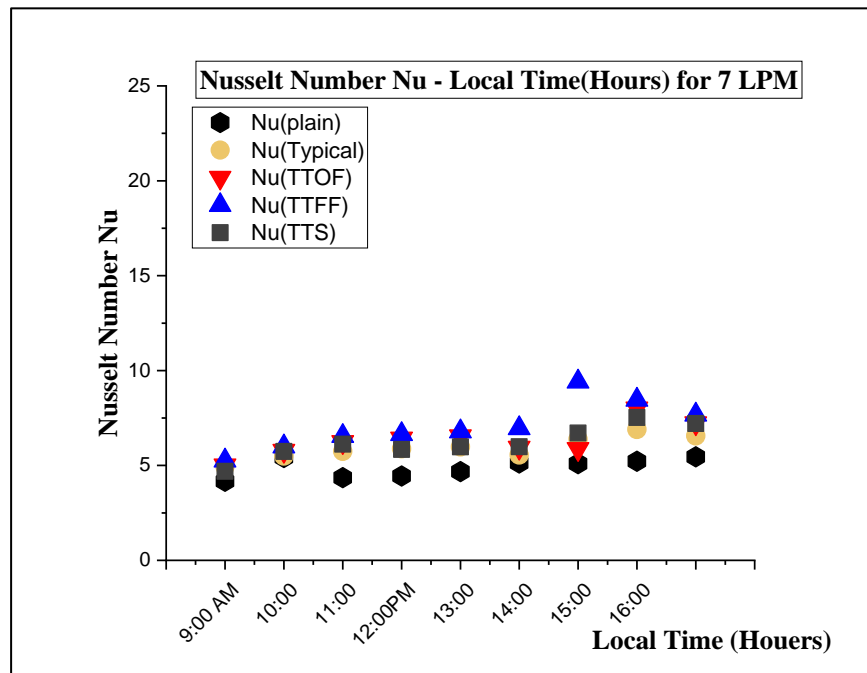


Fig. 5.13: The variation of Nusselt number versus local Time at 7L/min.

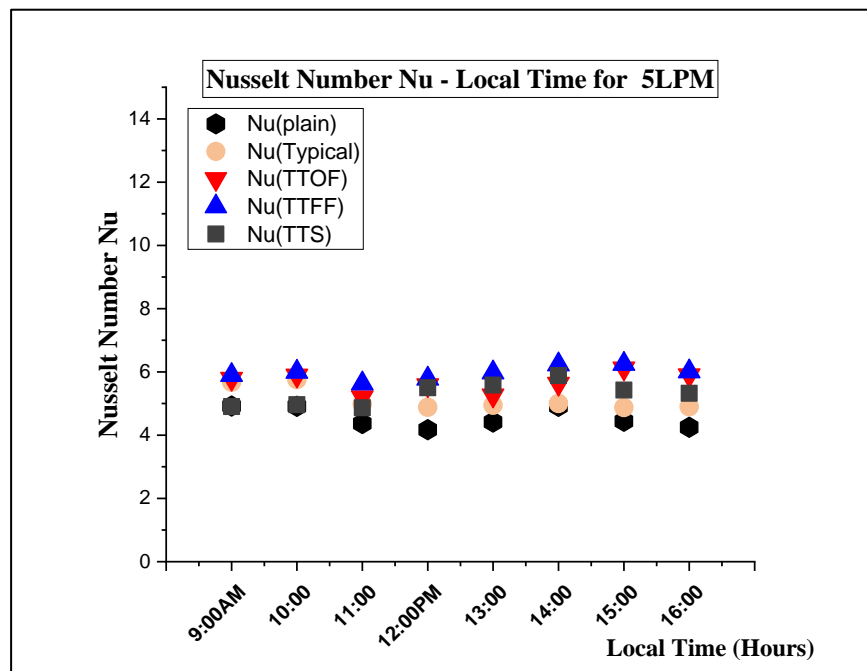


Fig. 5.14: The variation of Nusselt number versus local Time at 5L/min.

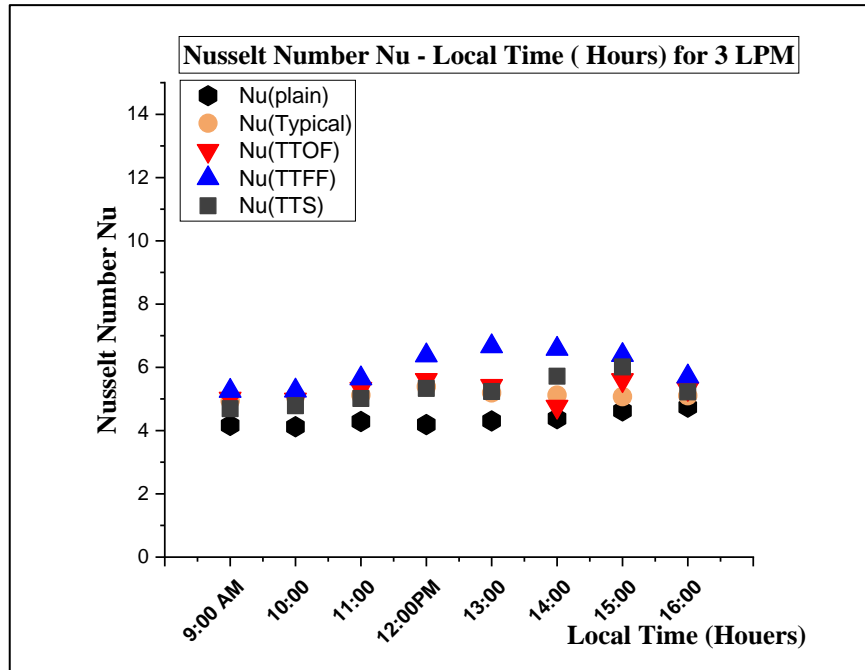


Fig. 5.15: The change of Nusselt Number against Local Time at 3L/min.

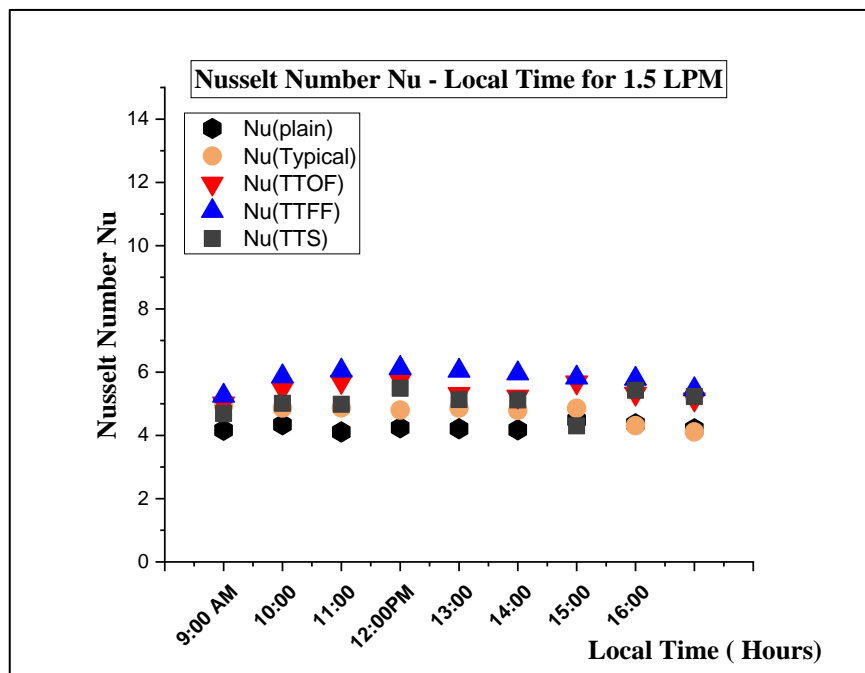


Fig. 5.16: The change of Nusselt Number against local Time at 1.5 L/min.

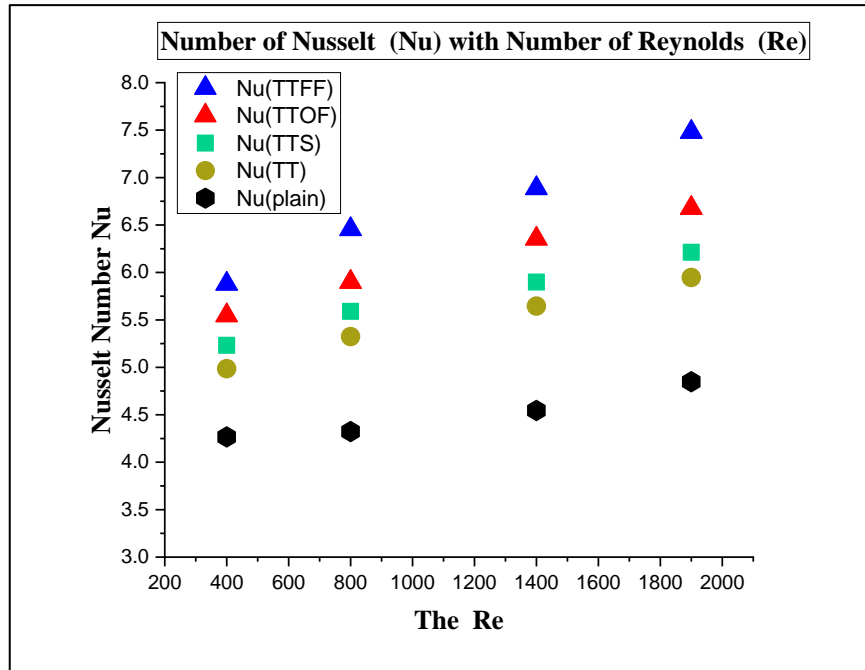


Fig. 5.17: The change of Nusselt number against number of Reynolds Re with (smooth tube TT, TTFF, TTOF, and TTS).

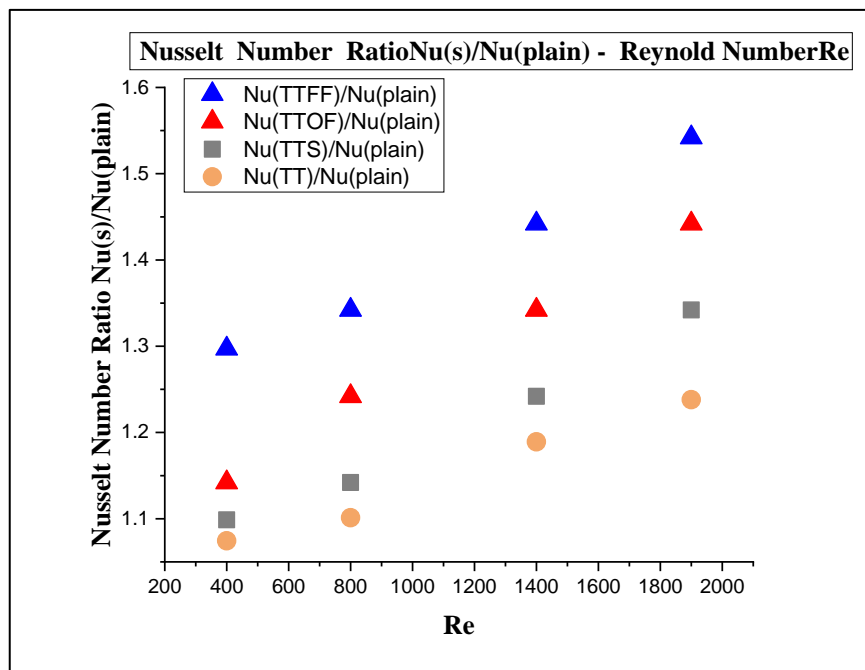


Fig. 5.18: Nusselt number ratio versus The Re with (TT, TTFF, TTOF, and TTS).

5.6 The Results of pressure drop

The factor of friction (f) represent the influence of four types of twisted tape on the pressure drop (Δp) across a tube of solar collector equipped with (TT, TTFF, TTOF, and TTS) was represented and comparesion with the plain tube the employment of combined device insert lead to a effective augment in factor of friction compare with the plain tube at decrease of Reynolds number Re , the twisted tape insert enhances the effective area of the thermal transfer and increases the friction between the fluid and the twisted tape also the tube wall which causes more pressure drop at constant pumping ratio (Manglik and Bergles 2003)[14]. The figures (5.19) to (5.22) illustrate the difference of friction factor for local time to tube equipped with (TT, TTFF, TTOF, and TTS) and compare with plain tube at four volumetric flow rates (7,5,3 and 1.5 LPM), and the figures (5.23) and (5.24) represent the change of friction effect (f) and friction factor ratio $f(s) / f(\text{plain})$ for Reynolds Number respectively.

The figures (5.19) to (5.22) showed the friction factor associated in a tube equipped with (TTFF, TTOF, and TTS) and comparison with (TT) alone and plain tube at four volumetric flow rates (7,5,3 and 1.5 L / min) for the local time from 9:00 AM to 4:00 PM, the friction factor was higher across pipes fitted with twisted strips with vortex generator comparsion with typical convolute strip and plain tube, due to existing vortex generator causes additional pressure loss across the tube. Figures (5.23) and (5.24) shown the variation of the friction effect and the ratio of friction factor for the number of Reynolds respectively. The effect of the convolute strip on the factor of friction shown in fig. (5.23), the friction impact increases at decreases number of Reynolds and the maximum friction effect was created in the tube fitted with (TTFF, TTOF, and TTS) compared to normal strip and smooth tube, the factor of friction (f) in a tube fitted with a TTFF increase around 18%-30% above the plain tube. Fig. (5.24) shown the ratio of $f(s) / f(\text{plain})$ tend to decrease with increase Re .

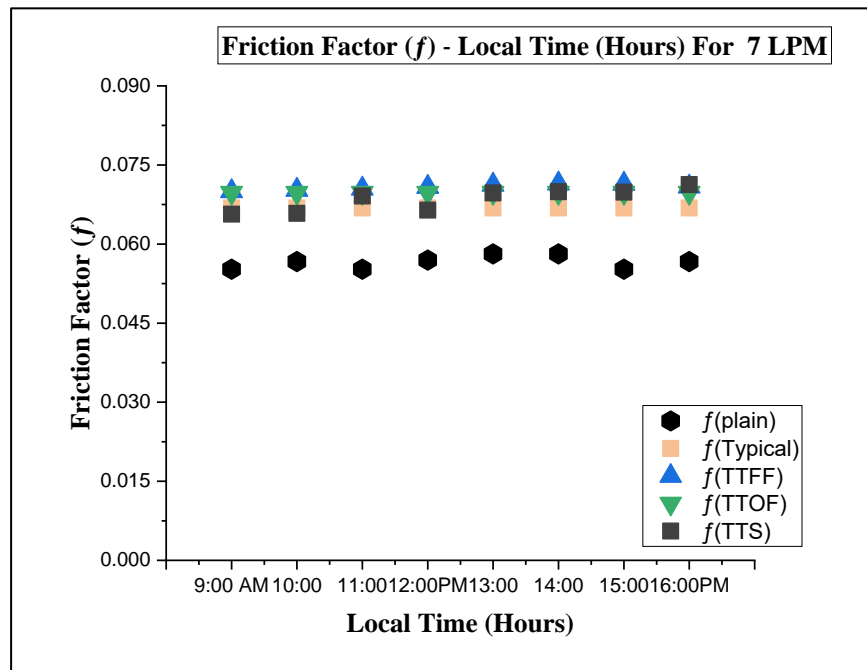


Fig. 5.19: The Factor of Friction change with Local Time at 7L /min.

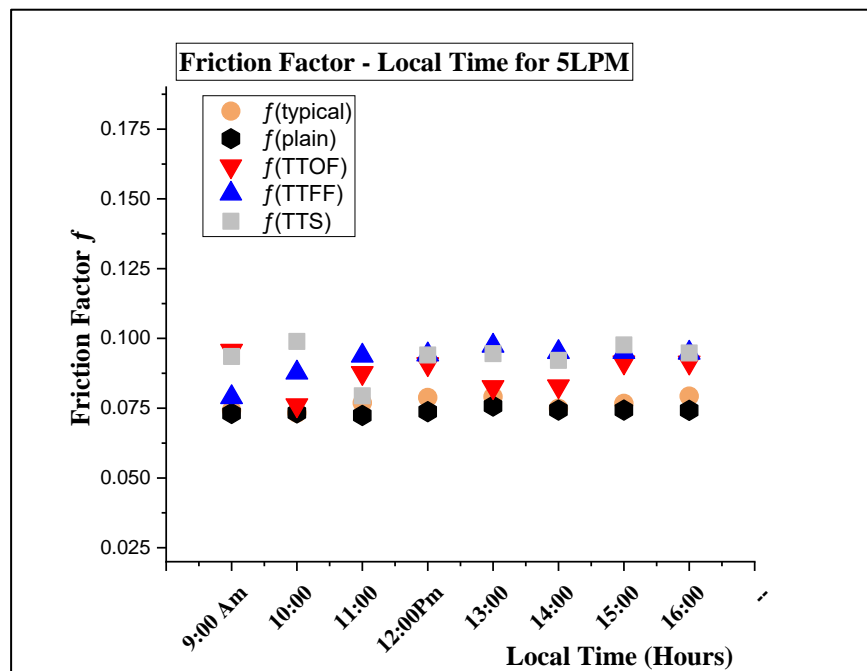


Fig. 5.20: The Factor of Friction variation for Local Time at 5 L/min.

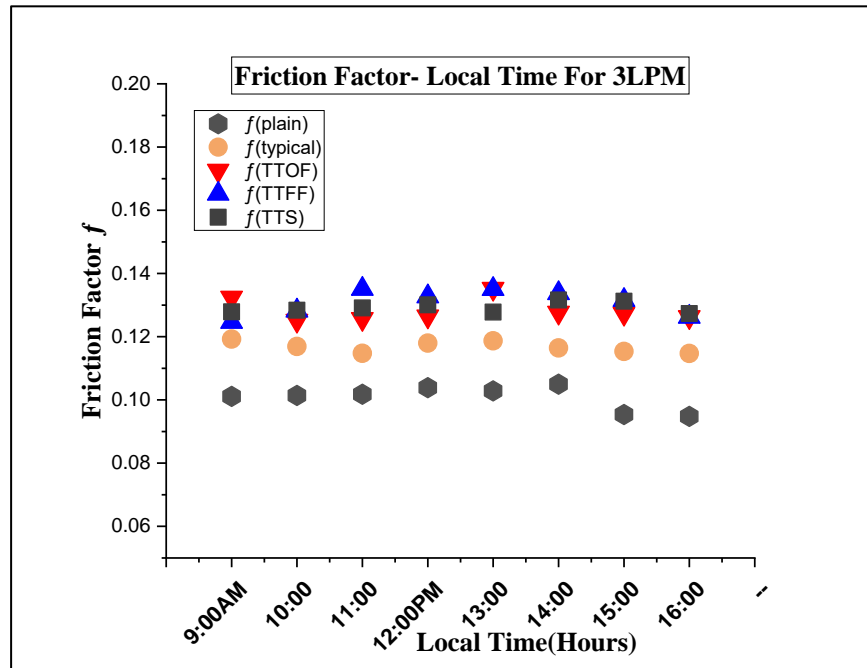


Fig. 5.21: The Friction Factor Variation With Local Time For 3L/min.

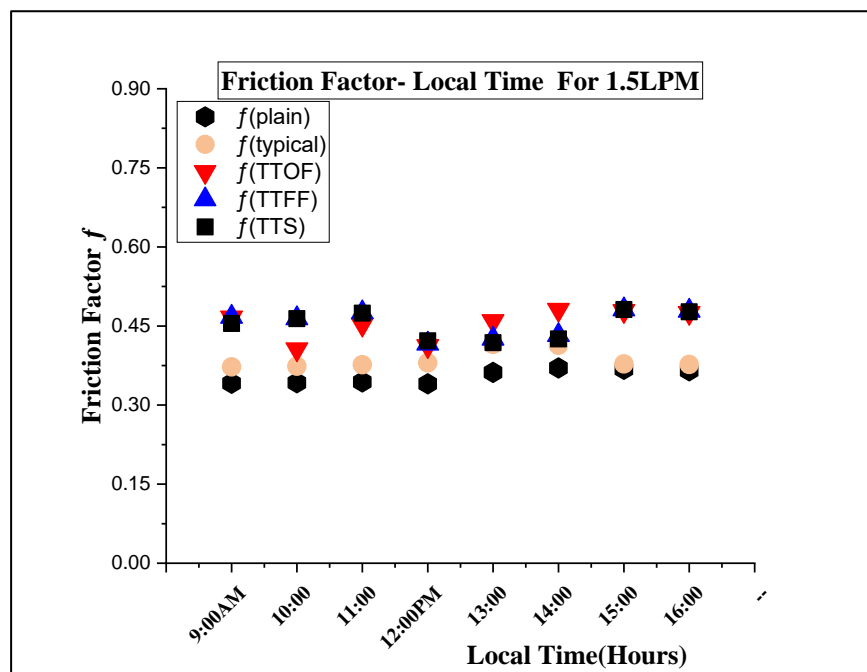


Fig. 5.22: The Friction Factor Variation with Local Time For 1.5 L/min.

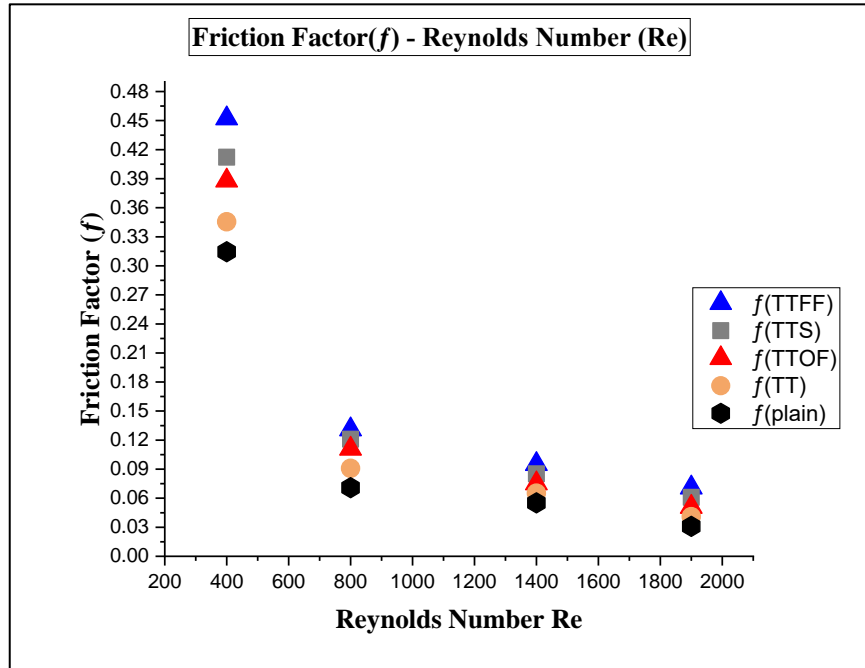


Fig. 5.23: The Factor of Friction versus with Number of Reynolds to (smooth pipe TT, TTFF, TTOF, and TTS)

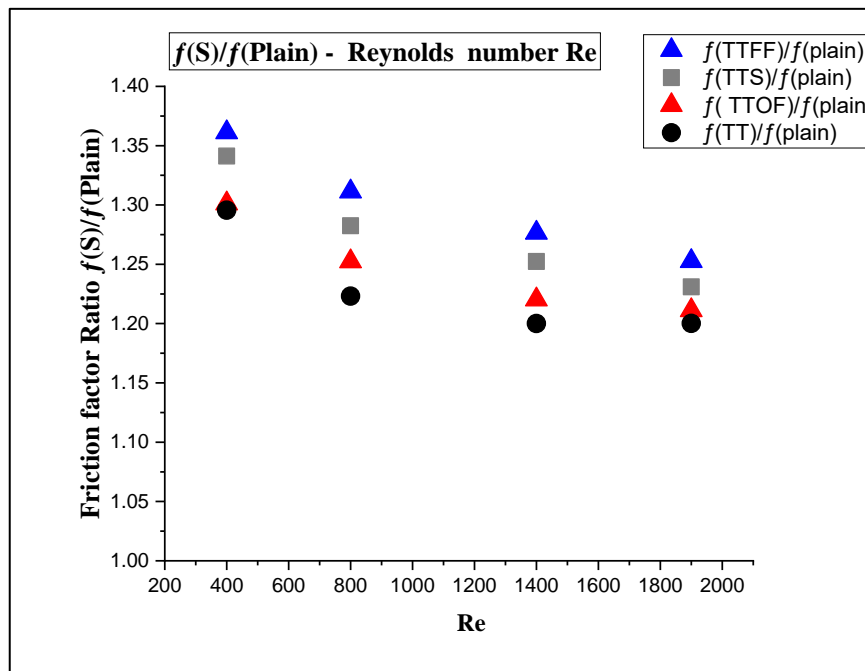


Fig. 5.24: The friction factor ratio versus for Number of Reynolds to (TT, TTFF, TTOF, and TTS)

5.7 The factor of thermal performance (TPF)

The performance ratio (TPF) showing the practical advantage it is obtained from equation (3.34), in which heat transfer rate and factor of friction are simultaneously calculated within pipe with and without twisted tape at constant pumping ratio. The figures (5.25) to (5.28) shows the performance ratio to different twisted tapes variations for local time at four volumetric flow rates (7.5, 3 and 1.5 L / min) and the fig.(5.29) displays the variability of performance ratio for tube fitted with four twisted tapes (TTS, TTFF, TTOF, and TT) with Reynolds number Re .

The figures (5.25) to (5.28) showed that the thermal performance factors (TPF) for TTFF, TTOF, and TTS, they were greater than one and much higher than normal twisted tape (TT). The figure(5.29) represents the change in TPF for the number of Reynolds Re , the TPF for TTFF is higher than the other twisted tapes with the same pumping power and due to additional fluid disturbance, the maximum performance ratio was generated within pipe equipped with convolute strip with vortex generators, which also indicates excellent mixing of fluids leading to higher heat transfer rates than pressure loss, this discovers the feature of convolute strip with vortex generators and comparison with normal strip, considering power saving and vortex generators have a beneficial impact on the efficiency of collector over a typical convolute strip alone. The maximum performance ratio in pipe equipped with (TTFF) of 1.4.

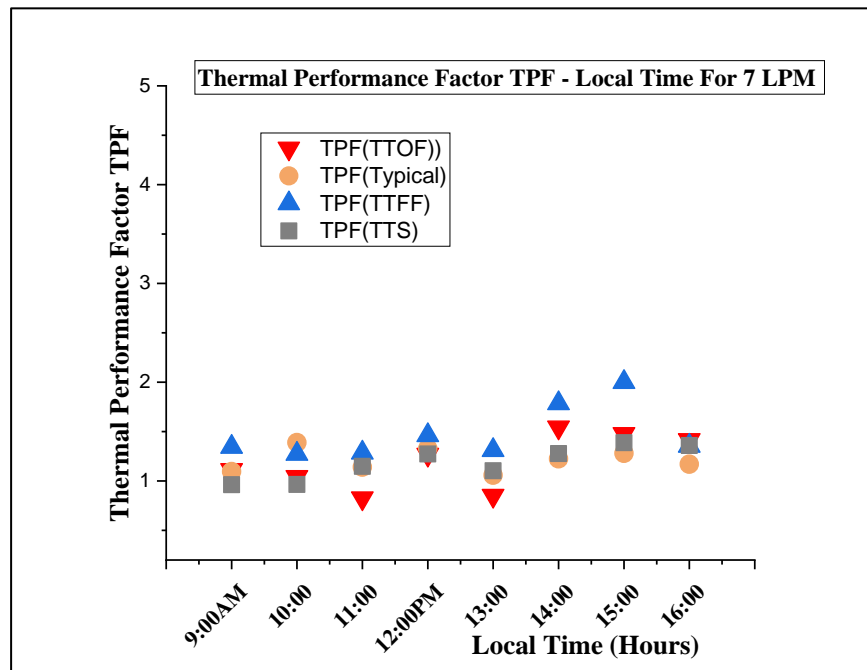


Fig. 5.25: Thermal Performance Factor with Local Time for 7 L/min.

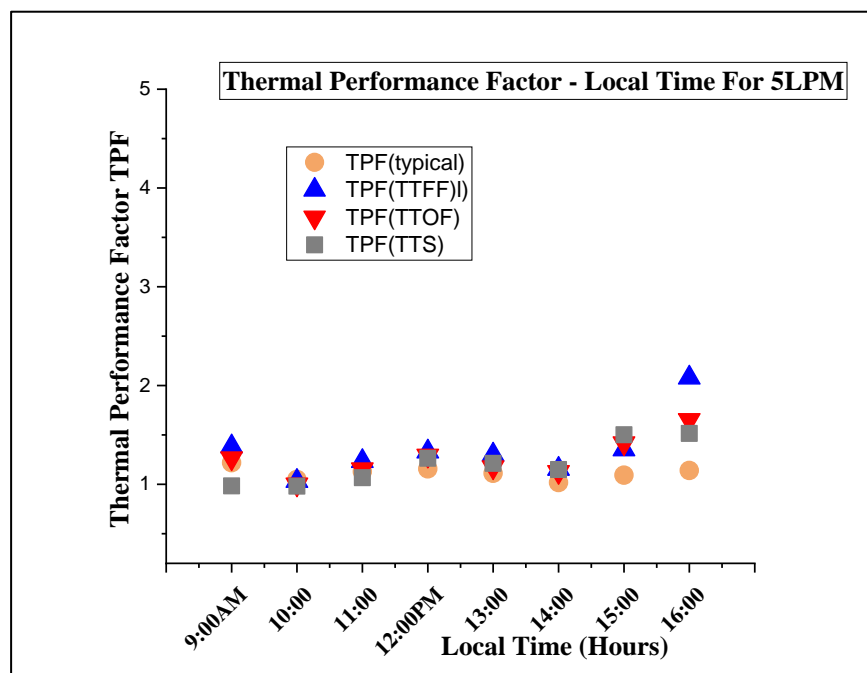


Fig. 5.26: Thermal Performance Factor with Local Time For 5 L/min.

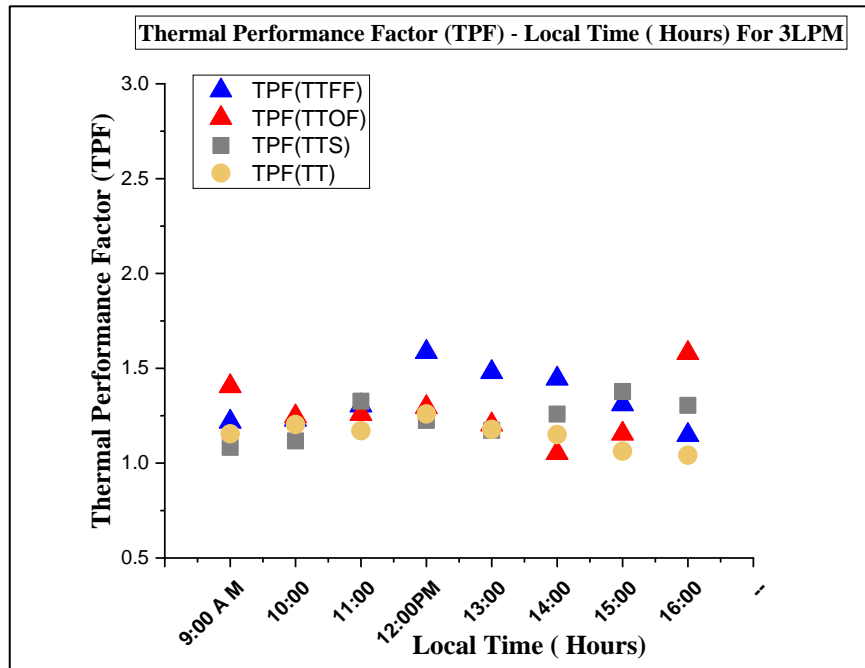


Fig. 5.27: Thermal Performance Factor with Local Time For 3LPM.

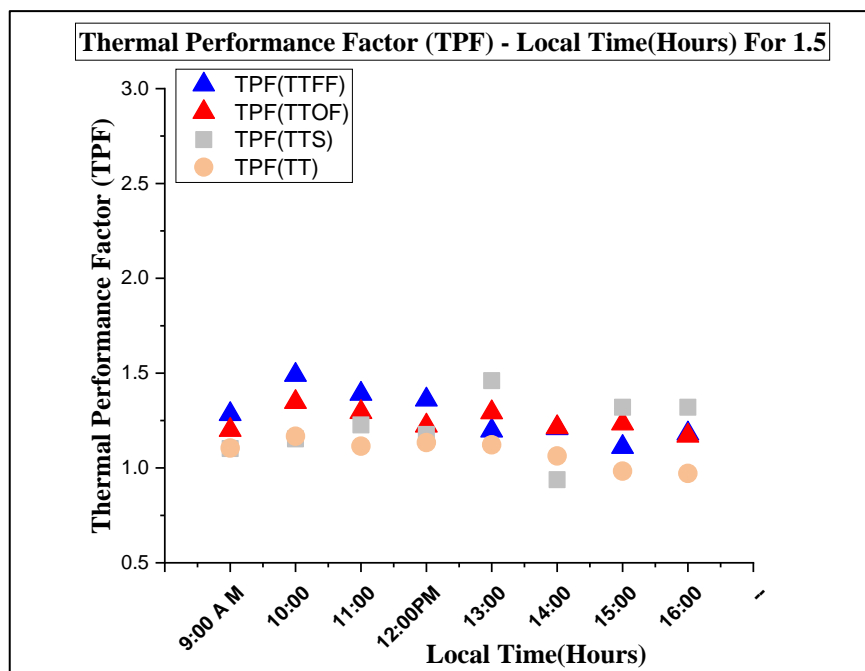


Fig. 5.28: Thermal Performance Factor with Local Time for 1.5 L/min.

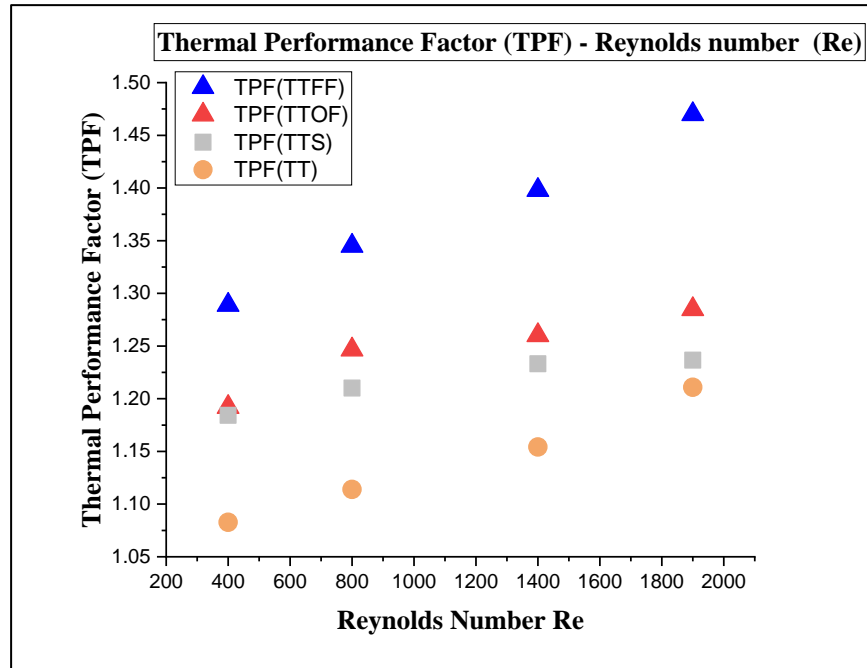


Fig. 5.29: The Performance ratio (TPF) versus Number of Reynolds Re for TT, TTFF, TTOF, and TTS

5.8 Collector efficiency

Figure(5.30) illustrated the influence of convolute strip includ a vortex generator on solar collector efficiency for the Reynolds number. The figure showed maximum efficiency(η) in the riser tube fitted with (TTFF) for constant pumping power and stable condition. This is the fact that the twisted profile of the aluminum strip generates eddy motion and decrease the size of hydraulic, which ensures the effective fluid blending, at the same time the presence of a curvature vortex generator(CVG) in front flow in the twisted tapes improves the time the fluid remains in the riser tubes which rises the heat flow. Hence the heat transfer improvement is higher than the friction factor increasement lead to maximum efficiency [22]. The maximum efficiency found 64.7% in a tube with TTFF.

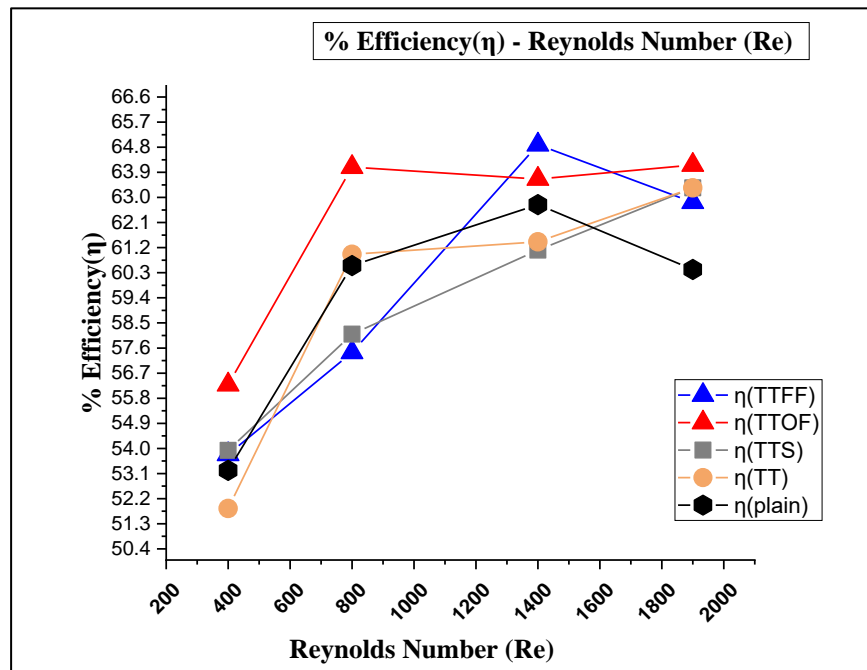


Fig. 5.30: The efficiency of solar collector verse with Reynolds number Re for(TT, TTFF, TTOF, TTS, and plain tube)

Chapter Six

Conclusions

&

Recommendation

Chapter Six

Conclusion and Recommendation

The research aimed to study the impact of four different twisted tapes (TT, TTFF, TTOF, and TTS) on the performance of solar collectors with the laminar flow regime ($300 < Re < 2000$) under stable conditions and constant pumping power at different volumetric flow rates (7, 5, 3 and 1.5 L / min) and to analyze the influence on heat rate and drop of pressure . Chapter abbreviated the principal conclusion of this study, and suggestions for further research are also mentioned.

6.1 The conclusion

The concluded study topics are as follows:

1. The maximum temperature difference achieved for solar collector fitted with TTFF was 5.9 ° C, 8.3 ° C, 13.4 ° C and 18.3 ° C for volume flow rates 7, 5, 3 and 1.5 LPM respectively.
2. The outlet temperature of the water increases within pipe equipped with vortex generator twisted strip over because makes the vortex in the twisted tape more disrupt the thermal layer. The maximum outlet temperature reached in a TTFF tube was 75 ° C, 77.88 ° C, and 97.9 ° C, from (7 L / min to 1.5 LPM) respectively.
3. The twisted tape generally increased the heat rate in term Nu and drop in pressure in term friction factor due to fluid swirling that produces a secondary flow and reduces hydraulic diameters. The TTFF increased the heat transfer rate that improved to 31.4%, 38.1%, 39.9% and 54.3% at ($300 < R < 2000$) respectively.

4. The extra pressure dropped and the friction factor increase around 18% - 30% with increment the Reynolds number.
5. The performance ratio (TPF) in the tube equipped with convolute strip with vortex generators was larger than the typical twisted tape and plain tube, the maximum TPF was 1.4 for tube fitted with TTFF.
6. The fact that the twisted tape induces swirl flow and decreases the hydraulic diameter which ensures a best blending of the fluid.
7. The maximum efficiency was 64.7 % in the riser tube fitted with TTFF at constant pump ratio and laminar flow regime ($300 < Re < 2000$).

6.2 The recommendations

Following are the recommendations for future work:

1. Investigating the impact of twisted tape with vortex generator on the efficiency of solar collectors using water and nanofluid as working fluids.
2. Investigating the influence of variation of curvature vortex generator twisted tape geometric and design parameters of solar collectors on the performance ratio of system.
3. Studying the influence of vortex generator convolute strip on the thermal performance of solar collectors under turbulent and laminar flow regimes with water and nanofluid.
4. Investigating the effect of another type of vortex generators convolute strips on the efficiency of the solar collector.
5. Comparison of the circular and other cross-sections of riser tubes (for example, square and rectangular) to detect the influence of convolute curvature tape on the performance of solar collectors.

References

References

- [1] S. A. Kalogirou, “Solar Energy Engineering: Processes and Systems: Second Edition,” *Sol. Energy Eng. Process. Syst. Second Ed.*, pp. 1–819, 2014, doi: 10.1016/C2011-0-07038-2.
- [2] M. Hallquits, “Heat Transfer and Pressure Drop Characteristics of Smooth Tubes At a Constant Heat Flux in the Transitional Flow Regime,” no. December, pp. 1–145, 2011.
- [3] A. R. A. Khaled, M. Siddique, N. I. Abdulhafiz, and A. Y. Boukhary, “Recent advances in heat transfer enhancements: A review report,” *Int. J. Chem. Eng.*, vol. 2010, no. 1, 2010, doi: 10.1155/2010/106461.
- [4] A. H. Yousif and M. R. Khudhair, “Enhancement Heat Transfer in a Tube Fitted with Passive Technique as Twisted Tape Insert - A Comprehensive Review,” vol. 7, no. 1, pp. 20–34, 2019, doi: 10.12691/ajme-7-1-3.
- [5] G. R. Saraf and F. A. W. Hamad, “Optimum tilt angle for a flat plate solar collector,” *Energy Convers. Manag.*, vol. 28, no. 2, pp. 185–191, 1988, doi: 10.1016/0196-8904(88)90044-1.
- [6] C. Stanciu and D. Stanciu, “Optimum tilt angle for flat plate collectors all over the World - A declination dependence formula and comparisons of three solar radiation models,” *Energy Convers. Manag.*, vol. 81, pp. 133–143, 2014, doi: 10.1016/j.enconman.2014.02.016.

- [7] A. E. Bergles, G. S. Brown, R. A. Lee, R. R. Snider, and S. W.D., “Investigation of Heat Transfer Augmentation Through Use of Internally Finned and Roughened Tubes,” *Eng. Proj. Lab. MIT*, no. May 1970, doi: 10.1109/AOE.2006.307325.
- [8] E. Bergles and H. L. Morton, “Survey and evaluation of techniques to augment convective heat transfer,” no. February 1965.
- [9] A. Dewan, P. Mahanta, K. S. Raju, and P. Suresh Kumar, “Review of passive heat transfer augmentation techniques,” *Proc. Inst. Mech. Eng. Part A J. Power Energy*, vol. 218, no. 7, pp. 509–527, 2004, doi: 10.1243/0957650042456953.
- [10] E. A. M. Elshafei, M. Safwat Mohamed, H. Mansour, and M. Sakr, “Experimental study of heat transfer in pulsating turbulent flow in a pipe,” *Int. J. Heat Fluid Flow*, vol. 29, no. 4, pp. 1029–1038, 2008, doi: 10.1016/j.ijheatfluidflow.2008.03.018.
- [11] S. Liu and M. Sakr, “A comprehensive review on passive heat transfer enhancements in pipe exchangers,” *Renew. Sustain. Energy Rev.*, vol. 19, pp. 64–81, 2013, doi: 10.1016/j.rser.2012.11.021.
- [12] C. Man, C. Wang, and J. Yao, “The current situation of the study on twisted tape inserts in pipe exchangers,” *J. Mar. Sci. Appl.*, vol. 13, no. 4, pp. 477–483, 2014, doi: 10.1007/s11804-014-1273-7.

- [13] R. Ecke, "The Turbulence Problem," no. 29, pp. 124–141, 2004.
- [14] R. M. Manglik and A. E. Bergles, *Swirl flow heat transfer and pressure drop with twisted-tape inserts*, vol. 36, no. C. 2003.
- [15] S. Zhang, L. Lu, C. Dong, and S. Hyun, "Performance evaluation of a double-pipe heat exchanger fitted with self-rotating twisted tapes," *Appl. Therm. Eng.*, vol. 158, no. May, p. 113770, 2019, doi: 10.1016/j.applthermaleng.2019.113770.
- [16] P. Taylor, S. V Patil, and P. V. V. Babu, "Square Duct Fitted With Increasing and Decreasing Heat Transfer and Pressure Drop Studies Through a Square Duct Fitted With Increasing and," no. October, pp. 37–41, 2014, doi: 10.1080/01457632.2013.877318.
- [17] S. V. P. P. V Vijaybabu, "Heat transfer enhancement through a square duct fitted with twisted tape inserts," pp. 1803–1811, 2012, doi: 10.1007/s00231-012-1031-9.
- [18] S. Eiamsa-ard, K. Wongcharee, and P. Promvonge, "Influence of Nonuniform Twisted Tape on Heat Transfer Enhancement Characteristics," *Chem. Eng. Commun.*, vol. 199, no. 10, pp. 1279–1297, 2012, doi: 10.1080/00986445.2012.668724.
- [19] M. Rahimi, S. Reza, and A. Abdulaziz, "Chemical Engineering and Processing : Process Intensification Experimental and CFD studies on heat transfer and friction factor characteristics of a tube equipped with modified twisted tape inserts," vol. 48, pp.

762–770, 2009, DOI: 10.1016/J.SEP2008.09.007.

- [20] S. R. Shabaniyan, M. Rahimi, M. Shahhosseini, and A. A. Alsaira, “CFD and experimental studies on heat transfer enhancement in an air cooler equipped with different tube inserts ☆,” vol. 38, pp. 383–390, 2011, doi: 10.1016/j.icheatmasstransfer.2010.12.015.
- [21] M. J. M. Sheikholeslami, Z. Li, and R. Moradi, “Nanofluid turbulent flow in a pipe under the effect of twisted tape with the alternate axis,” *J. Therm. Anal. Calorim.*, vol. 2, 2018, doi: 10.1007/s10973-018-7093-2.
- [22] M. Murugan, R. Vijayan, A. Saravanan, and S. Jaisankar, “Performance enhancement of centrally finned twist inserted solar collector using corrugated booster reflectors,” *Energy*, vol. 168, pp. 858–869, 2019, doi: 10.1016/j.energy.2018.11.134.
- [23] P. Sivashanmugam and P. K. Nagarajan, “Studies on heat transfer and friction factor characteristics of laminar flow through a circular tube fitted with right and left helical screw-tape inserts,” vol. 32, pp. 192–197, 2007, doi: 10.1016/j.expthermflusci.2007.03.005.
- [24] P. Sivashanmugam and S. Suresh, “Experimental studies on heat transfer and friction factor characteristics of turbulent flow through a circular tube fitted with regularly spaced helical screw-tape inserts,” vol. 27, pp. 1311–1319, 2007, doi: 10.1016/j.applthermaleng.2006.10.035.

- [25] M. Moawed, “Heat transfer and friction factor inside elliptic tubes fitted with helical screw-tape inserts,” pp. 1–16, 2011, doi: 10.1063/1.3582940.
- [26] M. M. K. Bhuiya *et al.*, “Heat transfer enhancement and development of correlation for turbulent flow through a tube with triple-helical tape inserts ☆,” *Int. Commun. Heat Mass Transf.*, vol. 39, no. 1, pp. 94–101, 2012, doi: 10.1016/j.icheatmasstransfer.2011.09.007.
- [27] A. El, A. Laknizi, S. Saadeddine, A. Ben, M. Meziane, and M. El, “Numerical design and investigation of heat transfer enhancement and performance for an annulus with continuous helical baffles in a double-pipe heat exchanger,” *Energy Convers. Manag.*, vol. 133, pp. 76–86, 2017, doi: 10.1016/j.enconman.2016.12.002.
- [28] K. Ahmed, O. Le, I. Andri, A. Pina, and J. Fournier, “ScienceDirect ScienceDirect study heat transfer enhancement and fluid flow 15th of CFD study of heat enhancement and fluid flow characteristics of laminar flow through the tube with helical helical screw tape t,” *Energy Procedia*, vol. 160, pp. 699–706, 2019, doi: 10.1016/j.egypro.2019.02.190.
- [29] S. K. Saha, A. Dutta, and S. K. Dhal, “Friction and heat transfer characteristics of laminar swirl flow through a circular tube ®

- fitted for orderly spaced convolute-strip elements,” vol. 44, PP. 7845–4545, 2001.
- [30] S. Eiamsa-ard, C. Thianpong, and P. Promvonge, “Experimental investigation of heat transfer and flow friction in a circular tube fitted with regularly spaced twisted tape elements ☆,” vol. 33, pp. 1225–1233, 2006, doi: 10.1016/j.icheatmasstransfer.2006.08.002.
- [31] S. Eiamsa-ard, C. Thianpong, P. Eiamsa-ard, and P. Promvonge, “Convective heat transfer in a circular tube with short-length twisted tape insert ☆,” *Int. Commun. Heat Mass Transf.*, vol. 36, no. 4, pp. 365–371, 2009, doi: 10.1016/j.icheatmasstransfer.2009.01.006.
- [32] S. N. Sarada, A. V. S. R. Raju, K. K. Radha, and L. S. Sunder, “Enhancement of heat transfer using varying width twisted tape inserts,” vol. 2, no. 6, pp. 107–118, 2010.
- [33] E. Esmaeilzadeh, H. Almohammadi, A. Nokhosteen, A. Motezaker, and A. N. Omrani, “International Journal of Thermal Sciences Study on heat transfer and friction factor characteristics of $g\text{-Al}_2\text{O}_3$ / water through a circular tube with twisted tape inserts with different thicknesses,” *Int. J. Therm. Sci.*, vol. 82, pp. 72–83, 2014, doi: 10.1016/j.ijthermalsci.2014.03.005.
- [34] N. Piriayarungrod, C. Thianpong, M. Pimsarn, and K. Nanan, “Heat transfer enhancement by tapered twisted tape inserts,”

Elsevier B.V., 2015, DOI: 10.1016/J.SEP.2015.08.002.

- [35] S. Eiamsa-ard, C. Thianpong, P. Eiamsa-ard, and P. Promvonge, “Thermal characteristics in a heat exchanger tube fitted with dual twisted tape elements in tandem,” *Int. Commun. Heat Mass Transf.*, vol. 37, no. 1, pp. 39–46, 2010, doi: 10.1016/j.icheatmasstransfer.2009.08.010.
- [36] S. Eiamsa-Ard and K. Wongcharee, “Heat transfer characteristics in micro -fin tube equipped with double twisted tapes: Effect of twisted tape and micro-fin tube arrangements,” *J. Hydrodyn.*, vol. 25, no. 2, pp. 205–214, 2013, doi: 10.1016/S1001-6058(13)60355-8.
- [37] M. M. K. Bhuiya, M. S. U. Chowdhury, M. Shahabuddin, M. Saha, and L. A. Memon, “Thermal characteristics in a heat exchanger tube fitted with triple twisted tape inserts,” *Int. Commun. Heat Mass Transf.*, vol. 48, pp. 124–132, 2013, doi: 10.1016/j.icheatmasstransfer.2013.08.024.
- [38] P. Li, Z. Liu, W. Liu, and G. Chen, “Numerical study on heat transfer enhancement characteristics of tube inserted with centrally hollow narrow twisted tapes,” *Int. J. Heat Mass Transf.*, vol. 88, pp. 481–491, 2015, doi: 10.1016/j.ijheatmasstransfer.2015.04.103.
- [39] P. Promvonge, “Thermal performance in the square-duct heat exchanger with quadruple V-finned twisted tapes,” *Appl. Therm.*

- ENG.*, vol. 98, pp. 278–307, 2016, doi: 10.1016/j.applthermaleng.2015.08.047.
- [40] C. Vashistha, A. K. Patil, and M. Kumar, “Experimental investigation of heat transfer and pressure drop in a circular tube with multiple inserts,” *Appl. Therm. Eng.*, vol. 96, pp. 117–129, 2016, doi: 10.1016/j.applthermaleng.2015.11.077.
- [41] S. Kumar, P. Dinesha, A. Narayanan, and R. Nanda, “Numerical investigation on the heat transfer characteristics in a circular pipe using multiple twisted tapes in laminar flow conditions,” *Heat Transf. - Asian Res.*, vol. 48, no. 7, pp. 3399–3419, 2019, doi: 10.1002/htj.21563.
- [42] S. Gunes, V. Ozceyhan, and O. Buyukalaca, “Heat transfer enhancement in a tube with equilateral triangle cross-sectioned coiled wire inserts,” *Exp. Therm. Fluid Sci.*, vol. 34, no. 6, pp. 684–691, 2010, doi: 10.1016/j.expthermflusci.2009.12.010.
- [43] S. Gunes, V. Ozceyhan, and O. Buyukalaca, “The experimental investigation of heat transfer and pressure drop in a tube with coiled wire inserts placed separately from the tube wall,” *Appl. Therm. Eng.*, vol. 30, no. 13, pp. 1719–1725, 2010, doi: 10.1016/j.applthermaleng.2010.04.001.
- [44] S. Gunes, E. Manay, E. Senyigit, and V. Ozceyhan, “A Taguchi approach for optimization of design parameters in a tube with coiled wire inserts,” *Appl. Therm. Eng.*, vol. 31, no. 14–15, pp.

2568–2577,2012, DOI: 10.1017/J.applthermaleng.2012.04.022.

- [45] A. García, J. P. Solano, P. G. Vicente, and A. Viedma, “The influence of artificial roughness shape on heat transfer enhancement : Corrugated tubes, dimpled tubes, and wire coils,” *Appl. Therm. Eng.*, vol. 35, pp. 196–201, 2012, doi: 10.1016/j.applthermaleng.2011.10.030.
- [46] S. Selvam, P. Thiyagarajan, and S. Suresh, “EFFECT OF WIRE COILED COIL MATRIX TURBULATORS WITH AND WITHOUT BONDING ON THE WALL OF THE TEST SECTION OF CONCENTRIC TUBE HEAT EXCHANGER,” vol. 16, no. 4, pp. 1151–1164, 2012, doi: 10.2298/TSCI110318117S.
- [47] P. K. Rout and S. K. Saha, “Laminar Flow Heat Transfer and Pressure Drop in a Circular Tube Having Wire-Coil and Helical Screw-Tape Inserts,” vol. 135, no. February 2013, 2014, doi: 10.1115/1.4007415.
- [48] S. S. P. R. T. S. Suresh, “Experimental Studies on Wire Coiled-Coil Matrix Turbulators with and Without Centre Core Rod,” no. m, 2012, doi: 10.1007/s13369-012-0498-5.
- [49] D. S. Martínez, A. García, J. P. Solano, and A. Viedma, “International Journal of Heat and Mass Transfer Heat transfer enhancement of laminar and transitional Newtonian and non-Newtonian flows in tubes with wire coil inserts,” vol. 76, pp.

- 540–546, 2014, DOI: 10.1017/JIJheatmasstransfer.2015.04.060.
- [50] J. San, W. Huang, and C. Chen, “Experimental investigation on heat transfer and fluid friction correlations for circular tubes with coiled-wire inserts ☆,” *Int. Commun. Heat Mass Transf.*, vol. 65, pp. 8–14, 2015, doi: 10.1016/j.icheatmasstransfer.2015.04.008.
- [51] S. Roy and S. K. Saha, “Thermal and Friction Characteristics of Laminar Flow through a Circular Duct having Helical Screw-Tape with Oblique Teeth Inserts and Wire Coil Insert Sarbendu Roy Sujoy Kumar Saha,” *Exp. Therm. FLUID Sci.*, 2015, doi: 10.1016/j.expthermflusci.2015.07.007.
- [52] Z. Feng, X. Luo, F. Guo, H. Li, and J. Zhang, “Numerical investigation on laminar flow and heat transfer in a rectangular microchannel heat sink with wire coil inserts,” *Appl. Therm. Eng.*, 2017, doi: 10.1016/j.applthermaleng.2017.01.091.
- [53] S. Ahmed, “Enhancement and Prediction of Heat Transfer Rate in Turbulent Flow Through Tube With Perforated Twisted Tape Inserts :” vol. 133, no. April 2011, pp. 1–9, 2013, doi: 10.1115/1.4002635.
- [54] C. T. P. Eiamsa-ard and S. Eiamsa-ard, “Heat transfer and thermal performance characteristics of heat exchanger tube fitted with perforated twisted-tapes,” pp. 881–892, 2012, doi: 10.1007/s00231-011-0943-0.

- [55] C. Thianpong, P. Eiamsa-ard, P. Promvonge, and S. Eiamsa-ard, “Energy Procedia Effect of perforated twisted-tapes with parallel wings on heat transfer enhancement in a heat exchanger tube,” pp. 0–6, 2012, doi: 10.1016/j.egypro.2011.12.887.
- [56] M. M. K. Bhuiya, M. S. U. Chowdhury, M. Saha, and M. T. Islam, “Heat transfer and friction factor characteristics in turbulent flow through a tube fitted with perforated twisted tape inserts,” *Int. Commun. Heat Mass Transf.*, vol. 46, pp. 49–57, 2013, doi: 10.1016/j.icheatmasstransfer.2013.05.012.
- [57] K. Nanan, C. Thianpong, P. Promvonge, and S. Eiamsa-ard, “Investigation of heat transfer enhancement by perforated helical twisted-tapes ☆,” *Int. Commun. Heat Mass Transf.*, vol. 52, pp. 106–112, 2014, doi: 10.1016/j.icheatmasstransfer.2014.01.018.
- [58] S. Skullong, P. Promvonge, C. Thianpong, and M. Pimsarn, “International Journal of Heat and Mass Transfer Heat transfer and turbulent flow friction in a round tube with staggered-winglet perforated-tapes,” *HEAT MASS Transf.*, vol. 95, pp. 230–242, 2016, doi: 10.1016/j.ijheatmasstransfer.2015.12.007.
- [59] S. Eiamsa-ard, K. Wongcharee, P. Eiamsa-ard, and C. Thianpong, “Heat transfer enhancement in a tube using delta-winglet twisted tape inserts,” *Appl. Therm. Eng.*, vol. 30, no. 4, pp. 310–318, 2010, doi: 10.1016/j.applthermaleng.2009.09.006.
- [60] S. Eiamsa-ard, K. Wongcharee, P. Eiamsa-ard, and C.

- Thianpong, “Thermohydraulic Investigation of turbulent flow into a circular tube fitted with middle wings and alternating axes twisted bands,” *Exp. Therm. Fluid Sci.*, vol. 34, no. 8, pp. 1151–1161, 2010, doi: 10.1016/j.expthermflusci.2010.04.004.
- [61] K. Wongcharee and S. Eiamsa-ard, “Chemical Engineering and Processing : Process Intensification Heat transfer enhancement by twisted tapes with alternate-axes and triangular, rectangular and trapezoidal wings,” *Chem. Eng. Process. Process Intensif.*, vol. 50, no. 2, pp. 211–219, 2011, doi: 10.1016/j.cep.2010.11.012.
- [62] P. Taylor, S. Eiamsa-ard, C. Nuntadusit, and P. Promvonge, “Effect of Twin Delta-Winged Twisted-Tape on Thermal Performance of Heat Exchanger Tube Effect of Twin Delta-Winged Twisted-Tape on Thermal Performance of Heat Exchanger Tube,” no. April 2015, pp. 37–41, doi: 10.1080/01457632.2013.793112.
- [63] Z. Lin, L. Wang, M. Lin, W. Dang, and Y. Zhang, “Numerical study of the laminar flow and heat transfer characteristics in a tube inserting a twisted tape having parallelogram winglet vortex generators”: Liang-Bi Wang,” *Appl. Therm. Eng.*, 2016, doi: 10.1016/j.applthermaleng.2016.12.142.
- [64] S. Tamna, Y. Kaewkohkiat, S. Skullong, and P. Promvonge, “Heat transfer enhancement in a tubular heat exchanger with

- double V-ribbed twisted-tapes,” *Case Stud. Therm. Eng.*, vol. 7, pp. 14–29, 2017, DOI: 10.1016/J.csite.2017.01.002.
- [65] S. E. Tarasevich, A. B. Yakovlev, A. A. Giniyatullin, and A. V. Shishkin, “IMECE2011-62088,” pp. 1–6, 2017.
- [66] B. S. Petukhov, “Heat Transfer and Friction in Turbulent Pipe Flow With Variable Physical Properties,” *Adv. Heat Transf.*, vol. 6, no. C, pp. 503–564, 1970, doi: 10.1016/S0065-2717(08)70153-9.
- [67] J. F. Jf, L. J. Marks, J. A. S. E. Stewart, M. L. Dorsy, W. Watson-wrighi, and J. S. F. Lawrsrrcs, “FluidMechanics-Streeter.pdf.” 1992, doi: 10.1016/0041-0101(92)90430-D.
- [68] W. H. Azmi, K. V. Sharma, R. Mamat, A. B. S. Alias, and I. Izwan Misnon, “Correlations for thermal conductivity and viscosity of water-based nanofluids,” *IOP Conf. Ser. Mater. Sci. Eng.*, vol. 36, no. 1, pp. 0–6, 2012, doi: 10.1088/1757-899X/36/1/012029.
- [69] W. A. B. John A. Duffie, *Wiley: Solar Engineering of Thermal Processes, 4th Edition - John A. Duffie, William A. Beckman.* 2013.
- [70] K. S. Ong, “Thermal performance of solar air heaters: Mathematical model and solution procedure,” *Sol. Energy*, vol. 55, no. 2, pp. 93–109, 1995, doi: 10.1016/0038-092X(95)00021I.

- [71] D. M. H. Al-Shamkhi, "Experimental study of the performance of low cost solar water heater in Najaf city," *Int. J. Mech. Mechatronics Eng.*, vol. 16, no. 1, pp. 109–121, 2016.
- [72] Ali Sh. Baqir, Hasan S.Khwayyir, Hiba Q.Mohammed " Effects of Air Bubble Injection on the Efficiency of a Flat Plate Solar Collector: An Experimental Study for the Open Flow System" *Journal of Engineering and Applied Sciences*, Vol. 15 No. 7, pp. 1703-1708
- [73] Hasan S.Khwayyir, Ali Sh. Baqir, Hiba Q.Mohammed, "Effect of Air Bubble Injection on the Thermal Performance of a Flat Plate Solar Collector", *Thermal Science and Engineering progress*, <https://doi.org/10.1016/j.tsep.2019.100476>
- [74] Ali Majeed. A, Ahmad. H. Yousif, and Ali Shakir Baqir, "Study the effect of twisted tapes on thermal performance solar collector with using curvature vortex generators," vol. 62, no. 07, pp. 3631–3643, 2020.
- [75] J. Shandal, Q. A. Abed, and D. M. Al-Shamkhee, "Simulation analysis of thermal performance of the solar air/water collector by using computational fluid dynamics," *E3S Web Conf.*, vol. 180, 2020, doi: 10.1051/e3sconf/202018002015.
- [76] R. J. Moffat, "Describing the uncertainties in experimental results," *Exp. Therm. Fluid Sci.*, vol. 1, no. 1, pp. 3–17, 1988, doi: 10.1016/0894-1777(88)90043-X.

APPENDICES

Appendix (A)

A. The calibration of Instruments used in the experiments

A.1 Calibration of solar collector meter:

Figure (A.1) represents the solar irradiance meter calibration. In the faculty of technical engineering / Najaf, the solar meter is calibrated with the solar energy research station. The data were collected for every thirty minutes between 9:00 AM and 3:00 PM.

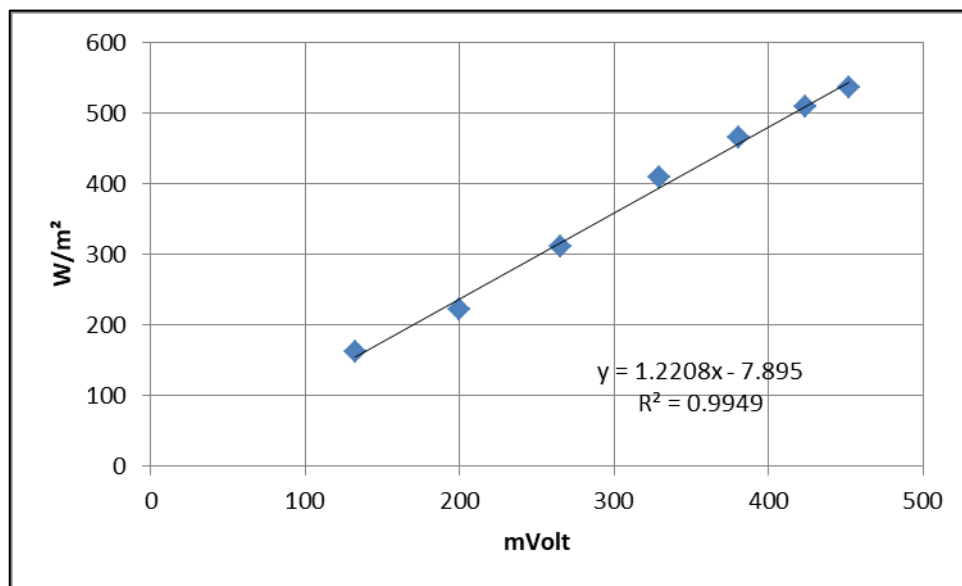


Fig. A.1: calibration of solar radiation meter.

A.2 Flow rate meter calibrate method

The volumetric rate device is adjusted utilizing cylindrical graduated glass vessels and stopwatch. The section below displays the calibration measures with test results. The calibrator time weight method used to calibrate the volume flow meter with a stopwatch and graduated glass vessel, The calibration is done

by flowing the water through a flow meter at different flow rates and at the same time measuring the flow time required by volume by the pail to fill the correct amount of working fluid.

Samples of volume flow meter calibration

The reading of volumetric flow rate of flow rate meter = 1 liter/min

Inspection no (1):

Monitoring time = for one minute

Water dischargh in graduate vessel = 0.97liter/min.

Inspection no (2):

Monitoring time = for one minute

Water dischargh in graduate vessel = 0.966 liter/min.

Inspection no (3):

Monitoring time = for one minute

Water dischargh in graduate vessel = 0.954liter/minute

Inspection no (4):

Monitoring time = for one minute

Water dischargh in graduate vessel = 0.994 liter/minute.

The average of volumetric flow rates

$V = (v_1 + v_2 + v_3 + v_4) / 4 = (0.994 + 0.954 + 0.966 + 0.97) / 4 = 0.971$ liter/minute
The error of the volume flow meter = $1 - 0.971 = 0.029$ liter/minute

$$\% \text{ Error} = \frac{1 - 0.029}{1} \times 100 = 2.9\%$$

A.3 Calibration of temperature sensors of 8- channel data logger and 4K type thermocouples with digital thermometers:

The two sets of sensors (S1 – S8) °C, (S9-S16) °C for two 8- channel data loggers and four thermocouples(T1-T4) °C for digital thermometer are calibrated by using a mercury thermometer. The calibration results were recorded in the tables (A-1),(A-2) and (A-3).

Table A.1: calibration results of first 8- channels data logger with 8 sensors

| Mercury Thermometer °c | S 1°c deeg. | S 2°c deeg | S 3°c deeg | S 4°c deeg | S 5°c deeg | S 6°c deeg | S 7°c deeg | S 8°c deeg |
|---------------------------------------|----------------|---------------|---------------|---------------|---------------|---------------|---------------|---------------|
| 20 | 20.4 | 20.4 | 20.3 | 19.8 | 19.7 | 20.3 | 20.4 | 19.6 |
| 25 | 25.5 | 25.4 | 24.6 | 24.7 | 25.4 | 25.3 | 25.4 | 24.7 |
| 30 | 30.4 | 30.3 | 30.5 | 29.7 | 30.4 | 30.3 | 30.4 | 29.6 |
| 35 | 35.4 | 35.4 | 35.3 | 35.4 | 34.6 | 35.4 | 35.2 | 34.7 |
| 40 | 40.3 | 40.2 | 40.2 | 40.2 | 39.9 | 39.8 | 40.2 | 40.3 |
| 45 | 45.2 | 45.4 | 44.7 | 44.6 | 45.2 | 45.2 | 45.3 | 44.9 |
| 50 | 50.3 | 50.4 | 49.6 | 49.7 | 50.1 | 50 | 50.3 | 50.2 |
| 55 | 55.4 | 55.3 | 54.6 | 55.1 | 55.3 | 54.6 | 55.2 | 55.3 |
| 60 | 60.3 | 60.4 | 60.3 | 60.1 | 59.7 | 60.2 | 60.2 | 60.2 |
| 65 | 64.5 | 65.4 | 64.5 | 64.5 | 65.5 | 64.6 | 64.8 | 64.6 |

Table A.2: calibration results of second 8- channels data logger with 8 sensors

| Mercury Thermometer deeg | S 9 °C deeg. | S 10 °C deeg. | S 11 °C deeg. | S 12 °C deeg. | S 13 °C deeg. | S 14 °C deeg. | S 15 °C deeg. | S16 °C deeg. |
|---|--------------------|---------------------|---------------------|---------------------|---------------------|---------------------|---------------------|--------------------|
| 20 | 20.4 | 19.4 | 20.4 | 19.8 | 20.4 | 19.7 | 20.3 | 19.8 |
| 25 | 24.8 | 25.4 | 25.4 | 25.3 | 25.4 | 24.7 | 25.3 | 25.3 |
| 30 | 30.4 | 30.5 | 30.3 | 29.7 | 30.3 | 29.8 | 29.6 | 30.4 |
| 35 | 35.5 | 35.3 | 35 | 34.6 | 35.3 | 34.7 | 34.9 | 34.7 |
| 40 | 40.4 | 40.3 | 40 | 39.7 | 39.6 | 40.4 | 39.8 | 39.8 |
| 45 | 45.4 | 45 | 44.7 | 44.6 | 45.4 | 44.8 | 45.4 | 45.3 |
| 50 | 50.3 | 50 | 50.4 | 49.6 | 49.8 | 50.1 | 50.3 | 50.2 |
| 55 | 55.3 | 55.2 | 55 | 54.6 | 54.7 | 55.4 | 55.3 | 54.6 |
| 60 | 60.4 | 60.3 | 60 | 60.4 | 59.7 | 59.8 | 60 | 60.4 |
| 65 | 64.3 | 65 | 64.7 | 64.7 | 64.8 | 64.5 | 65 | 64.4 |

Table A.3: the calibration of 4 k- type

| Mercury Thermometer °C | Temp1 °C | Temp.2 °C | Temp.3 °C | Temp.4 °C |
|------------------------------|-------------|--------------|--------------|--------------|
| 25 | 25.9 | 26 | 26 | 26 |
| 30 | 31 | 29.2 | 31 | 31 |
| 35 | 36 | 35.6 | 36 | 36.3 |
| 40 | 41 | 40.9 | 41 | 41 |
| 45 | 44.1 | 46 | 46 | 46 |
| 50 | 49.2 | 51 | 51 | 51 |
| 55 | 54.1 | 54 | 56 | 56 |
| 60 | 60 | 61 | 61.2 | 59 |
| 65 | 64 | 64 | 64.1 | 66 |

The values of sixteen temperature sensors for two 8- channel data loggers and four thermocouples are too close that they cannot be distinguished if plotted. Correlating the values above(straight lines) calibration curves.

a. The correlation values of the first set sensors (S_1 to S_8) as follows:

$$Ts_1=0.988 \times Ts_1(\text{real})+0.78 \quad \dots\dots\dots (A.1)$$

$$Ts_2=0.99 \times Ts_1(\text{real})+0.3752 \quad \dots\dots\dots (A.2)$$

$$Ts_3=0.9886 \times Ts_3(\text{real})+0.4442 \quad \dots\dots\dots (A.3)$$

$$Ts_4=0.9993 \times Ts_4(\text{real})-0.0841 \quad \dots\dots\dots (A.4)$$

$$Ts_5=1.0035 \times Ts_5(\text{real})-0.0794 \quad \dots\dots\dots (A.5)$$

$$Ts_6=0.9851 \times Ts_5(\text{real})+0.6836 \quad \dots\dots\dots (A.6)$$

$$Ts_7=0.991 \times Ts_7(\text{real})+0.6212 \quad \dots\dots\dots (A.7)$$

$$Ts_8=1.0064 \times Ts_8(\text{real})-0.263 \quad \dots\dots\dots (A.8)$$

Where: $Ts(\text{real})$ = measured values; $Ts_1 \dots Ts_8$ = correction values.

b. The correlation values of the second set sensors (S_9 to S_{16}) as follows:

$$T_{S_9} = 0.9918 \times T_{S_9(\text{real})} + 0.5703 \quad \dots\dots (A.9)$$

$$T_{S_{10}} = 1.0024 \times T_{S_{10}(\text{real})} + 0.37 \quad \dots\dots\dots (A.10)$$

$$T_{S_{11}} = 0.9882 \times T_{S_{11}(\text{real})} + 0.5897 \quad \dots\dots\dots (A.11)$$

$$T_{S_{12}} = 0.999 \times T_{S_{12}(\text{real})} - 0.1588 \quad \dots\dots\dots (A.12)$$

$$T_{S_{13}} = 0.983 \times T_{S_{13}(\text{real})} + 0.7612 \quad \dots\dots\dots (A.13)$$

$$T_{S_{14}} = 0.003 \times T_{S_{14}(\text{real})} - 0.2388 \quad \dots\dots\dots (A.14)$$

$$T_{S_{15}} = 1.0006 \times T_{S_{15}(\text{real})} + 0.0642 \quad \dots\dots\dots (A.15)$$

$$T_{S_{16}} = 0.9941 \times T_{S_{16}(\text{real})} + 0.2424 \quad \dots\dots\dots (A.16)$$

c. The correlation values of thermocouples (T_1 to T_4) as follows:

$$T_1 = 0.946 \times T_1(\text{real}) + 2.4633 \quad \dots\dots\dots (A.17)$$

$$T_2 = 0.978 \times T_2(\text{real}) + 1.8011 \quad \dots\dots\dots (A.18)$$

$$T_3 = 0.9767 \times T_3(\text{real}) + 1.8611 \quad \dots\dots\dots (A.19)$$

$$T_4 = 0.981 \times T_4(\text{real}) + 1.155 \quad \dots\dots\dots (A.20)$$

A.4 Calibration differential pressure manometer:

To calibrate the differential pressure manometer using a differential pressure gauge and a pneumatic system (air compressor), the calibration process carried out by open both ports of differential pressure gauge and exposed to ambient to obtain a zero needle position because no pressure is applied to both ports. Connected the pneumatic hose on the high or positive side and generate the required pressure and compare it with the manometer and record all details for 5 test points. The fig(A-2) represents the calibration of the differential pressure manometer.

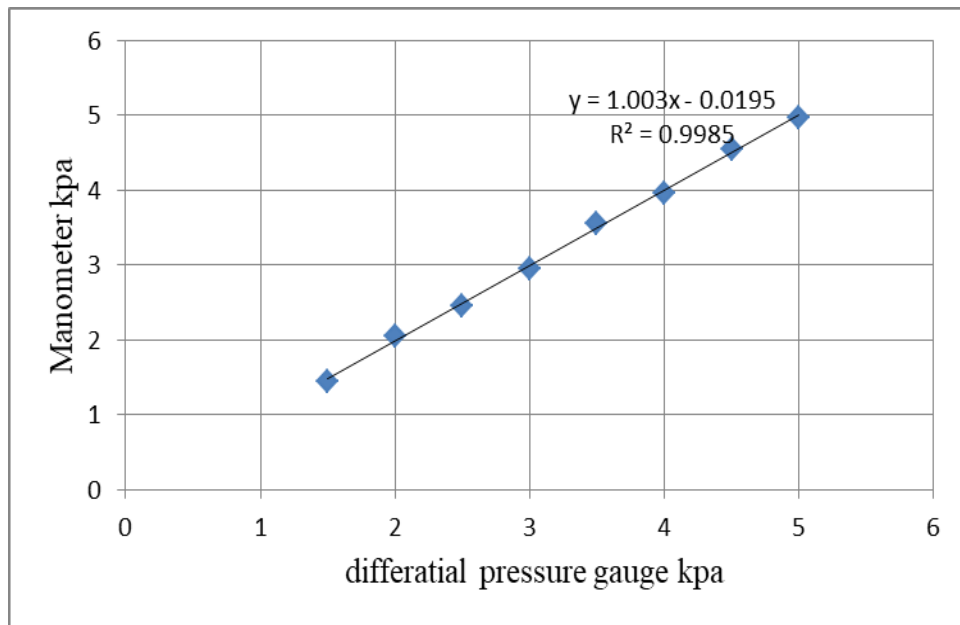


Fig. A.2: calibration of differential pressure manometer

Appendix (B)

B. Calculation of fin efficiency of straight configuration and the Average Transmittance-Absorptance ($\tau\alpha$) av

B.1 Calculating the efficiency (F) for rectangular shape and straight fins [1]

The figure(B.1) represents the cross-section for solar collector of flat plate type consider the temperature distribution between two tubes.

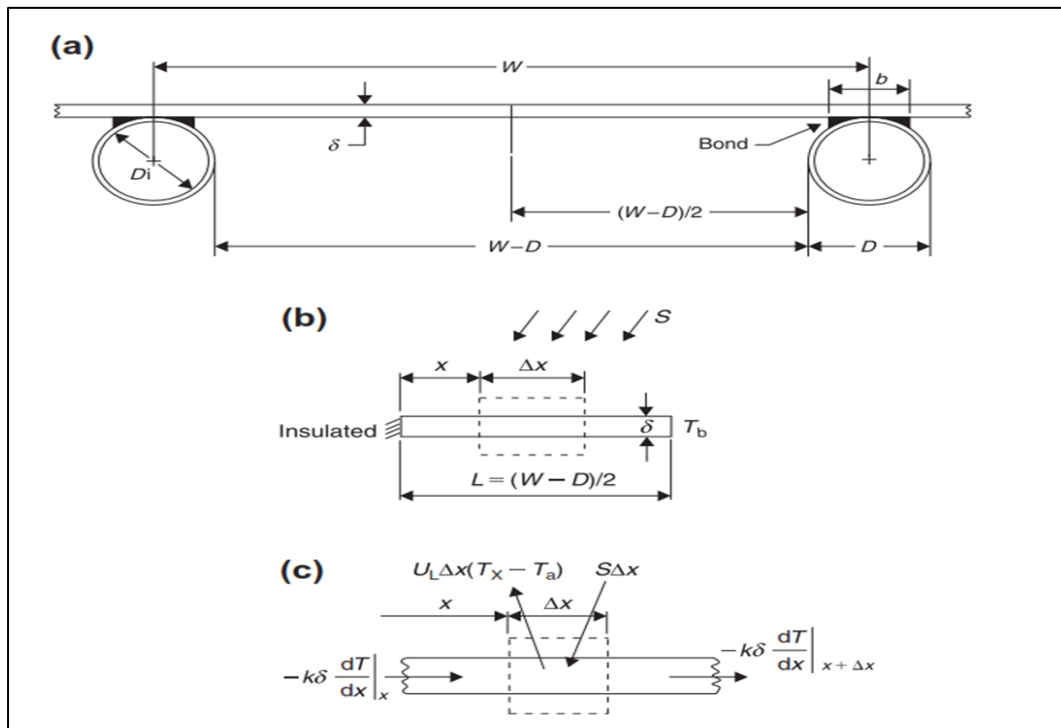


Fig. B.1: temperature distribution between two tubes in flat plate solar collector.

Evaluated the energy of thermal transferred by conduction within area of pipe per unit length by using Fourier low at the fin base can be expressed as follow:

$$q_{fin} = -k\delta \frac{dT}{dX} \Big|_{X=L} = \frac{k\delta m}{U_L} [S - U_L(T_b - T_a)] \tanh(mL) \dots \dots \dots (B.1)$$

The equation (B.1) represents the stored energy on only one part of the pipe from both aspect the energy copilation equation becomes:

$$q_{fin}=(W-D)[S-U_L(T_b - T_a)]\frac{\tanh[\frac{m(W-D)}{2}]}{m(W-D)/2} \dots\dots\dots(B.2)$$

From efficiency equation of straight fin

$$q_{fin}=[(W - D)] [F [S-U_L(T_b- T_a)]] \dots\dots\dots(B.3)$$

From eq (B.2)&(B.3) the efficiency (F) for straight fin with rectangular shap given by:

$$F = \frac{\tanh[\frac{m(W-D)}{2}]}{m(W-D)/2} \dots\dots\dots(B.4)$$

B.2 Calculate the Average Transmittance-Absorptance ($\tau\alpha$)_{av} [1]

In case the waves of solar irradiance beatings the roof of the diaphanous sheet with an angle θ_1 that call incidence angle, thereafter a portion of incidence irradianc is reflected and the residual is reflected to an angle θ_2 that call reflection angle as shown in the figure (B.2).The angles θ_1 and θ_2 are related by the Snell's law where:

$$n = \frac{\sin(\theta_1)}{\sin(\theta_2)} \dots\dots\dots(B.5)$$

Where n represents the ratio of reflection index for the tow media interface forming, n = 1.526 for glasses.

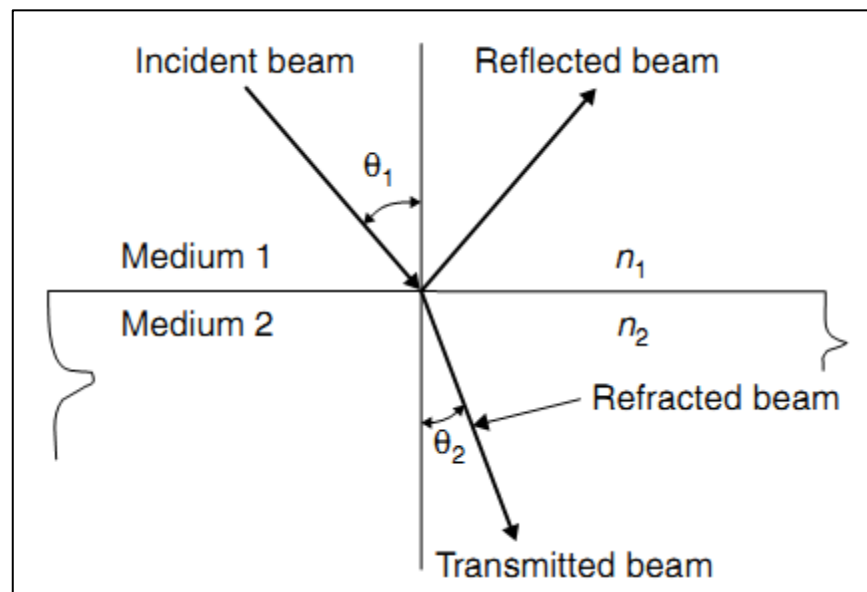


Fig. B.2: incidence and reflection angles for the irradiance beam from a medium with refractive index n_1 to a medium with refractive index n_2

Also, the incidence angle θ_1 can be evaluated from the following correlation

$$\cos\theta_1 = \cos(\vartheta - \beta) \cos\omega \cos\delta + \sin(\vartheta - \beta) \sin\delta \dots\dots\dots(B.6)$$

Where ϑ is The latitude of the city in degrees and the angle(ω) of solar hour calculated from the equation below:

$$\omega = 15(ST - 12) \dots\dots\dots(B.7)$$

The declination angle (δ) evaluated from the equation below:

$$\delta = 23.45 \sin \left(\frac{M + 284}{365} 360 \right) \dots\dots\dots (B.8)$$

M-represent the day number in the year

The parallel and perpendicular components of radiation for smooth surface correlated in the following relationship were derived by Fresnel:

$$e_{\perp} = \frac{\sin^2(\theta_1 - \theta_2)}{\sin^2(\theta_1 + \theta_2)} \dots\dots\dots (B.9)$$

$$e_{\parallel} = \frac{\tan^2(\theta_1 - \theta_2)}{\tan^2(\theta_1 + \theta_2)} \dots\dots\dots(B.10)$$

In similar the transmittance (τ_r) determined from an average of two transmittance components as below (the subscript e refers to reflection losses) :

$$\tau_r = \left(0.5 \times \left[\frac{(1 - e_{\parallel})}{(1 + e_{\parallel})} + \frac{(1 - e_{\perp})}{(1 + e_{\perp})} \right] \right) \dots\dots\dots(B.11)$$

The transmittance, τ_{α} can be computed from the following equation (the subscript α refers to absorption losses):

$$\tau_{\alpha} = e^{\left[\frac{-KL}{\cos(\theta_2)} \right]} \dots\dots\dots(B.12)$$

Where K is coefficient of extinction that change between ($4 m^{-1}$ and $32m^{-1}$) for low and high quality of glass respectively, L refer to thickness of cover

The transmittance for single glass the becomes :

$$\tau \cong \tau_{\alpha} \tau_r \dots\dots\dots(B.13)$$

The absorptance dependent angle from 0° to 80° can be calculated from the equation(Beckman et al., 1977)

$$\left(\frac{\alpha}{\alpha_n} \right) = 1 + 2.0345 \times 10^{-3} \theta_e - 1.99 \times 10^{-3} \theta_e^2 + 5.324 \times 10^{-6} \theta_e^3 - 4.799 \times 10^{-8} \theta_e^4 \dots\dots\dots(B.14)$$

Where :

θ_e is the efficient angle of incidence in degrees.

α_n is Absorptance at normal angle of incidence, that equals to(0.96) for black paint.

The average transmittance- absorptance product $(\tau\alpha)_{av}$ can be obtained from:

$$(\tau\alpha)_B = 1.01\tau\left(\frac{\alpha}{\alpha_n}\right)\alpha_n \dots\dots\dots(B.15)$$

$$(\tau\alpha)_{av} \cong 0.96(\tau\alpha)_B \dots\dots\dots(B.16)$$

Appendix(C)

C. Uncertainties analysis

In the present analysis, some of the sources of error which could be defined as sources of uncertainty in estimating volumetric flow rates, temperatures and drops in pressure and solar radiation which could lead to errors in the predicted values:

1. Instability of electric power.
2. Uncertainty in temperature reading resulted from defects in manufacturing in temperature reader devices and thermocouples.
3. Errors inflow measurements.

R. J. Moffat (Moffat.R.J1988)[76] based on the Kline and McClintock method was used for calculating an inaccuracy of results.

Consideration the results(R) be a function of m independent variables: $S_1, S_2, S_3 \dots S_m$

$$R = R(S_1, S_2, S_3, \dots, S_m) \quad (C.1)$$

For small changes in variables, it is possible to express this relationship in linear Form as:

$$\delta R = R_{S_1} \delta S_1 + R_{S_2} \delta S_2 + R_{S_3} \delta S_3 + \dots + R_{S_m} \delta S_m \quad (C.2)$$

The resulting uncertainty interval (e) may, therefore, be given as:

$$\left(\frac{e_R}{R}\right)^2 = \left[\left(R_{S_1} \frac{e_{S_1}}{S_1} \right)^2 + \left(R_{S_2} \frac{e_{S_2}}{S_2} \right)^2 + \left(R_{S_3} \frac{e_{S_3}}{S_3} \right)^2 + \dots + \left(R_{S_m} \frac{e_{S_m}}{S_m} \right)^2 \right]$$

(C.3)

$$\text{Where : } R_{S_m} = \frac{\partial R}{\partial S_m} \quad (C.4)$$

C.1 Friction factor derivation

$$f = \left(\frac{d_i}{L}\right) \left(\frac{2\Delta P}{\rho_w U^2}\right) \quad (C/1)$$

$$f = 2 \left(\frac{\Delta P}{L}\right) \left(\frac{\rho_w d_i^3}{Re^2 \mu_w^2}\right) \quad (C/2)$$

$$\frac{\partial f}{\partial(\Delta P)} = \frac{2}{L} \left(\frac{\rho_w d_i^3}{Re^2 \mu_w^2}\right)$$

$$\frac{\partial f}{\partial(L)} = 2 \Delta P \left(\frac{\rho_w d_i^3}{Re^2 \mu_w^2}\right) \left(-\frac{1}{L^2}\right)$$

$$\frac{\partial f}{\partial(d_i)} = \frac{2 \Delta P}{L} \left(\frac{\rho_w}{Re^2 \mu_w^2}\right) (3 d_i^2)$$

$$\frac{\partial f}{\partial(Re)} = \frac{2 \Delta P}{L} \left(\frac{\rho_w d_i^3}{\mu_w^2}\right) \left(\frac{-2}{Re^3}\right)$$

Take the amount of error on either side of the equation (C/1)

$$\Delta f = \left[\left\{ \frac{\partial f}{\partial(\Delta P)} \Delta(\Delta P) \right\}^2 + \left\{ \frac{\partial f}{\partial(L)} \Delta(L) \right\}^2 + \left\{ \frac{\partial f}{\partial(d_i)} \Delta(d_i) \right\}^2 + \left\{ \frac{\partial f}{\partial(Re)} \Delta(Re) \right\}^2 \right]^{0.5} \quad (C/3)$$

$$\begin{aligned} \frac{\partial f}{\partial(\Delta P)} \Delta(\Delta P) &= \frac{2}{L} \left(\frac{\rho_w d_i^3}{Re^2 \mu_w^2}\right) \Delta(\Delta P) \\ &= \frac{2\Delta P}{L} \left(\frac{\rho_w d_i^3}{Re^2 \mu_w^2}\right) \frac{\Delta(\Delta P)}{\Delta P} \\ &= f \frac{\Delta(\Delta P)}{\Delta P} \end{aligned} \quad (C/4)$$

$$\begin{aligned} \frac{\partial f}{\partial(L)} \Delta(L) &= 2 \Delta P \left(\frac{\rho_w d_i^3}{Re^2 \mu_w^2}\right) \left(-\frac{1}{L^2}\right) \Delta(L) \\ &= -2 \left(\frac{\Delta P}{L}\right) \left(\frac{\rho_w d_i^3}{Re^2 \mu_w^2}\right) \frac{\Delta(L)}{L} = -f \frac{\Delta(L)}{L} \end{aligned} \quad (C/5)$$

$$\begin{aligned} \frac{\partial f}{\partial(d_i)} \Delta(d_i) &= \frac{2 \Delta P}{L} \left(\frac{\rho_w}{Re^2 \mu_w^2}\right) (3 d_i^2) \Delta(d_i) \\ &= 3 \left(\frac{\Delta P}{L}\right) \left(\frac{\rho_w d_i^3}{Re^2 \mu_w^2}\right) \frac{\Delta(d_i)}{d_i} = 3f \frac{\Delta(d_i)}{d_i} \end{aligned} \quad (C/6)$$

$$\begin{aligned} \frac{\partial f}{\partial(Re)} \Delta(Re) &= \frac{2 \Delta P}{L} \left(\frac{\rho_w d_i^3}{\mu_w^2}\right) \left(\frac{-2}{Re^3}\right) \Delta(Re) \\ &= \frac{2 \Delta P}{L} \left(\frac{\rho_w d_i^3}{\mu_w^2 Re^2}\right) \left(\frac{-2\Delta(Re)}{Re}\right) = -2 f \left(\frac{\Delta(Re)}{Re}\right) \end{aligned} \quad (C/7)$$

By replacing equations (C /4) , (C/5) , (C/6) and (C/7) in equation (C/3), we can get:

$$\begin{aligned}\Delta f &= \left[\left\{ f \frac{\Delta(\Delta P)}{\Delta P} \right\}^2 + \left\{ -f \frac{\Delta(L)}{L} \right\}^2 + \left\{ 3f \frac{\Delta(d_i)}{d_i} \right\}^2 + \left\{ -2f \left(\frac{\Delta(Re)}{Re} \right) \right\}^2 \right]^{0.5} \\ &= \left[f^2 \left\{ \frac{\Delta(\Delta P)}{\Delta P} \right\}^2 + f^2 \left\{ \frac{\Delta(L)}{L} \right\}^2 + f^2 \left\{ \frac{3\Delta(d_i)}{d_i} \right\}^2 + f^2 \left\{ \frac{2\Delta(Re)}{Re} \right\}^2 \right]^{0.5} \\ \Delta f &= f \left[\left\{ \frac{\Delta(\Delta P)}{\Delta P} \right\}^2 + \left\{ \frac{\Delta(L)}{L} \right\}^2 + \left\{ \frac{3\Delta(d_i)}{d_i} \right\}^2 + \left\{ \frac{2\Delta(Re)}{Re} \right\}^2 \right]^{0.5} \\ \frac{\Delta f}{f} &= \left[\left\{ \frac{\Delta(\Delta P)}{\Delta P} \right\}^2 + \left\{ \frac{\Delta(L)}{L} \right\}^2 + \left\{ \frac{3\Delta(d_i)}{d_i} \right\}^2 + \left\{ \frac{2\Delta(Re)}{Re} \right\}^2 \right]^{0.5} \quad (C/8)\end{aligned}$$

where ΔP directly evaluated from forced circulation or $\Delta P = (\rho_{mercury} - \rho_w) \Delta h$ where;

h is the difference between mercury and water columns in meter).

$\rho_{mercury}$ is the density of mercury in kg/m^3 .

$$\frac{\Delta(\Delta P)}{\Delta P} = \frac{\Delta h}{h} \quad (C/9)$$

$$Re = \frac{\rho_w d_i U}{\mu_w} \quad \text{and} \quad \dot{m} = \frac{\pi}{4} d_i^2 \rho_w U$$

$$\text{Thus} \quad Re = \frac{4 \dot{m}}{\pi d_i \mu_w} \quad (C/10)$$

$$\frac{\Delta(Re)}{Re} = \left[\left\{ \frac{\Delta \dot{m}}{\dot{m}} \right\}^2 + \left\{ \frac{\Delta d_i}{d_i} \right\}^2 \right]^{0.5} \quad (C/11)$$

C.2 Nusselt number derivation

$$Nu = \frac{h_i d_i}{k} \quad (C/12)$$

$$\frac{\Delta Nu}{Nu} = \left[\left\{ \frac{\Delta h_i}{h_i} \right\}^2 + \left\{ \frac{\Delta d_i}{d_i} \right\}^2 + \left\{ \frac{\Delta k}{k} \right\}^2 \right]^{0.5} \quad (C/13)$$

From equations (3.25)& (3.26)

$$h_i = \frac{1}{A_i \left[\frac{q}{T_p - T_m} - \frac{\ln\left(\frac{d_o}{d_i}\right)}{2\pi k_w L} \right]} \quad (C/14)$$

$$\begin{aligned}
 \Delta h_i &= \frac{1}{A_i} \left[\left\{ \frac{\partial h_i}{\partial q} \Delta q \right\}^2 + \left\{ \frac{\partial h_i}{\partial T_p} \Delta T_p \right\}^2 + \left\{ \frac{\partial h_i}{\partial T_m} \Delta T_m \right\}^2 + \left\{ \frac{\partial h_i}{\partial (\ln(\frac{d_o}{d_i}))} \Delta (\ln(\frac{d_o}{d_i})) \right\}^2 \right]^{0.5} \\
 \frac{\Delta h_i}{h_i} &= \frac{1}{A_i} \frac{1}{h_i} \left[\left\{ \frac{\partial h_i}{\partial q} \Delta q \right\}^2 + \left\{ \frac{\partial h_i}{\partial T_p} \Delta T_p \right\}^2 + \left\{ \frac{\partial h_i}{\partial T_m} \Delta T_m \right\}^2 + \left\{ \frac{\partial h_i}{\partial (\ln(\frac{d_o}{d_i}))} \Delta (\ln(\frac{d_o}{d_i})) \right\}^2 \right]^{0.5} \\
 &= \frac{1}{A_i} \left[\frac{1}{h_i^2} \left\{ \frac{\partial h_i}{\partial Q} \Delta Q \right\}^2 + \frac{1}{h_i^2} \left\{ \frac{\partial h_i}{\partial T_p} \Delta T_p \right\}^2 + \frac{1}{h_i^2} \left\{ \frac{\partial h_i}{\partial T_m} \Delta T_m \right\}^2 + \frac{1}{h_i^2} \left\{ \frac{\partial h_i}{\partial (\ln(\frac{d_o}{d_i}))} \right. \right. \\
 &\quad \left. \left. \Delta (\ln(\frac{d_o}{d_i})) \right\}^2 \right]^{0.5} \\
 &= \frac{1}{A_i} \left[\left(\frac{\Delta q}{q} \right)^2 \frac{1}{\left[\left\{ \frac{q}{T_p - T_m} \right\} - \frac{\ln(\frac{d_o}{d_i})}{2\pi k_{WL}} \right]^2} \frac{1}{h_i^2} + \left(\frac{\Delta T_p}{T_p} \right)^2 \frac{1}{\left[\left\{ \frac{q}{T_p - T_m} \right\} - \frac{\ln(\frac{d_o}{d_i})}{2\pi k_{WL}} \right]^2} \frac{1}{h_i^2} + \right. \\
 &\quad \left. \left(\frac{\Delta T_m}{T_m} \right)^2 \frac{1}{\left[\left\{ \frac{q}{T_p - T_m} \right\} - \frac{\ln(\frac{d_o}{d_i})}{2\pi k_{WL}} \right]^2} \frac{1}{h_i^2} + \left(\frac{\Delta (\ln(\frac{d_o}{d_i}))}{\ln(\frac{d_o}{d_i})} \right)^2 \frac{1}{\left[\left\{ \frac{q}{T_p - T_m} \right\} - \frac{\ln(\frac{d_o}{d_i})}{2\pi k_{WL}} \right]^2} \frac{1}{h_i^2} \right]^{0.5} \\
 \frac{\Delta h_i}{h_i} &= A_i \left[\left\{ \frac{\Delta Q_{out}}{Q_{out}} \right\}^2 + \left\{ \frac{\Delta T_p}{T_p} \right\}^2 + \left\{ \frac{\Delta T_m}{T_m} \right\}^2 + \left\{ \frac{\Delta (\ln(\frac{d_o}{d_i}))}{\ln(\frac{d_o}{d_i})} \right\}^2 \right]^{0.5} \quad (C/15)
 \end{aligned}$$

C.3 collector efficiency derivation

collector efficiency is calculated from the ratio of output heat to input heat for solar collector .

$$\eta = \left(\frac{Q_{out}}{Q_{in}} \right), \quad \eta = \frac{\left(\frac{\Delta Q}{Q} \right)_{out}}{\left(\frac{\Delta Q}{Q} \right)_{in}}$$

where the Q_{out} represents the heat gained by the water from the inlet to outlet. Thus Q_{out} is given by:

$$Q_{out} = \dot{m} \times C_p \times (T_o - T_i)$$

$$\left(\frac{\Delta Q}{Q} \right)_{out} = \left(\frac{1}{Q_{out}} \right) \left[\left\{ \frac{\partial Q_{out}}{\partial \dot{m}} \Delta \dot{m} \right\}^2 + \left\{ \frac{\partial Q_{out}}{\partial T_o} \Delta T_o \right\}^2 + \left\{ \frac{\partial Q_{out}}{\partial T_i} \Delta T_i \right\}^2 \right]^{0.5}$$

$$\left(\frac{\Delta Q}{Q} \right)_{out} = \left[\left\{ \frac{\Delta \dot{m}}{\dot{m}} \right\}^2 + \left\{ \frac{\Delta T_o}{T_o} \right\}^2 + \left\{ \frac{\Delta T_i}{T_i} \right\}^2 \right]^{0.5} \quad (C/16)$$

Q_{in} is the input heat evaluated from atmospheric temperature and inlet temperature of water:

$$\left(\frac{\Delta Q}{Q}\right)_{in} = \frac{1}{Q_{in}} \left[\left\{ \frac{\partial Q_{in}}{\partial T_i} \Delta T_i \right\}^2 + \left\{ \frac{\partial Q_{in}}{\partial T_a} \Delta T_a \right\}^2 + \left\{ \frac{\partial Q_{in}}{\partial G_T} \Delta G_T \right\}^2 \right]^{0.5}$$

$$\left(\frac{\Delta Q}{Q}\right)_{in} = \left[\left\{ \frac{\Delta T_i}{T_i} \right\}^2 + \left\{ \frac{\Delta T_a}{T_a} \right\}^2 + \left\{ \frac{\Delta G_T}{G_T} \right\}^2 \right]^{0.5} \quad (C/17)$$

$$\frac{\Delta \eta}{\eta} = \frac{1}{\eta} \left[\left\{ \frac{\partial \eta}{\partial Q_{in}} \Delta Q_{in} \right\}^2 + \left\{ \frac{\partial \eta}{\partial Q_{out}} \Delta Q_{out} \right\}^2 \right]^{0.5}$$

$$\frac{\Delta \eta}{\eta} = \left[\left\{ \frac{\Delta Q_{in}}{Q_{in}} \right\}^2 + \left\{ \frac{\Delta Q_{out}}{Q_{out}} \right\}^2 \right]^{0.5} \quad (C/18)$$

C.4 Uncertainty analysis for forced circulation condition:

The errors obtained in this experiment study care based on the least counts and the accuracy of the devices used. Table(C.1) represents the errors in the devices used in this experimental study.

Table C.1: The errors in the instruments used in experiments

| S. No. | parameter | amount | potential inaccuracy |
|--------|------------|---------------------|----------------------|
| 1 | d_i | 0.0115 m | 0.0008m |
| 2 | d_o | 0.0125m | 0.0008m |
| 3 | L | 1.6m | 0.001m |
| 4 | \dot{m} | 0.025kg/sec | 0.48 ec |
| 5 | T_p | 42°C | 0.5°C |
| 6 | T_i | 35.6°C | 0.5°C |
| 7 | T_o | 39.8°C | 0.5°C |
| 8 | T_m | 37.7°C | 0.5°C |
| 9 | T_a | 28.6°C | 0.5°C |
| 10 | G_T | 708W/m ² | 10W/m ² |
| 11 | ΔP | 65 mbar | 0.05mbar |

C.4.1 Friction factor evaluated

From eq.(C/11)

$$\frac{\Delta(\text{Re})}{\text{Re}} = \left[\left\{ \frac{\Delta \dot{m}}{\dot{m}} \right\}^2 + \left\{ \frac{\Delta d_i}{d_i} \right\}^2 \right]^{0.5} = \left[\left\{ \frac{0.00048}{0.025} \right\}^2 + \left\{ \frac{0.0008}{0.0115} \right\}^2 \right]^{0.5} = 7.21\%$$

From eq.(C.9)

$$\frac{\Delta(\Delta P)}{\Delta P} = \frac{0.05 \text{ mbar}}{65 \text{ mbar}} = 7.69 \times 10^{-4}$$

From eq.(C.8)

$$\frac{\Delta f}{f} = \left[\left\{ \frac{\Delta(\Delta P)}{\Delta P} \right\}^2 + \left\{ \frac{\Delta(L)}{L} \right\}^2 + \left\{ \frac{3\Delta(d_i)}{d_i} \right\}^2 + \left\{ \frac{2 \Delta(\text{Re})}{\text{Re}} \right\}^2 \right]^{0.5}$$

$$\frac{\Delta f}{f} = \left[\left\{ 7.69 \times 10^{-4} \right\}^2 + \left\{ \frac{0.001}{1.6} \right\}^2 + \left\{ \frac{3 \times 0.0008}{0.0115} \right\}^2 + \left\{ 2 \times 0.0721 \right\}^2 \right]^{0.5} = 0.253$$

C.4.2 The Nusselt number calculation

From the equation(C/16)

$$\left(\frac{\Delta Q}{Q} \right)_{\text{out}} = \left[\left\{ \frac{\Delta \dot{m}}{\dot{m}} \right\}^2 + \left\{ \frac{\Delta T_o}{T_o} \right\}^2 + \left\{ \frac{\Delta T_i}{T_i} \right\}^2 \right]^{0.5} = \left[\left\{ \frac{0.00048}{0.025} \right\}^2 + \left\{ \frac{0.5}{39.8} \right\}^2 + \left\{ \frac{0.5}{35.6} \right\}^2 \right]^{0.5}$$

$$= 2.68\%$$

From equations (C/14) and (C/15)

$$\frac{\Delta h_i}{h_i} = A_i \left[\left\{ \frac{\Delta Q_{\text{out}}}{Q_{\text{out}}} \right\}^2 + \left\{ \frac{\Delta T_p}{T_p} \right\}^2 + \left\{ \frac{\Delta T_m}{T_m} \right\}^2 + \left\{ \frac{\Delta(\ln(\frac{d_o}{d_i}))}{\ln(\frac{d_o}{d_i})} \right\}^2 \right]^{0.5}$$

$$= 1.039 \times 10^{-4} \left[\left\{ 0.0268 \right\}^2 + \left\{ 0.0119 \right\}^2 + \left\{ 0.0133 \right\}^2 + \left\{ \frac{0}{0.0883} \right\}^2 \right]^{0.5}$$

$$= 1.382 \times 10^{-6}$$

$$\frac{\Delta \text{Nu}}{\text{Nu}} = \left[\left\{ \frac{\Delta h_i}{h_i} \right\}^2 + \left\{ \frac{\Delta d_i}{d_i} \right\}^2 \right]^{0.5} = \left[\left\{ \frac{\Delta h_i}{h_i} \right\}^2 + \left\{ \frac{\Delta d_i}{d_i} \right\}^2 \right]^{0.5}$$

$$= \left[\left\{ 1.382 \times 10^{-6} \right\}^2 + \left\{ 0.0695 \right\}^2 \right]^{0.5} = 6.95\%$$

C.4.3 Efficiency calculation

From the equations (C/17) and (C/18)

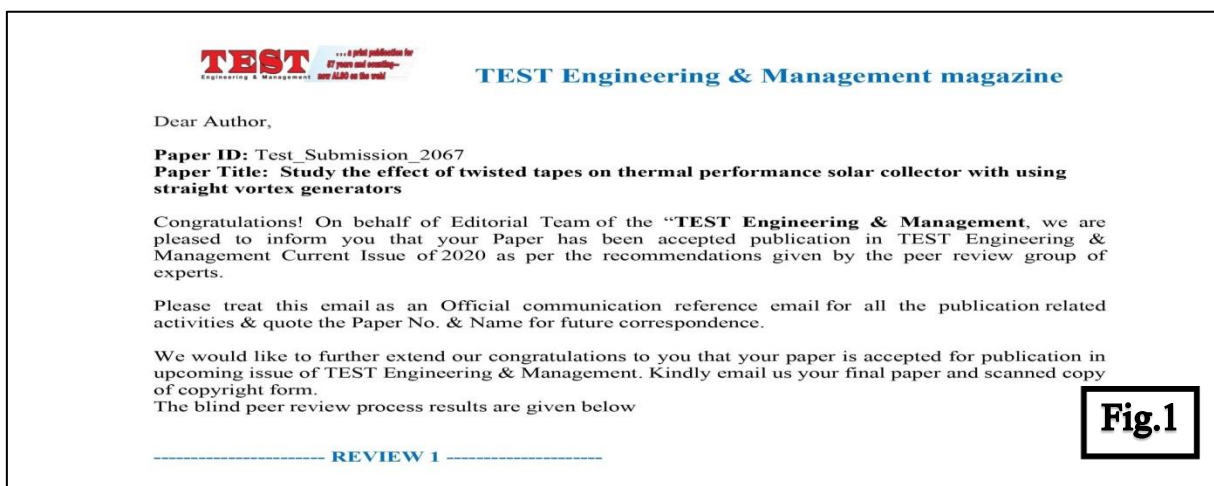
$$\left(\frac{\Delta Q}{Q}\right)_{in} = \left[\left\{ \frac{\Delta T_i}{T_i} \right\}^2 + \left\{ \frac{\Delta T_a}{T_a} \right\}^2 + \left\{ \frac{\Delta G_T}{G_T} \right\}^2 \right]^{0.5} = \left[\{0.0140\}^2 + \{0.0174\}^2 + \{0.0141\}^2 \right]^{0.5} = 2.64\%$$

$$\frac{\Delta \eta}{\eta} = \left[\left\{ \frac{\Delta Q_{in}}{Q_{in}} \right\}^2 + \left\{ \frac{\Delta Q_{out}}{Q_{out}} \right\}^2 \right]^{0.5} = \left[0.0264 \right]^2 + \left[0.0268 \right]^2 \right]^{0.5} = 3.76\%$$

Appendix(D)

D. List of publications

1. Accept the publication of the research (STUDY THE EFFECT OF TWISTED TAPES ON THERMAL PERFORMANCE OF SOLAR COLLECTOR WITH USING STRAIGHT VORTEX GENERATOR) in the journal (TEST Engineering & Management).Fig.1.
2. Publication of the resserch(STUDY THE EFFECT OF TWISTED TAPES ON THERMAL PERFORMANCE OF SOLAR COLLECTOR WITH USING CURVATUER VORTEX GENERATORS) in the journal (Technology Reports of Kansai University) .Fig2.



الخلاصة

الهدف من هذا البحث هو دراسة عملية لتأثير استخدام اشربة ملتوية من الالمنيوم كا معززات اضطراب على معدل أنتقال الحرارة بدلالة رقم نسلت NU , خسائر الضغط بدلالة معامل الاحتكاك f , معامل الاداء الحراري TPF و الكفاءة للمجمع الشمسي المسطح .هذا البحث ركز على عملية حفظ الطاقة تحت ظروف مستقلة وللجريان الطباقى وللماء المقطر المائع الاختبارى.

الجانب العملي يشتمل على تصنيع مجمع شمسي مسطح و تصنيع اربعة انواع مختلفة من الاشربة الملتوية مع مولد الدوامات (VG) مع نسبة الالتواء $Y=2$ (شريط ملتوي مع مولد دوامات منحنى الشكل يكون باتجاه جريان المائع TTF , شريط ملتوي مع مولد دوامات منحنى الشكل عكس اتجاه جريان المائع $TTOF$, شريط ملتوي يتضمن مولد دوامات مستقيمة وشريط ملتوي عادي) , ابعاد مولد الدوامات يكون بارتفاع ٢ ملم وسمك ١ ملم. أجهزة القياس المستخدمة كانت جهاز قياس الاشعاع الشمسي, جهاز قياس التدفق الحجمي للمائع, جهاز قياس فرق الضغط, أجهزة قياس درجات الحرارة مع حساسات الحرارة. التجارب اجريت في محافظة بابل حسب خط العرض $32^{\circ}, 13', 27 N$ وخط الطول $44^{\circ}, 22', 36 E$ مدى التدفق الحجمي المستخدم في التجارب كان (1.5, 3, 5, 7) لتر/ثانية ورقم رينولد Re يتغير من ٤٠٠ الى ٢٠٠٠. النتائج الاختبارية بينت ان انخفاض معدل التدفق الحجمي يزيد في فرق درجة الحرارة بين درجة حرارة الدخول والخروج للماء وكان اعلى فرق درجة حرارة للتدفق الحجمي ١.٥ لتر/ثانية هو $18.3^{\circ} C$ في الانابيب التي تحتوي على اشربة ملتوية مع مولد دوامات منحنى باتجاه الجريان TTF وبنفس الوقت ان اعلى درجة حرارة $98^{\circ} C$ خروج كانت لنفس التدفق اعلاه و لأنابيب التي بداخلها اشربة ملتوية نوع TTF . بالإضافة الى ان معدل انتقال الحرارة بدلالة رقم نسلت خسائر الضغط بدلالة معامل الاحتكاك تزداد في الانابيب التي تكون مزودة بأشربة نوع TTF

مقارنة مع الحالات الأخرى والأنبوب الأملس حيث ان رقم نسلت ازداد في الأنابيب التي تحتوي على
اشرطة نوع TTFF الى 40%,38.2%,31% و 54.2% بالمقارنة مع الأنبوب الأملس للجريين الطباقى
و لرقم رينولد من ٤٠٠ الى ٢٠٠٠ على التوالي أضافة الى ان معامل الاحتكاك يقل بزيادة رقم رينولد
,حيث يزداد معامل الاحتكاك في الأنابيب التي تكون مزودة بالشرطة ملتوية مع مولد دوامات (TTFF,
TTOF و TTS) بالمقارنة مع الأنبوب الأملس والشريط الاعتيادي لوحده حيث تكون الزيادة حوالى
من 18% الى 30%. وبينت النتائج العملية ان اعلى معامل اداء حراري وكفاءة يكون في الأنابيب
التي تزود بأشرطة من نوع TTFF بالمقارنة مع الحالات الأخرى, حيث ان اعلى معامل اداء حراري كان
١.٤ واعلى كفاءة ايضا ٦٤.٧%.



جمهورية العراق
وزارة التعليم العالي والبحث العلمي
جامعة الفرات الاوسط التقنية
الكلية التقنية الهندسية – نجف

دراسة تأثير انواع مختلفة من الاشرطة الملثوية على الأداء الحراري للمجمع الشمسي

رسالة مقدمة الى

قسم هندسة تقنيات ميكانيك القوى في الكلية التقنية الهندسية- نجف/جامعة الفرات الاوسط التقنية كجزء من متطلبات نيل درجة الماجستير التقني في هندسة تقنيات الميكانيك

تقدم بها

علي مجيد عبد الكريم

بكلوريوس هندسة ميكانيكية - ميكانيك عام

٢٠٠٠

إشراف

الأستاذ الدكتور

علي شاکر باقر

الأستاذ المساعد الدكتور

أحمد هاشم يوسف

ذي الحجة ١٤٤١